ORNL/NRC/LTR-08/03

Contract Program or Project Title:	**Technical Update of Reactor Pressure Vessel Structural Integrity Program** **Materials Science and Technology Division**
Subject of this Document:	**Review of Draft NUREG Report on Technical Basis for Revision of Regulatory Guide 1.99**
Type of Document:	**Letter Report**
Authors (in Alphabetical Order):	**R. K. Nanstad (Oak Ridge National Laboratory)** **G. R. Odette (University of California, Santa Barbara)** **R. E. Stoller (Oak Ridge National Laboratory)** **T. Yamamoto (University of California, Santa Barbara)**
Date of Document:	**March 31, 2008**
Responsible NRC Individual And NRC Office or Division	**Mark EricksonKirk, (301) 415-6015** **Division of Engineering Technology** **Office of Nuclear Regulatory Research**

Prepared for
U. S. Nuclear Regulatory Commission
Washington, D.C. 20555-0001
Under Interagency Agreement DOE 1886-N653-3Y
NRC JCN No. N6459

OAK RIDGE NATIONAL LABORATORY
Oak Ridge, Tennessee 37831-8056
Managed and Operated by
UT-Battelle, LLC
For the
U. S. DEPARTMENT OF ENERGY
Under Contract No. DE-AC05-00OR22725

ORNL/NRC/LTR-08/03

Review of Draft NUREG Report on Technical Basis for Revision of Regulatory Guide 1.99

(Authors in Alphabetical Order)

Randy K. Nanstad
Oak Ridge National Laboratory
Oak Ridge, Tennessee

G. Robert Odette
University of California, Santa Barbara
Santa Barbara, California

Roger E. Stoller
Oak Ridge National Laboratory
Oak Ridge, Tennessee

Takuya Yamamoto
University of California, Santa Barbara
Santa Barbara, California

Date Published –March 31, 2008

Prepared for
U. S. Nuclear Regulatory Commission
Office of Nuclear Regulatory Research
Under Interagency Agreement DOE 1886-N653-3Y
NRC JCN No. N6459

Prepared by
OAK RIDGE NATIONAL LABORATORY
Oak Ridge, Tennessee 37831-8056
Managed and Operated by
UT-Battelle, LLC
For the
U. S. DEPARTMENT OF ENERGY
Under Contract No. DE-AC05-00OR22725

CONTENTS

FIGURES

TABLES

ABBREVIATED TERMS

Acronyms and Abbreviations

3FTTS	three-feature transition temperature shift
AMES	Ageing Materials European Strategy
AMSE	American Society of Mechanical Engineers
ASTM	American Society for Testing and Materials
B&W	Babcock and Wilcox
BWR	boiling water reactor
CE	Combustion Engineering
CRP	copper-rich precipitate
DBT	ductile-brittle transition
DBTT	ductile-brittle transition temperature
dpa	displacements per atom
DRE	dose rate effect
EFPY	effective full-power years
EOL	end of life
EONY	Eason, Odette, Nanstad, and Yamamoto
EPRI	Electric Power Research Institute
EWO	Eason, Wright, and Odette
HSSI	Heavy Section Steel Irradiation (program)
IAEA	International Atomic Energy Agency
IVAR	Irradiation Variable (program)
JRQ	Japanese designation for a specific heat of RPV steel
LBP	late-blooming phase
LV	Laval
MD	matrix defect
MEK	Mark EricksonKirk
MF	matrix feature
MNP	Mn-Ni-Si-rich precipitate
NRC	U.S. Nuclear Regulatory Commission
NRT	Norgett, Robinson, and Torrens
ORNL	Oak Ridge National Laboratory
PF	product form
PIA	postirradiation annealing
PWR	pressurized water reactor
RED	radiation-enhanced diffusion
RPV	reactor pressure vessel
SDB	U.S. power reactor surveillance database
SE	standard error
SER	solute trap enhanced recombination
SIA	self-interstitial atom
SMD	stable matrix defect
TMS	The Minerals, Metals, and Materials Society
TTS	transition temperature shift
UCSB	University of California, Santa Barbara
UMD	unstable matrix defect

Nomenclature

$\Delta\sigma_y$	change in yield strength
ΔH	change in microhardness
ΔT_{30}	transition temperature shift
ΔUSE	change in Charpy upper shelf energy due to irradiation (= USE_i-USE_u)
ϕt	fluence, n/cm^2, E > 1 MeV
ϕ_{eff}	effective fluence
Cu_{min}	minimum Cu needed for CRP formation
Cu_{max}	maximum effective dissolved Cu prior to irradiation
fluence	n/cm^2, E > 1 MeV
flux	n/cm^2/s, E > 1 MeV
sqrt	square root
T_{30}	temperature at 30 ft-lb (41 J) in Charpy tests
tanh	hyperbolic tangent

Unit Conversions

Fahrenheit to Celsius: $T_C = (T_F - 32)/1.8$

Foot-pounds to Joules: 1 ft-lb = 1.356 J

Note: The U.S. RPV surveillance database is maintained in English units. Thus, the modeling tasks for the NUREG report and parts of this letter report were performed and are reported in English units. Data in other parts of this letter report are reported in SI units.

Review of Draft NUREG Report on Technical Basis for Revision of Regulatory Guide 1.99

R. K. Nanstad[1], G. R. Odette[2], R. E. Stoller[1], and T. Yamamoto[2]
(in alphabetical order)

SUMMARY

A panel of reviewers from Oak Ridge National Laboratory and University of California, Santa Barbara, (UCSB) was appointed by the Nuclear Regulatory Commission (NRC) to provide a technical review of the draft NUREG report by Mark EricksonKirk, *Technical Basis for Revision of Regulatory Guide 1.99: NRC Guidance on Methods to Estimate the Effects of Radiation Embrittlement on the Charpy V-Notch Impact Toughness of Reactor Vessel Materials.* This letter report provides the results of that review. As requested, the review focused on the portions of the draft NUREG dealing with the embrittlement trend curve, the upper-shelf energy, and attenuation. In consideration of the embrittlement trend curve, additional specific discussions are included on the use of test reactor data at high flux and high fluence as well as the more general influence of neutron flux, or dose rate effects (DREs).

As part of the review, the panel performed detailed analyses of various subsets of data from the U.S. surveillance database (SDB) and other sources of data to evaluate the predictive capability of the transition temperature shift (TTS) RM-9 correlation/model (the term "model" will be used throughout this report) developed by Dr. Mark EricksonKirk (MEK). Variants of the MEK model were compared with those for a similar TTS model developed by Eason, Odette, Nanstad, and Yamamoto (EONY). These analyses also included further statistical optimization of the models to try to avoid limitations that are associated with the use of the Excel® solver. The comparisons show that both the EONY and MEK models provide reasonably good fits to a wide variety of subsets of TTS and yield strength increase ($\Delta\sigma_y$) data from the SDB and the UCSB Irradiation Variable (IVAR) database, respectively. While the general trends in flux, fluence, temperature, copper, nickel, and phosphorous are broadly consistent with one another, there are significant differences in the TTS predicted by the two models, depending on the specific combination of variables. The largest differences are associated with variations in the treatment of product form (PF) effects and maximum Copper (Cu_{max}) levels. However, we did not find a clear-cut reason to select one model over the other.

The draft NUREG proposes the use of a TTS model derived from the high-flux RADAMO database at high fluence. However, current understanding of radiation damage mechanisms suggests that it is not appropriate to directly use high-flux data or TTS models derived from such data to directly predict high fluence behavior for reactor pressure vessel (RPV) or surveillance conditions. This conclusion was reinforced by the development and application of a physically based three-feature TTS (3FTTS) model to the high-flux data that included the effects of so-called "unstable matrix defects" (UMDs) that are very important for highly accelerated test reactor irradiations. The 3FTTS model was based on adding UMD effects to the low flux MEK (or EONY) model. The 3FTTS model is in much better agreement with the high-flux RADAMO

[1] Materials Science and Technology Division, Oak Ridge National Laboratory
[2] Mechanical Engineering and Materials Departments, University of California, Santa Barbara

data in Appendix G of the draft NUREG report and minimizes the trend of underprediction of TTS below fluences of more than 6×10^{19} n/cm^2. The UMDs are not significant at low flux surveillance conditions and, in almost all the cases examined, the 3FTTS gives good predictions of the TTS in the surveillance, IVAR, and RADAMO databases.

However, the panel agrees with the concern expressed in the draft NUREG report about the paucity of high fluence data in the SDB. We believe that this is a major issue for the operation of plants over extended lifetime to 60 effective full power years or more. Based on the analysis of the high fluence subset of the existing SDB, we recommend that the low flux models not be used at fluences greater than 5×10^{19} n/cm^2 without further consideration. Consistent with the concerns expressed in the draft NUREG report, perhaps some caution should be exercised above 3×10^{19} n/cm^2. (Fluence is for E > 1 MeV in all cases except as otherwise noted.)

The change in Charpy upper shelf energy due to radiation (ΔUSE) correlation recommended in the draft NUREG provides a reasonable basis for prediction with the current database. However, the current Regulatory Guide 1.99, Revision 2 procedure recommended in the draft NUREG for attenuation should not be employed. An alternate approach, based on attenuation of the physically based displacement per atom (dpa) dose unit combined with a self-consistent treatment of dose rate effects, is described and should be used for predicting TTS in an RPV. The review does not directly provide recommendations regarding the development of Regulatory Guide 1.99, Revision 3.

1. INTRODUCTION AND OVERVIEW

In late 2007, the Component Integrity Branch of the Division of Engineering in the Nuclear Regulatory Commission (NRC) Office of Research convened a panel to review the draft NUREG report prepared by Dr. Mark EricksonKirk, *Technical Basis for Revision of Regulatory Guide 1.99: NRC Guidance on Methods to Estimate the Effects of Radiation Embrittlement on the Charpy V-Notch Impact Toughness of Reactor Vessel Materials* (EricksonKirk 07). This letter report presents the results of a review by the panel members from Oak Ridge National Laboratory (ORNL) and University of California, Santa Barbara. The statement of work provided to the panel requested particular focus on assessing the soundness of the technical basis supporting the recommended revisions to Regulatory Guide 1.99, Revision 3 (RG 1.99-3). Specifically, the reviewers were asked to determine whether the recommendations made in the report regarding (1) the ΔT_{30} embrittlement trend curve (which we hereafter will refer to as the Mark Erickson-Kirk transition temperature shift [MEK TTS] model), (2) the decrease in upper-shelf energy (ΔUSE) equation, and (3) the attenuation equation, are wholly consistent, generally consistent, or inconsistent with the current technical state of knowledge that is published in the open literature. The draft NUREG report includes a number of appendices, including the draft RG 1.99-3, that are not specifically reviewed or discussed in this letter report.

In the overall analysis, the draft NUREG uses data from the U.S. power reactor surveillance database (SDB), some surveillance data from the French and Japanese databases, and various test reactor data (e.g., data from the RADAMO and Irradiation Variable [IVAR] databases). The embrittlement trend curve model, designated RM 6(2) and recommended in the draft NUREG report, was based on fitting the SDB. The draft NUREG report recommends a fluence limit (e.g., Sect. 9.4.1.1) of 3×10^{19} n/cm^2 for the RM 6(2) model, whereas a TTS model derived from accelerated test reactor data (RADAMO) was used to develop an embrittlement TTS trend curve for fluence at and beyond 4×10^{19} n/cm^2. In addition to the draft NUREG report, Dr. EricksonKirk transmitted a revised SDB model, designated RM-9, to the panel members requesting that the revised model be used in the review process. As part of the review process, the panel performed detailed analyses of various subsets of data from the SDB to evaluate the predictive capability of the MEK (RM-9) TTS; analyses of the same datasets were performed with the Eason, Odette, Nanstad, and Yamamoto (EONY) TTS model (Eason 07). Additional analyses were performed of many datasets from the Irradiation Variable (IVAR) database (Odette 08). The analyses also included further statistical optimization of both the EONY and MEK models. A detailed evaluation of the statistical constructs used in the draft NUREG was not performed, but comments regarding the basic approach are provided.

The NUREG recommendation is to restrict the use of the MEK model to 3×10^{19} n/cm^2 and to use the RADAMO model above 4×10^{19} n/cm^2. A simple linear weighting function using the equation from surveillance data and the equation from test reactor data was then developed to provide the predictive embrittlement between 2 and 4×10^{19} n/cm^2. Thus, our report provides comments and analysis regarding displacement rate effects (DREs) and the use of high-flux test reactor data. The analysis included development and application of a physically based three-feature TTS (3FTTS) model. In addition to contributions from matrix defects (MDs) and copper rich precipitates (CRPs), the 3FTTS model treats both direct hardening and indirect sink effects of thermally unstable matrix defects (UMDs) that both form and dissolve (anneal) under irradiation. The 3FTTS model used the optimized MEK model modified for UMD sink effects to treat the MD and CRP contributions and simply added the UMD hardening. The UMDs are not

significant at low flux surveillance conditions but are very important for high-flux test reactor irradiations. A complete analysis of the extensive database compiled in the draft NUREG report is beyond the support provided for our current effort. However, a limited analysis shows that the 3FTTS model can rationalize most of the trends observed in the high-flux RADAMO database to fluences greater than 6×10^{19} n/cm^2. At low flux the 3FTTS model (basically an optimized MEK model) predictions are in generally good agreement with both the surveillance and IVAR databases.

Our report also provides analysis and recommendations on attenuation. Consistent with international understanding of radiation damage mechanisms, we propose that attenuation of displacement per atom (dpa) in the vessel represents the proper treatment of spectral variations in establishing the effective neutron dose inside the vessel. We show that this can be done by scaling the fluence (E > 1 MeV) with the ratio of the dpa at prototypic surveillance locations with the corresponding attenuated dpa in the vessel. However, both the MEK and EONY TTS models include flux as a variable in both the MD and CRP terms. Thus, it is also important to scale the flux used in the TTS evaluations in the vessel with the dpa ratio.

Our report also provides brief comments on the ΔUSE equation and some other aspects of the draft NUREG report.

2. REVIEW COMMENTS AND DISCUSSION OF CHAPTER 4, TRANSITION TEMPERATURE SHIFT

This chapter provides some comments on specific issues in Chap. 4 and presents a detailed analysis of the draft NUREG RM-9 model as it relates to U.S. reactor surveillance data and data from the IVAR database. A brief discussion of statistical considerations is presented in Sect. 2.2, followed by the RM-9 analysis in Sect. 2.3. Finally, a short summary of observations of the RM-9 model is presented in Sect. 2.4.

2.1 Comments on Chapter 4

The draft NUREG report clearly represents an enormous and impressive effort, and Dr. EricksonKirk is to be applauded for his initiative in gathering and analyzing data in the literature to help guide the development and validation of TTS models. The information assembled in Appendix G of the draft NUREG report is especially useful and represents a substantial contribution to the field. While we do not agree with all his conclusions, Dr. EricksonKirk's effort to raise the issue of the paucity of high fluence data in the SDB and to find approaches to dealing with this important issue are also to be greatly commended. Further, we note that our work was greatly facilitated by Dr. EricksonKirk's very effective and easy-to-use spreadsheets. However, we think it important to communicate some concerns about specific items in Chap. 4 as well as to offer constructive comments on the overall approach to evaluating data trends. The approach that we preferred to use differs from that in the draft NUREG. We outline the reasons for our preference, but leave it to others to judge the merits of various approaches.

We are impressed with the effort to identify variable trends described in Chap. 4 of the draft NUREG report as well as the extensive comparisons of the TTS models with independent sources of data that were not used in the model calibration. However, it is useful to note that the basic approach in Chap. 4 differs somewhat in philosophy from the approach that we prefer. Our analysis emphasizes single-variable evaluations to allow for determination of the effect of specified variables whenever possible, as well as analysis of well-defined subsets of data that are most pertinent to TTS predictions for RPV surveillance and vessel irradiation conditions. This contrasts to the acknowledged approach in Chap. 4, which assesses trends from either (1) data for combinations of alloys in the IVAR database within the general composition limits of the SDB and (2) generally high-flux data on a variety of steels and model ferritic alloys (e.g., Chaouadi 05 and Debarberis 05). In our opinion, a limitation in the draft NUREG approach derives from the fact that hardening and embrittlement depend in a sensitive way on the combination of a large number of variables. As a result, the effects of variables that are clearly apparent and statistically significant in controlled single-variable comparisons, for example of the effect of flux for a specified alloy and irradiation temperature over an overlapping range of fluence in the IVAR database, are more difficult to discern when a range of compositional variables are included in trend plots such as Fig. 4-3 in the draft NUREG. We believe that such confounding is also the case for Figs. 4-5 (Ni), 4-7 (P), 4-8 (Mn), 4-11 (Cu), 4-12 (Cu), 4-13 (flux) and 4-16 (Ni and Mn). Further, for reasons discussed later in this report, variable effects trends in high-flux TTS and $\Delta\sigma_y$ (e.g., from the RADAMO database), differ from those at low flux, as found in IVAR and SDB. These differences are seen in the RADAMO model itself, for example in the balance of CRP and MD contributions to the TTS and Ni effects, as well as in the 3FTTS model analysis described in Sect. 3.1 of this report. These differences are due to variations in the underlying microstructures in the low vs high-flux regimes. Thus, in summary, our approach to assessing the effects of pertinent variables is, whenever possible, to use

controlled single or few variable comparisons, or using physically justifiable subsets of data, for relatively low flux irradiations. Indeed, such trends in essentially all the key variables can be extracted from the IVAR controlled, single-variable database.

We also note that the basic form of the MEK TTS model does not vary fundamentally from those used in previous database correlation studies, such as that in NUREG 6551 (Eason 98) and EONY (Eason 07). Thus, while they are cited in Chap. 4 of the draft NUREG report, we would recommend even more extensive utilization of the detailed discussions of mechanisms and variable effects trends in Chaps. 2 and 6 of the EONY report (also included in Appendix A of the draft NUREG report). Further, for reasons discussed below, we recommend caution in using the insight from the RADAMO and other high-flux or model alloy data sets or the use of TTS models derived from such data. We recognize that there are merits to the development of a TTS model from an even more independent set of information than, for example, that provided by the IVAR database. However, this approach may bear some costs in terms of fidelity and relevance.

We have a number of specific concerns about Chap. 4 that are generally minor but may be worth briefly noting. First and foremost, several of the conclusions in Chap. 4 regarding items such as flux effects on CRP contributions to TTS need to be modified because they are inconsistent with the final MEK (RM-9) model. Other, generally minor comments include (in sequence referencing the appropriate page number) are as follows.

- 4-11. The Electric Power Research Institute (Carter 02) report suggests that there will be flux effects if the MD hardening features depend on radiation-enhanced diffusion (RED). Well formed Mn-Ni precipitates are one cited example. This also now seems to be the case for MDs.
- 4-13. It is not clear that nonhardening embrittlement has a cut-off below 0.03% P. However, we agree on the more general points made in that paragraph.
- 4-14. We do not agree that product form effects lie entirely in the TTS and that they do not occur in irradiation hardening ($\Delta\sigma_y$). For example, in the IVAR database the differences between welds and plates cannot be totally explained by the TTS-$\Delta\sigma_y$ relation. Moreover, we do not agree that product form effects are simply artifacts of fitting CVN data with tanh functions rather than using linear fits in the transition. We do agree that product form and starting properties affect this relation as discussed in Chaps. 2 and 6 of the EONY report as well as shown long ago with semi-empirical micromechanical models of the TTS-$\Delta\sigma_y$ relation (Odette 85, Nanstad 93). We do not agree that Fig. 4-9 of the draft NUREG demonstrates a lack of product form effect on $\Delta\sigma_y$ because the weld data generally fall well above the data for plates and forgings.
- 4-19. The high Cu_{min} is based on very limited data on low-Ni Rolls Royce welds. The Cu_{min} for high-Ni welds is lower and is currently taken as 0.072 Cu (Williams 02).
- 4-19 (Sect. 4.1.2.2). A temperature dependence in the CRP term has been recognized prior to the development of the IVAR database (Odette 96). The IVAR assessment was primarily based on subtracting the $\Delta\sigma_y$ for steels with low Cu from the corresponding $\Delta\sigma_y$ for steels with high Cu that are otherwise very similar in their composition and heat treatment and that have been irradiated at the same conditions (Odette 05). As discussed elsewhere there are also microstructural data that support this conclusion (Odette 95, Odette 05, Eason 07).

- 4-19 (Sect. 4.1.2.3). The analysis in Chap. 2 of the EONY report did not conclude that flux effects vanish below 10^{10} n/cm^2-s. Rather, the EONY report proposed that flux effects in that regime could be expected due to contributions of thermal diffusion to solute transport and clustering. Further, neither we nor the EONY report concludes that the flux effect on ϕt_{sat} (or in ϕ_{eff}) in the IVAR database is modest, but rather the DRE is statistically significant and very systematic.
- 4-20 (Sect. 4.1.2.4). Single-variable analysis of the IVAR database shows that Mn and P also have statistically significant and systematic effects on $\Delta\sigma_y$.
- 4-20 (Sect. 4.1.2.5). We previously commented on the product form effect on $\Delta\sigma_y$ as well as on TTS.
- 4-28. In light of the preceding discussion, and the use of the RM-9 vs RM-6(2) model, we believe that Table 4.2 must be extensively revised. We also believe that mechanisms and data trends are well described in Chap. 2 of the EONY report and could be used more effectively in the draft NUREG.
- 4-88. There are what appear to be some nonphysical features in the RADAMO model, which basically derives from the original model of Fisher (Fisher 88). For example, the activation energy for thermal diffusion of Cu depends on flux, fluence, and temperature in the RADAMO model. That does not make physical sense. However, the main effect of that part of the RADAMO model is at lower Cu levels. Thus, this treatment may just be a convenient, albeit artificial, way to model the slow precipitation in this composition regime, which is a trend observed in IVAR and other datasets. The mechanism is most likely lower nucleation rates. Other, more significant concerns about use of the RADAMO model are discussed below.

2.2 Statistical Considerations

None of the panel members is a professional statistician. Thus, while we offer a number of *opinions* on the statistical approach used in the draft NUREG, they are just opinions based mainly on our experience and on physical as well as statistical considerations. We leave it to others to judge the relative merits of various approaches and strongly recommend that comments be sought from professional statisticians as part of the continuing review process (e.g., brief discussions were held with Dr. K. O. Bowman of ORNL). The following points are offered in that context.

- In development of an embrittlement model, simplification of the model equations, which are intrinsically greatly oversimplified to begin with relative to the complicated nature of radiation damage, should not be an overriding objective. The equation used for the model should be guided by mechanistic considerations, the statistical success of the resulting fits, and residual analysis for the variables and key subsets of data.
- Our understanding is that the t-statistic is generally used for evaluating the quality of modeling of an independent variable and the significance of that variable's influence on the dependent variable. The use of the t-statistic is based on a set of assumptions that may not be appropriate for this particular analysis, involving nonlinear fitting of approximate equations to the highly scattered and ill-distributed surveillance database.

- Demanding high statistical confidence levels for including the effect of a variable (such as flux) for a highly scattered surveillance database is not appropriate when there is independent information, subsets of data, and mechanistic considerations that support the effect of the variable. The insight provided by the independent information should be rejected only if its inclusion significantly degrades the fit.
- Minimizing the individual and sum of t-statistics (spreading the errors) for the variables in a particular model is an interesting statistical approach. However, in our judgment, there are two possible limitations to that approach. The first is that spreading the errors may mask effects that are subtle and primarily reflected in subsets of the SDB or other independent sources of data. For example, the DRE at fluxes greater than 4×10^{10} n/cm^2/s observed in the IVAR database are not found in either the EONY or RM-6(2) models. It appears that the standard error (SE) and t-statistics are slightly better for the SDB if a DRE is absent in this flux regime. However, this slight statistical benefit is outweighed by the availability of independent and high-quality data. We are pleased to note that this conclusion is represented in the RM-9 model. A second issue with the t-statistic approach is that it sums the contributions for the individual variables rather than the squared values of these statistics. This issue might benefit from review and comment by a professional statistician. However, having raised these concerns, as will be seen in the following sections of this report, the overall capability of the MEK (RM-9) model to fit the SDB is good and we have exploited the approach to further optimize both the MEK and EONY models.
- The systematic approach adopted in the draft NUREG to describe how a final model was reached from the assumed starting point (model equation, variables, and parameterization) is also interesting and innovative. However, since the final result depends on many details of the starting point and optimization path, we do not believe that the approach is intrinsically superior to less obviously systematic approaches. Of course, the choice of general approach is a matter of judgment and depends on the objective.

There are issues with any nonlinear least squares method when used to fit an approximate model with many variables to an imperfect database. This is particularly true of the Excel® solver. We found that the fit results, including the standard error (SE) and various t-statistic measures, were sensitive to how the solver was used. Specifically, the statistics could be improved by employing tighter convergence criteria. However, it is clear that, even in that case, the Excel® solver can get stuck in local minima in parameter space.

Thus, we developed a macro within Excel® to address the issue. The macro enabled fits for a specified set of values for a selected model parameter. For each value of the specified parameter, all the other parameters were optimized to obtain the best t-statistic and SE. The parameterized model was then used as the starting point for a set of specified values for another parameter. This process was repeated in sequence for a number of variables until it appeared that an overall statistical optimum had been achieved. The results of this exercise are described in the next section. The procedure, in effect, forces the Excel® solver out of local minima, allowing it to explore a larger range of parameter space. However, even in that case, there is no guarantee that the solver finds the true minimum, and the final results are still path dependent to some extent. Nevertheless, by that point there is little that can be achieved by going further.

The derivation of a specific final model from the starting point depends on the fitting considerations, such as those described in the paragraph above. Thus, even accepting the draft

NUREG approach, the sequence of steps might be different from those described in Chap. 4 of that document, depending on details of the fitting procedure, perhaps leading to a different final model. We did not attempt to examine this possibility in detail.

Rather, our optimization started with the RM-9 model, which replaced the RM-6(2) model, discussed in the draft NUREG. We also carried out a similar optimization of the simplified EONY model (Eason 07). The effects of these optimizations on the model parameters are generally modest. These results are discussed in the following section.

2.3 Analysis of the RM-9 Model

The RM-9 MEK TTS model is a major improvement over the RM-6(2) model and has an acceptable physical basis that is similar to all modern physically based TTS models (Eason 98, Eason 07, Williams 02, ASTM E900, Fisher 88). It provides a generally acceptable fit to the SDB. Perhaps most notably, both the CRP and MD terms in the RM-9 model depend on flux in a way that is similar (but not identical) to the EONY model and that are qualitatively consistent with trends observed in the IVAR database.

To provide a basis for reference, the MEK (RM-9) model is compared with the EONY model and subsets of various databases. Three versions of each model were evaluated: (1) the original baseline model (b), which was the simplified model in the EONY07 case; (2) an improved model (i), derived from tighter convergence criteria; and (3) what we have designated a super optimized model (o) derived using the macro search scheme described above. Table 2.1 summarizes the statistical results. Appendix A provides a table with further details.

Table 2.1. Summary of results from optimization of the MEK and EONY embrittlement models using Excel® statistics package

Statistic	EricksonKirk			Eason		
	b	i	o	b	i	o
t-total	7.44	2.37	2.04	12.9	7.9	1.57
S-error	24.3	23.8	23.7	22.7	22.7	22.6
t-max	1.75	1.16	1.70	4.43	2.79	1.38

The effects of the primary variables (T, ϕ, ϕt, Cu, Ni, P) are generally similar for the six TTS models. However, there are significant quantitative differences in some cases, depending on the particular set of variables. The major differences are the product form (PF) factors and maximum Cu (Cu_{max}) parameters. However, the optimized EONY and MEK models are generally closer to one another than the base models. This is shown in the plots of the differences in the predicted MEK-EONY TTS as a function of the measured TTS in the SDB for the base and optimized models (top and bottom, respectively) in charts (a)–(f) in Fig. 2.1 for the various product form groupings. These differences for the optimized EONY and MEK models are generally relatively small, except for the Linde 80 weld due to the high Cu_{max} in that case. Thus, the optimized models will generally be the focus of further discussion. In Fig. 2.2, charts (a)–(l) show residual plots for the two optimized models.

Figure 2.3 (a) compares the fluence dependence for the optimized MEK and EONY models for CE plates and a set of compositional variables that are close to the average for the overall surveillance database (0.15 Cu, 0.6 Ni, 1.4 Mn, 0.012 P) at 288°C and 3×10^{10} n/cm^2-s, which gives an end of life (EOL) fluence of 6×10^{19} n/cm^2 in 2×10^9 s for 60 effective full power years (EFPYs).of operation In Fig. 2.3, charts (b)–(d) show the corresponding plots for the other three

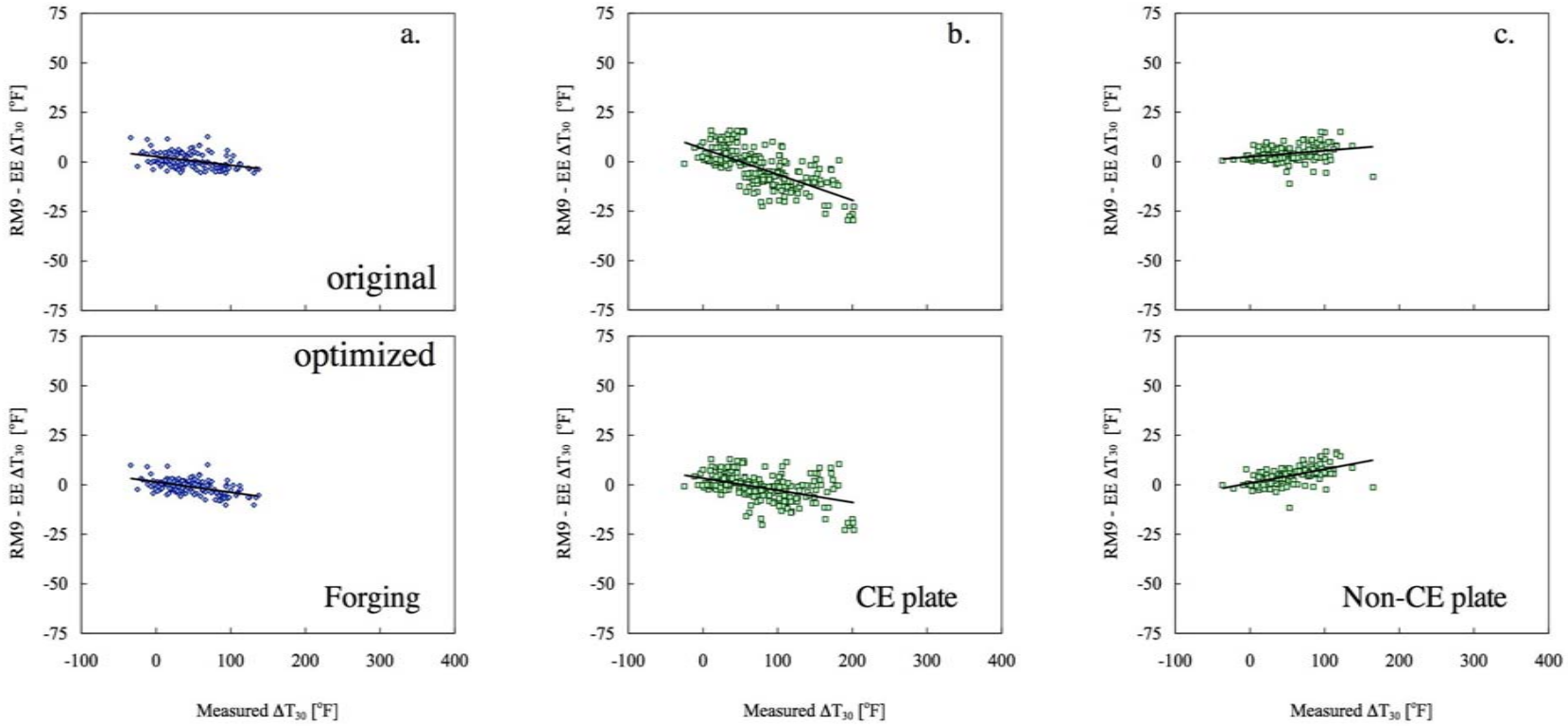

Fig. 2.1. Plots showing TTS differences between RM-9 and EONY models vs TTS (ΔT_{30}) (with base models in top plot and optimized models in bottom plots) for (a) forgings, (b) CE plates, (c) Non-CE plates, (d) standard reference materials, (e) Linde 80 welds, and (f) other than Linde 80 welds.

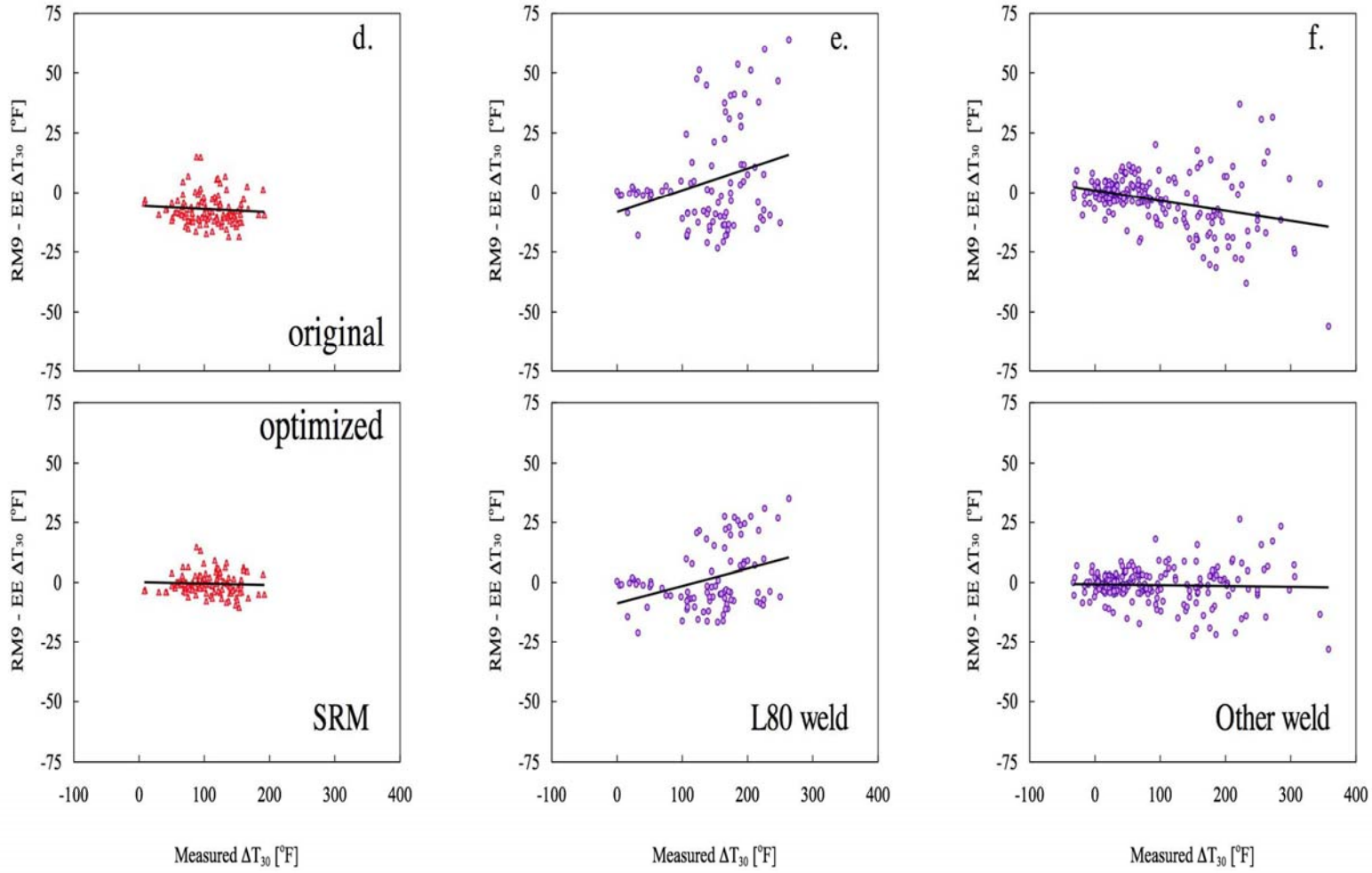

Fig. 2.1. (continued)

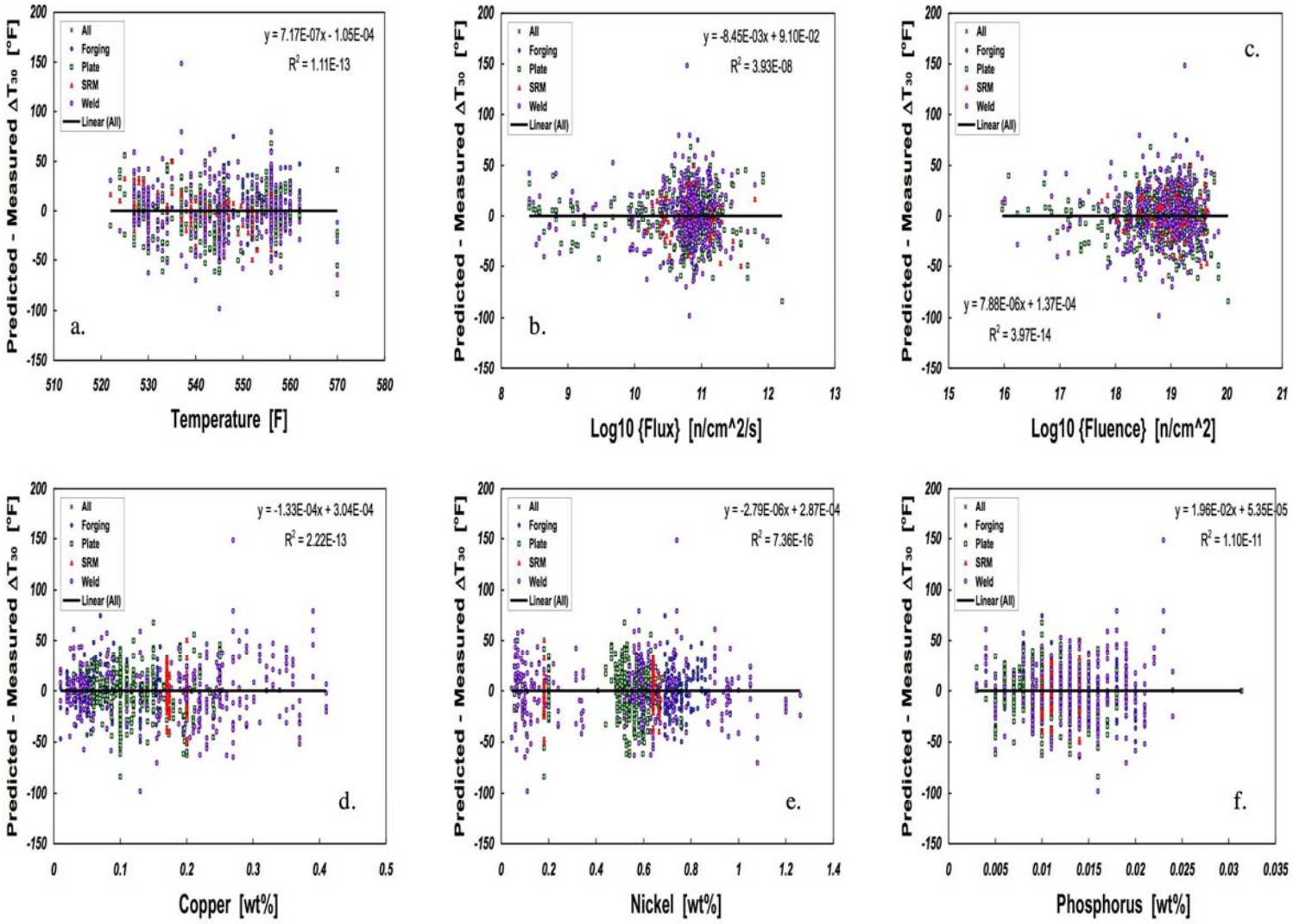

Fig. 2.2. Residual plots for the optimized MEK (a-f) and EONY (g-l) TTS models.

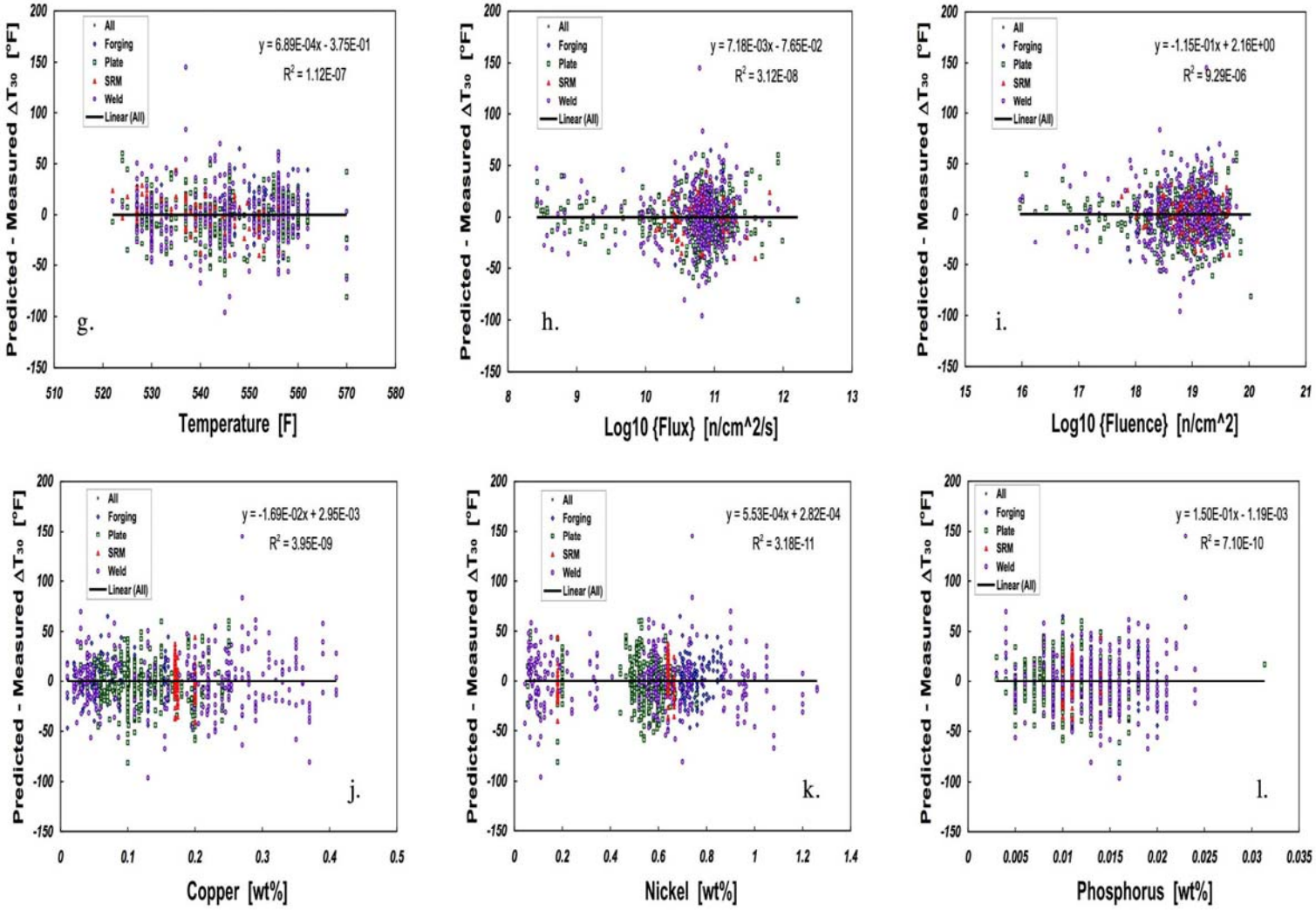

Fig. 2.2. (continued)

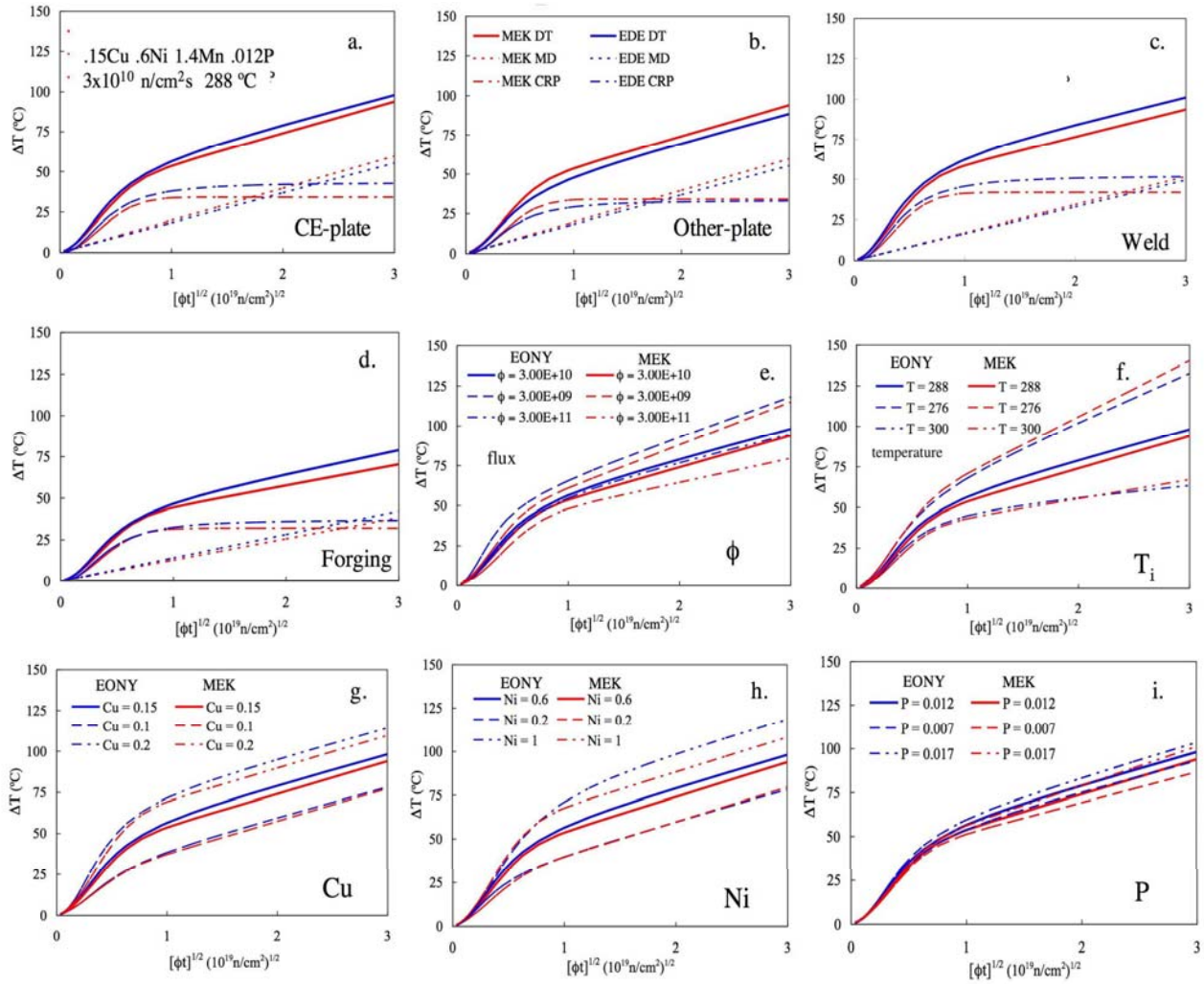

Fig. 2.3. Plots of the MEK and EONY model predictions of the TTS (ΔT) vs sqrt fluence where (a) base case compares the fluence dependence for the optimized MEK and EONY models for CE plates and a set of compositional variables close to the average for the overall SDB (0.15 Cu, 0.6 Ni, 1.4 Mn, 0.012 P, 3 × 10^{10} n/cm^2/s, and 288°C); (b-d) show corresponding plots for the other three product forms: a non-CE plate, a weld, and a forging; and (e-i) show similar plots for the specified variations in Cu, Ni, irradiation temperature, flux, and phosphorus, where the other unspecified variables in each case have the base case values.

product forms. Charts (e–i) in Fig. 2.3 show similar plots for specified variations in Cu (0.10, 0.15, and 0.20%), Ni (0.2, 0.6 and 1%), irradiation temperature (276, 288 and 300°C), flux (0.3, 3 and 30 × 10^{10} n/cm^2/s), and P (0.007, 0.012 and 0.017), where the other unspecified variables in each case have the base values noted above. The largest variations are associated with the differences in the dose rate effect at higher fluxes in the MEK vs EONY models and TTS predictions for high Ni.

In Fig. 2.4, charts (a)–(f) compare cross plots for the TTS predictions of the two models for the base composition for a wider range of flux (a), temperature (b), Cu (c), Ni (d) , P (e), and Mn (f). In the case of the lower Mn (< 1%), we have used the PF for forgings instead of CE plates. Again the TTS model predictions are similar, with the largest differences being in the effect of higher flux and Cu_{max}, especially for the Linde 80 welds.

Figure 2.5 shows model TTS predictions for sensitive alloy compositions similar to the Palisades (0.23%Cu/1.2%Ni at 276°C) and Maine Yankee (0.35%Cu/0.8%Ni at 288°C) welds. In general, the results are fairly similar except for the high-Cu Linde 80 welds. In that case, the MEK model predicts the highest TTS because of the high Cu_{max}. The flux in all of these cases was 3 × 10^{10} n/cm^2-s.

Comparisons of sensitive weld compositions for conditions more pertinent to BWRs are shown in Fig. 2.6 at nominal fluxes of 1 and 3 × 10^9 n/cm^2/s (left and right plots, respectively) at 276°C. In those cases, at the lowest flux and low fluence, the EONY model predicts slightly higher TTS results than the MEK model except for the Linde 80 weld at 3 × 10^9 n/cm^2/s, in which case the Cu_{max} term plays the determining role.

In Fig. 2.7, charts (a)–(h) compare the models to the IVAR database for Babcock and Wilcox (B&W) and Heavy Section Steel Irradiation (HSSI) Program surveillance plates and welds (some of the Linde 80 welds evaluated by the HSSI Program were also exposed in B&W surveillance capsules). The IVAR data at low, medium, and high flux have been adjusted to a common flux of 3 × 10^{11} n/cm^2/s by the fitted recombination model described in Chap. 6 of the EONY report (Eason 07). The TTS model predictions have been converted to yield stress changes ($\Delta\sigma_y$) using the procedure that is also described in Chap. 6 of the EONY report. In Fig. 2.8, charts (a)–(d) show similar plots for the A533B-1 plate JRQ (the International Atomic Energy Agency [IAEA] reference plate), an EPRI high-copper weld, the high-copper (0.31 wt %) Linde 124 HSSI weld 73W, an A302B plate and an A508 forging. In the case of the A508 steel, the IVAR data are compared to the models using the forging product form factor and the plate product form factor in Figs. 2.8d and 2.8e, respectively. Both models provide remarkably good fits. The EONY model generally gives slightly higher predictions than those for MEK except for the high-Cu 73W.

In Fig. 2.9, charts (a)–(e) compare the models to the IVAR plate data for no/low-Cu steels representative of compositions within the SDB. The MEK model is in good agreement with the data and gives generally better predictions than the EONY model.

In Fig. 2.10, charts (a)–(e) compare the models to the IVAR Laval (LV) plate data for the Cu-bearing steels representative of compositions within the SDB. The compositions of the high-Cu plates (code designations LB, LC, and LD) are essentially the same except for their low (0.2%), medium (0.8%), and high (1.3%) nickel content, respectively. Both models fit the data reasonably well at high nickel, but they both underpredict the low and medium nickel data at low fluence. Note the compositions of the L and CM-series alloys can be found in Chapter 6 of the

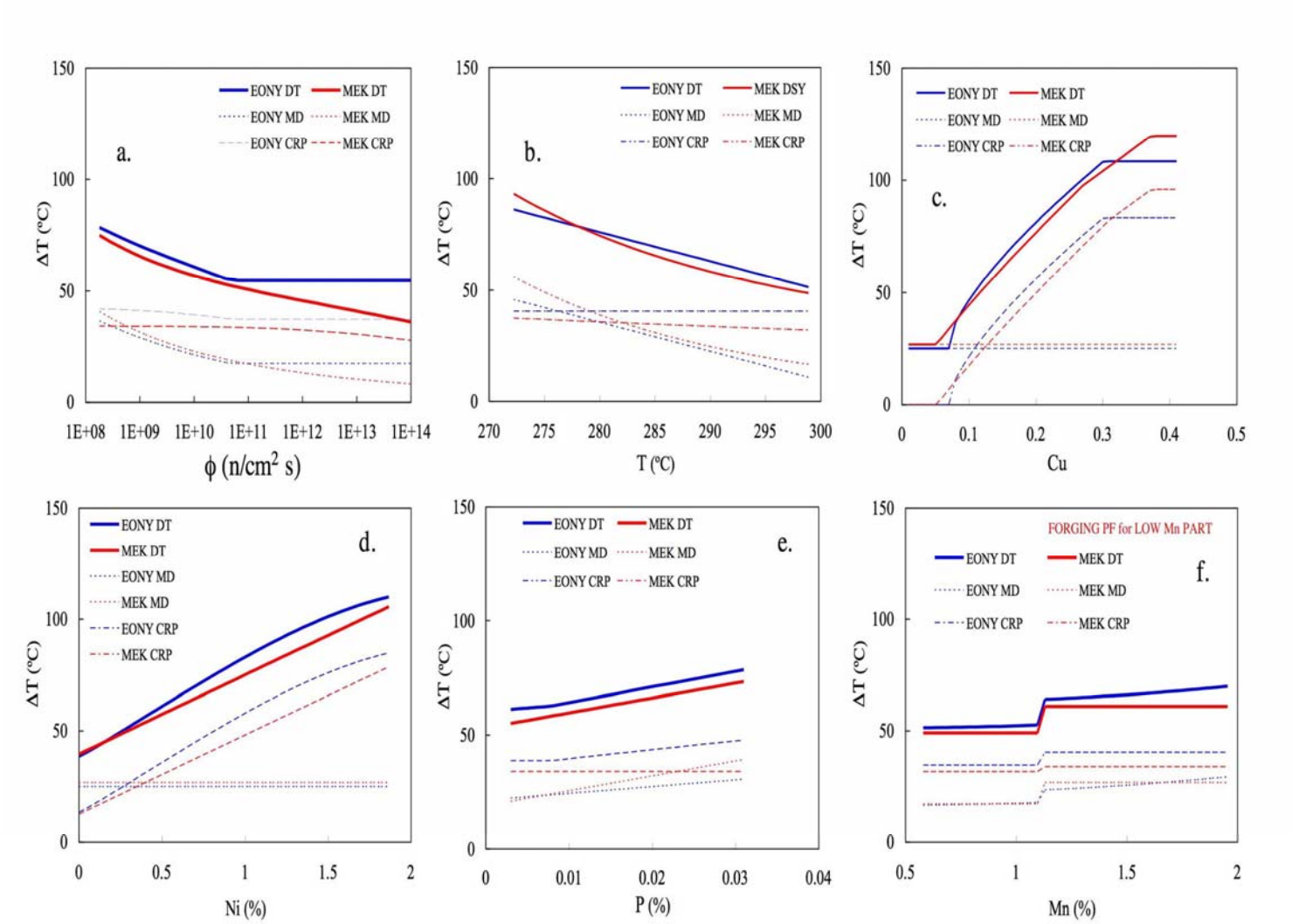

Fig. 2.4. Cross plots for TTS (ΔT) predictions of the MEK and EONY models for the base case composition (see Fig. 2.3) for a wider range of (a) flux, (b) temperature, (c) Cu, (d) Ni, (e) phosphorus, and (f) manganese. Note that for Mn < 1% in (f), the forging product form has been used (see text).

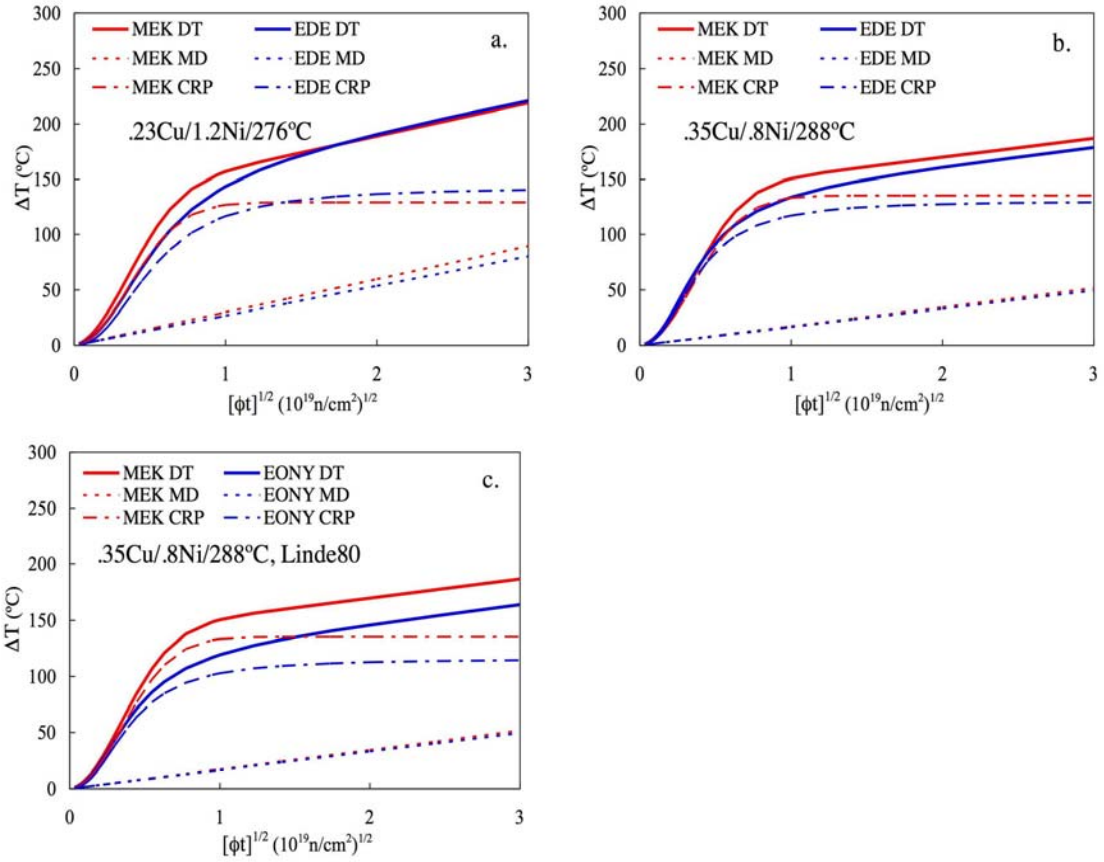

Fig. 2.5. Plots of the MEK and EONY model predictions of the TTS (ΔT) vs sqrt fluence for the sensitive welds (0.23%Cu/1.2%Ni irradiated at 276°C and 0.35%Cu/0.8%Ni at 288°C). The flux in these cases is 3×10^{10} n/cm^2/s, which gives an EOL fluence of 6×10^{19} n/cm^2 in 2×10^9 s (60 EFPY).

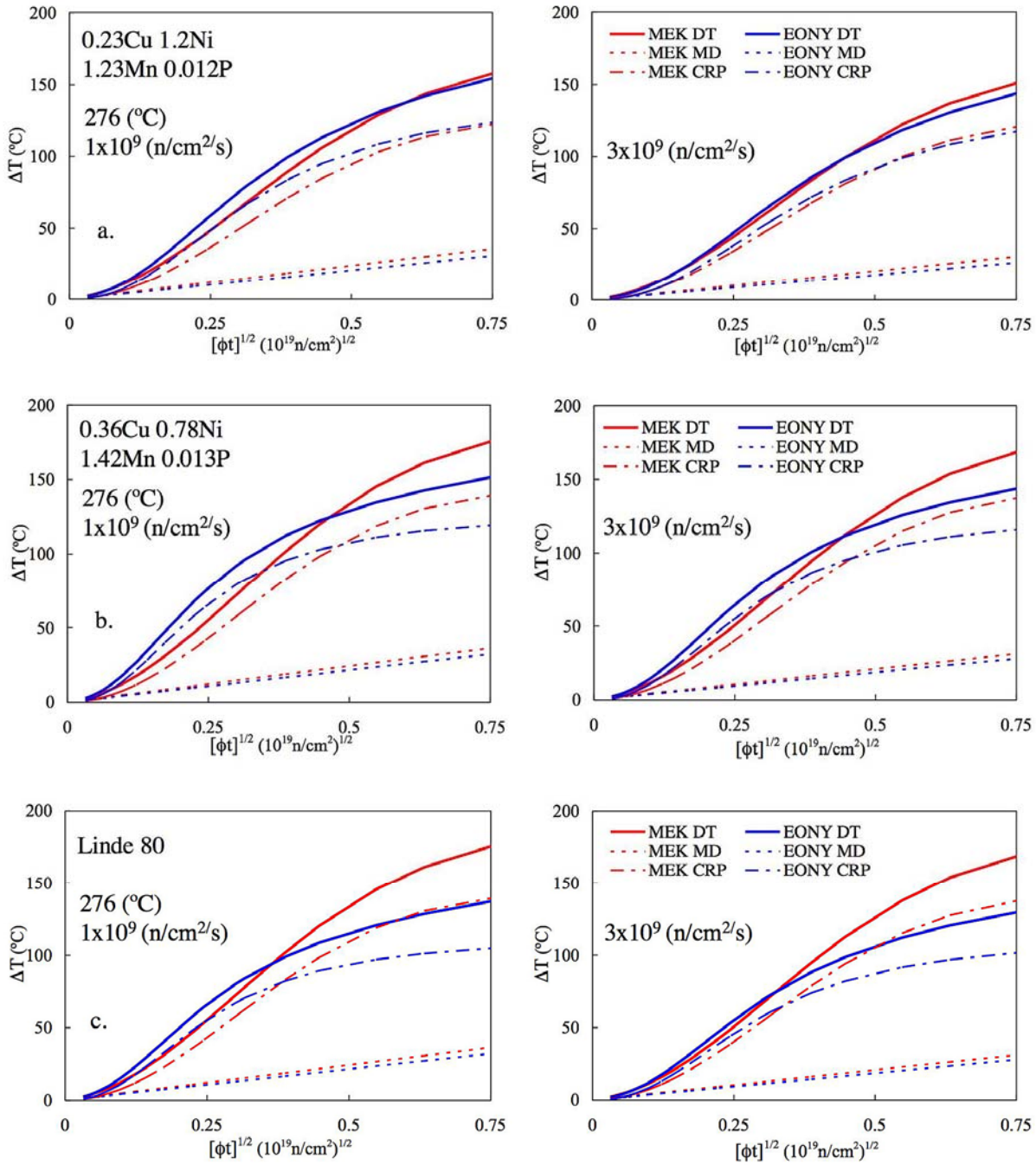

Fig. 2.6. Plots of the MEK and EONY model predictions of the TTS (ΔT) vs sqrt fluence for sensitive welds and for conditions pertinent to BWRs, at nominal fluxes of 1×10^9 and 3×10^9 n/cm^2/s (left- and right-hand plots, respectively) and for an irradiation temperature of 276°C.

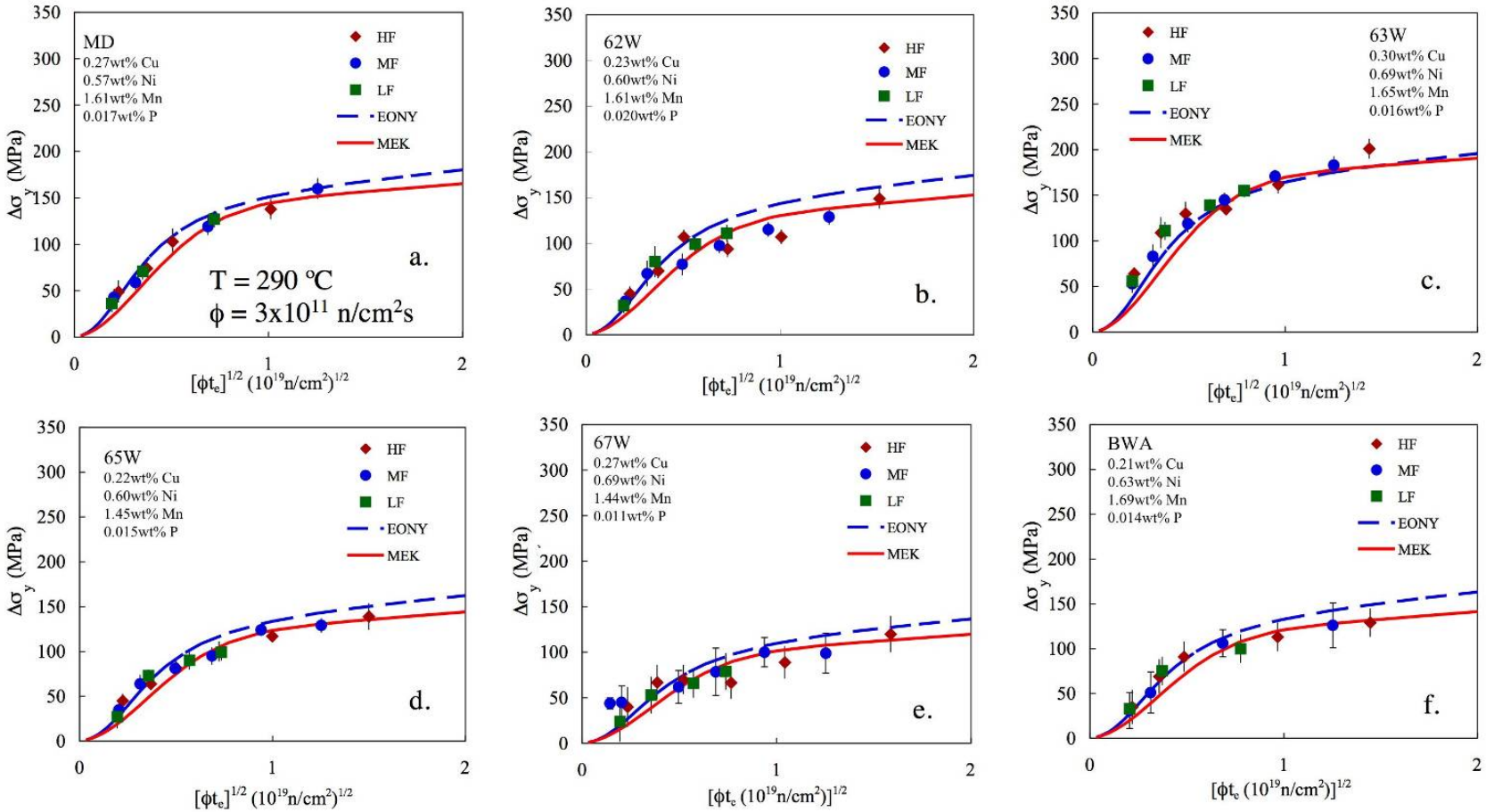

Fig. 2.7. Plots of the MEK and EONY model predictions of $\Delta\sigma_y$ vs the sqrt of fluence compared to data from IVAR at low, medium, and high flux, adjusted to a common flux of 3×10^{11} n/cm^2/s (see text). The materials from left to right and top to bottom are Midland Reactor vessel beltline weld (MD), HSSI Welds 62W, 63W, 65W, and 67W, and the Babcock & Wilcox "A," "B," and "C" welds.

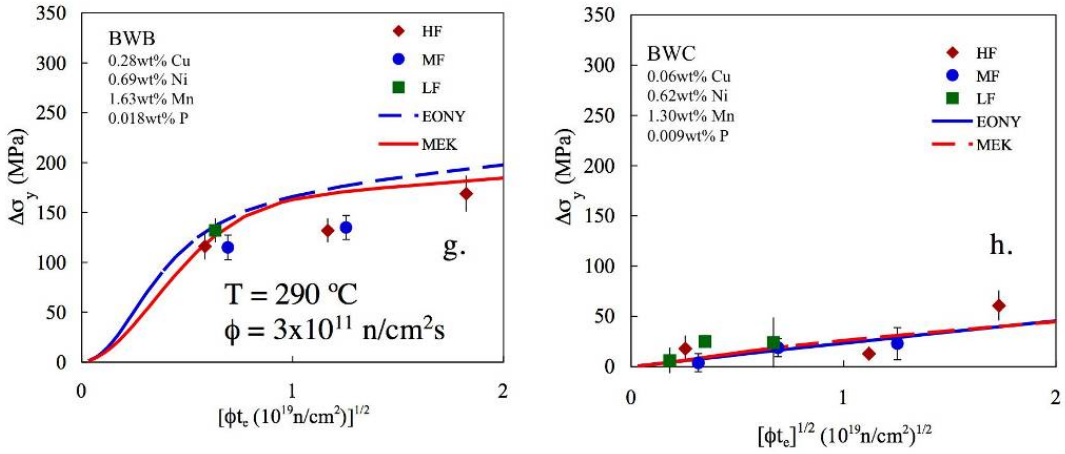

Fig. 2.7. continued

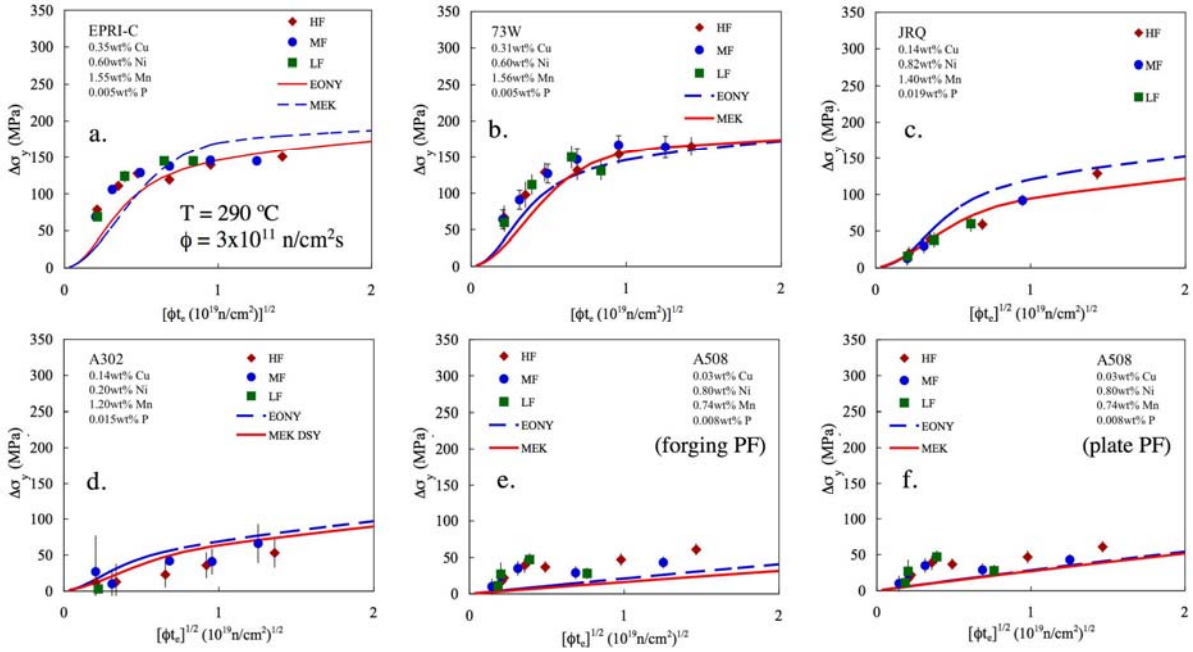

Fig. 2.8. Six plots similar to those in Fig. 2.7 for the A533B-1 plate JRQ (the IAEA reference plate), an EPRI high-copper weld, the high-copper (0.31 wt %) Linde 124 HSSI weld 73W, an A302B plate, and an A508 forging using both forging and plate product forms.

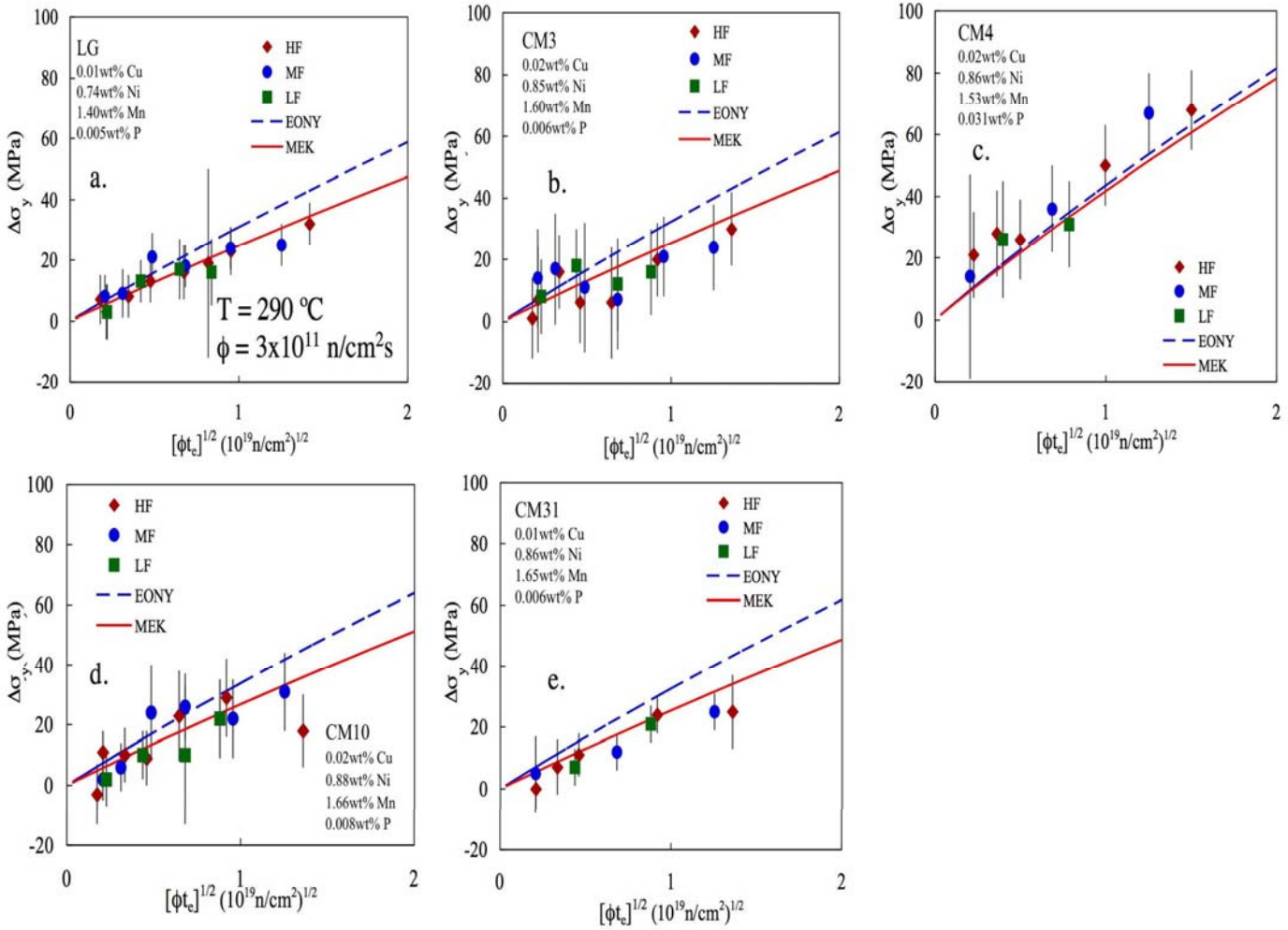

Fig. 2.9. Plots of the MEK and EONY model predictions of $\Delta\sigma_y$ vs the sqrt of fluence compared to plate data from the IVAR for low, medium, and high flux, adjusted to a common flux of 3×10^{11} n/cm^2/s. The data are for low/no Cu steels representative of compositions within the surveillance database.

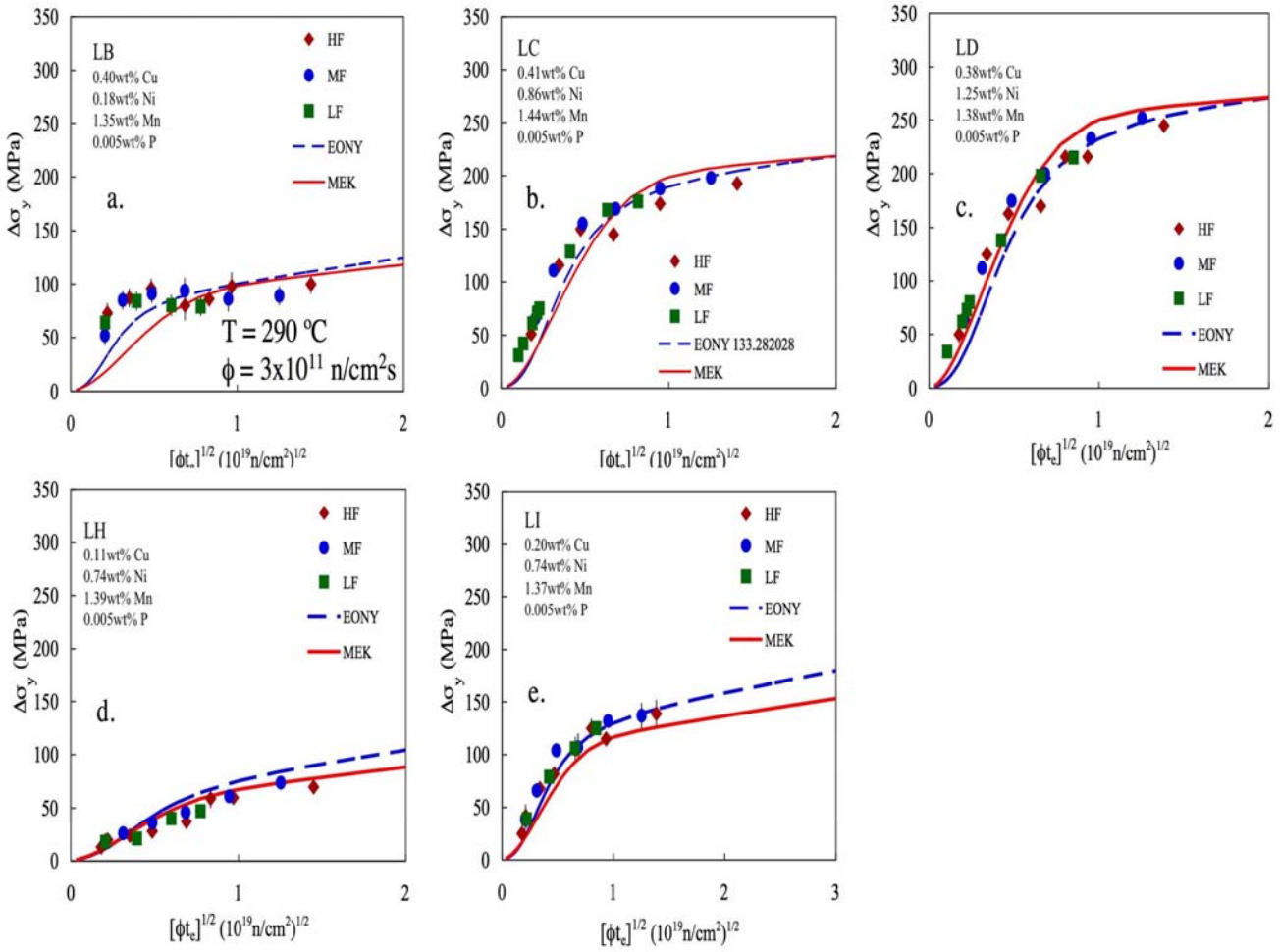

Fig. 2.10. Plots of the MEK and EONY model predictions of $\Delta\sigma_y$ vs the sqrt of fluence compared to plate data from IVAR for low, medium, and high flux, adjusted to a common flux of 3×10^{11} n/cm^2/s. The data are for the Laval (LV series) plate data for Cu-bearing steels representative of compositions within the surveillance database, with high 0.4% Cu and low (0.2%), medium (0.8%), and high (1.2%) Ni contents, as well as for which the medium 0.8% Ni plates with low, (0.1%) medium (0.2%), and high (0.4%) Cu, respectively).

EONY report (Eason 07). The compositions for the medium 0.8%-Ni LH, LI and LC plates are essentially the same, except for their low (0.1%), medium (0.2%) and high (0.4%) copper contents, respectively. The two models provide similar fits to the data, the EONY $\Delta\sigma_y$ being generally slightly higher than that for the MEK model.In Fig. 2.11, charts (a)–(e) compare the models to the IVAR CM plate data for the Cu-bearing steels for compositions within the SDB. The $\Delta\sigma_y$ values for the CM11 steel with 0.3% Cu are almost identical to those for CM19 (0.4% Cu), indicating a saturation in the effect of copper. Chart (e) in Fig. 2.11 shows that both models overpredict the $\Delta\sigma_y$ for the lower Mn IVAR steel CM22.

In Fig. 2.12, charts (a)–(c) cross plot IVAR data as a function of Cu, Ni, and Mn at two fluences. In the case of Mn < 1 wt % (see Fig. 2.12 [c]) the forging PF is used for both models. The Cu_{max} in the EONY model is 0.3%. Both models predict the observed $\Delta\sigma_y$ trends with Cu and Ni. Overall, the EONY model shows slightly better agreement with the high-fluence $\Delta\sigma_y$ data.

In Fig. 2.13, charts (a)–(d) compare the optimized models to cross plots of the IVAR data for low-Cu IVAR plates. The obvious effects of Ni and Mn in the $\Delta\sigma_y$ data are not reflected in either model, although the effects may be captured in the product form in the case of Mn (i.e., plate vs forging). Overall, the MEK model is in better agreement with the low-Cu IVAR data.

The two optimized model $\Delta\sigma_y$ predictions to IVAR data at irradiation temperatures from 270 to 310°C are compared in Figs. 2.14–2.16. In Fig. 2.14, charts (a)–(d) compare the irradiation temperature dependence of the IVAR data to the optimized models at two fluences for three

Linde 80 welds (HSSI welds 62W, 63W, and 65W), two B&W Linde 80 welds (BWA and BWC), and the A302B plate. While the predictions are similar overall, the EONY model is somewhat more conservative than the MEK model, which is in better agreement with the IVAR data. The exception is that both models significantly overpredict the $\Delta\sigma_y$ data at 270°C for the low-Cu BWC weld and A302B plate.

Charts (a) and (b) in Fig. 2.15 show similar plots for medium-Ni LV series alloys LH, LI, and LC, which have nominal Cu contents of 0.1, 0.2, and 0.4 %, respectively. In Fig. 2.15, charts (c) and (d) show the corresponding plots for high-Cu alloys with 0.2, 0.8, and 1.3% Ni. Again, the $\Delta\sigma_y$ MEK model predictions are in better agreement with the $\Delta\sigma_y$ data. Both models underpredict the $\Delta\sigma_y$ at 270°C for the LI alloy (0.8% Ni, 0.2% Cu).

In Fig. 2.16, charts (a) and (b) show similar plots for low-Cu (≤ 0.05 wt %) IVAR steels. Unlike the higher-Cu alloys, the predicted temperature dependence of $\Delta\sigma_y$ is greater than those observed in the IVAR data for both models. However, the MEK model is again in somewhat better agreement with the data.

In Figs. 2.17 and 2.18, the EONY, MEK, and combined MEK-RADAMO models are compared to a number of datasets from the SDB in selected cases for which there are at least four TTS values. In Fig. 2.17, charts (a)–(g) compare the models with PWR datasets from the SDB that include TTS at high fluence ($> 4 \times 10^{19}$ n/cm^2). Some of the data fall systematically high and some systematically low, while the predictions of the EONY and MEK models are generally in good agreement in most cases. The systematic high and low variations may be due to the uncertainty in the unirradiated TTS value and/or a combination of the chemistry factor and product form uncertainties. More generally, there is no sudden change in the fluence dependence in the observed TTS or any indication of a major breakdown in the MEK and EONY models within the observed fluence range. Charts (a)–(h) in Fig. 2.18 show multiple fluence data for a

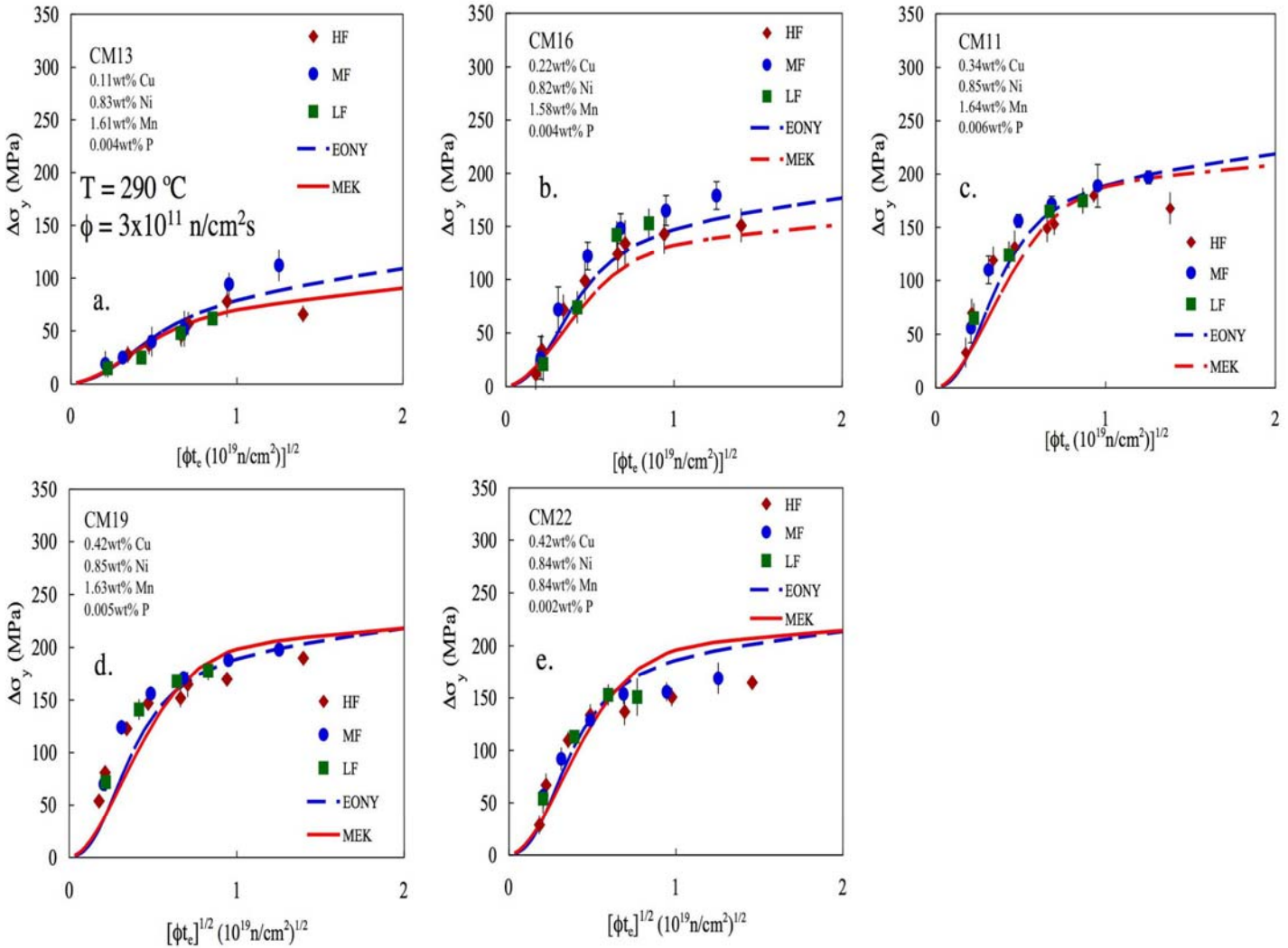

Fig. 2.11. Plots of the MEK and EONY model predictions of $\Delta\sigma_y$ vs the sqrt of fluence compared to plate data from IVAR for low, medium, and high flux, adjusted to a common flux of 3×10^{11} n/cm^2/s. The data are for the CM-series plate data for Cu-bearing steels representative of compositions within the surveillance database for medium 0.8% Ni and 1.6% Mn with (0.1%), medium (0.2%), and high (0.4%) Cu. A comparison is also shown for a steels with 0.8% Ni and 0.4% Cu with 0.8% and 1.6% Mn.

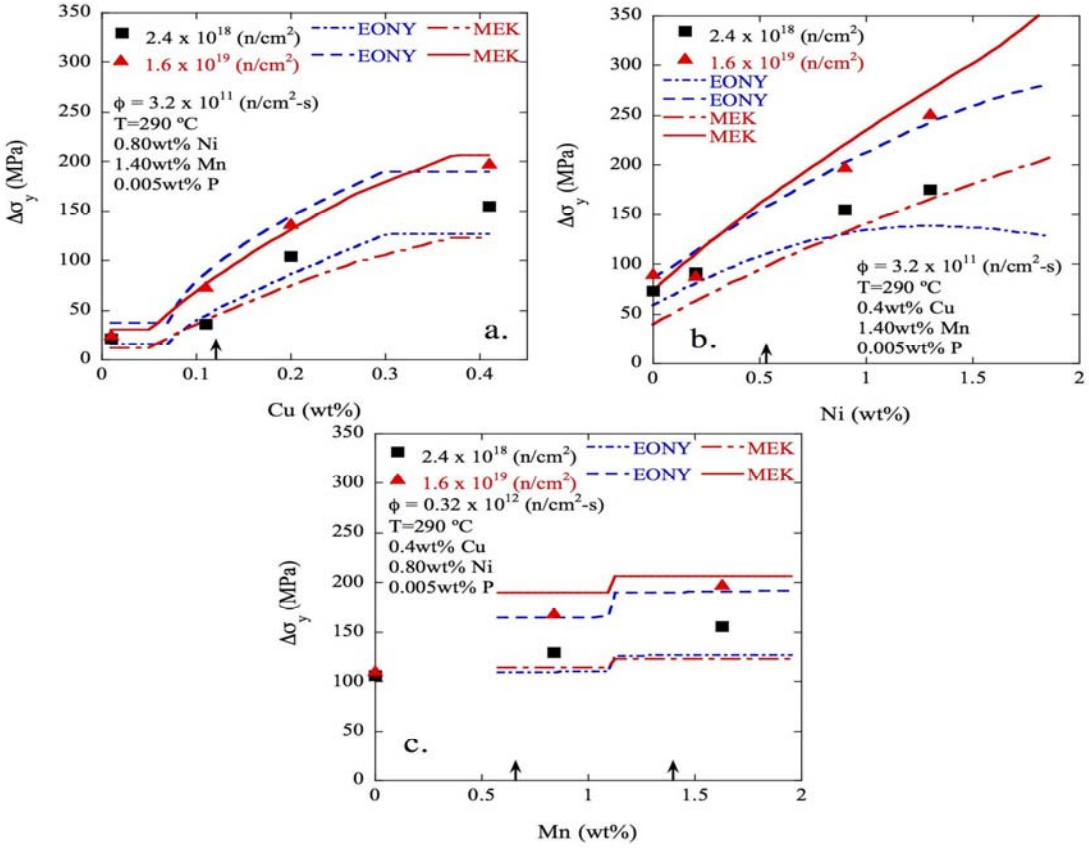

Fig. 2.12. Cross-plots (a-c) compare the MEK and EONY model predictions of $\Delta\sigma_y$ to IVAR data for alloys at two fluences, showing the effects of Cu (0.8% Ni, 1.6% Mn), Ni (1.6% Mn, 0.4% Cu), and Mn (0.8% Ni, 0.4% Cu). In cases with Mn < 1% in (c), the forging product form was used in both models.

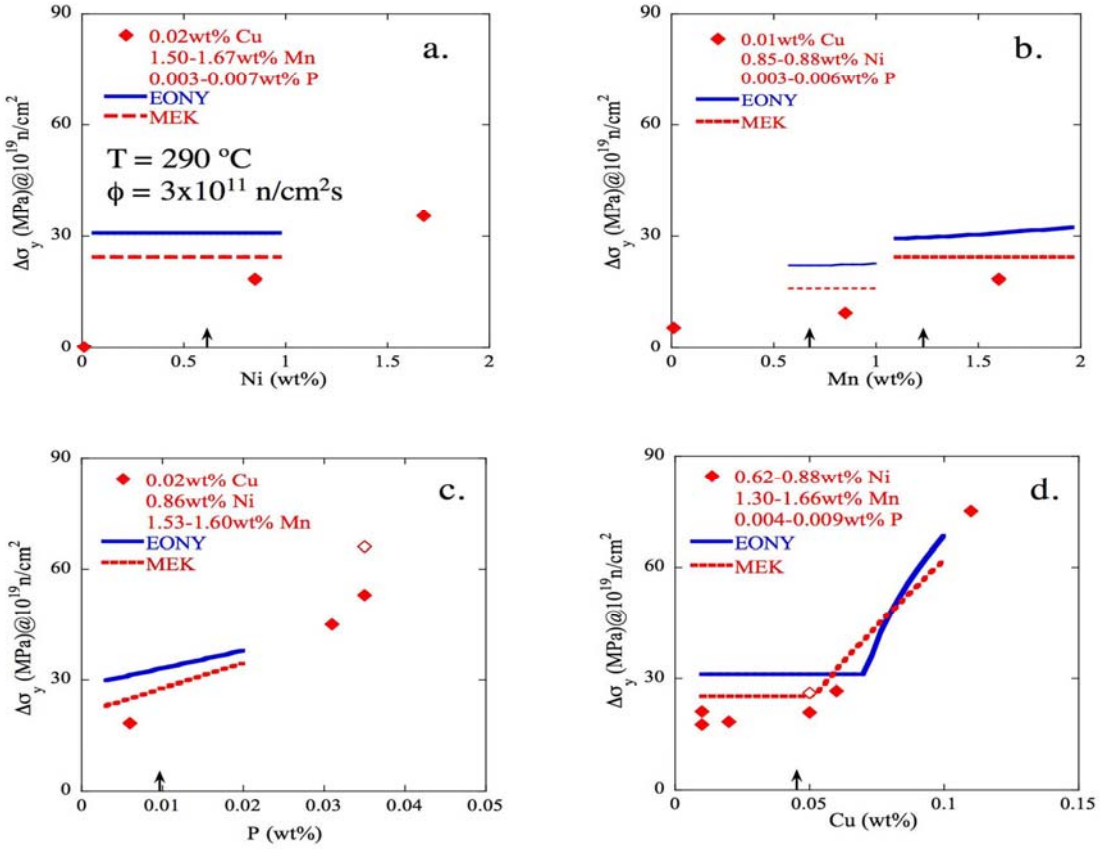

Fig. 2.13. Cross-plots (a-c) compare the MEK and EONY model predictions of $\Delta\sigma_y$ to IVAR data for low-no Cu alloys at two fluences, showing the effects of Ni (1.6% Mn and 0.005% P), Mn (0.4% Cu and 0.005% P) and P (0.8% Ni). In cases with Mn < 1% in (c), the forging product form was used in both models. The cross plot (d) shows the effect of Cu (0.8% Ni and 0.005% P).

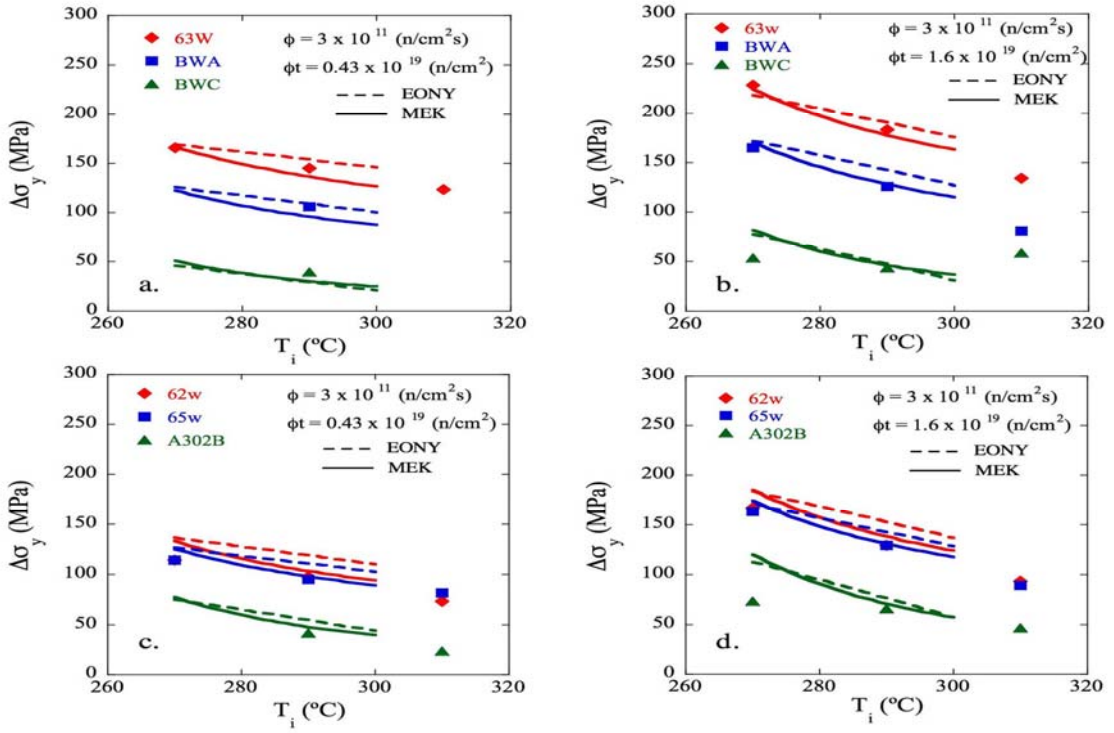

Alloy	Cu	Ni	Mn	P
63W	0.3	0.69	1.65	0.016
BWA	0.21	0.63	1.69	0.014
BWC	0.06	0.62	1.30	0.009

Alloy	Cu	Ni	Mn	P
62W	0.23	0.60	1.61	0.020
65W	0.22	0.60	1.45	0.015
A302B	0.14	0.20	1.20	0.015

Fig. 2.14. Comparisons of the MEK and EONY model predictions of the temperature dependence of $\Delta\sigma_y$ (from 270 to 310°C) at two fluences (0.43 and 1.6 × 10^{19} n/cm^2) to IVAR data for three Linde 80 welds, two B&W welds, and the A302B plate.

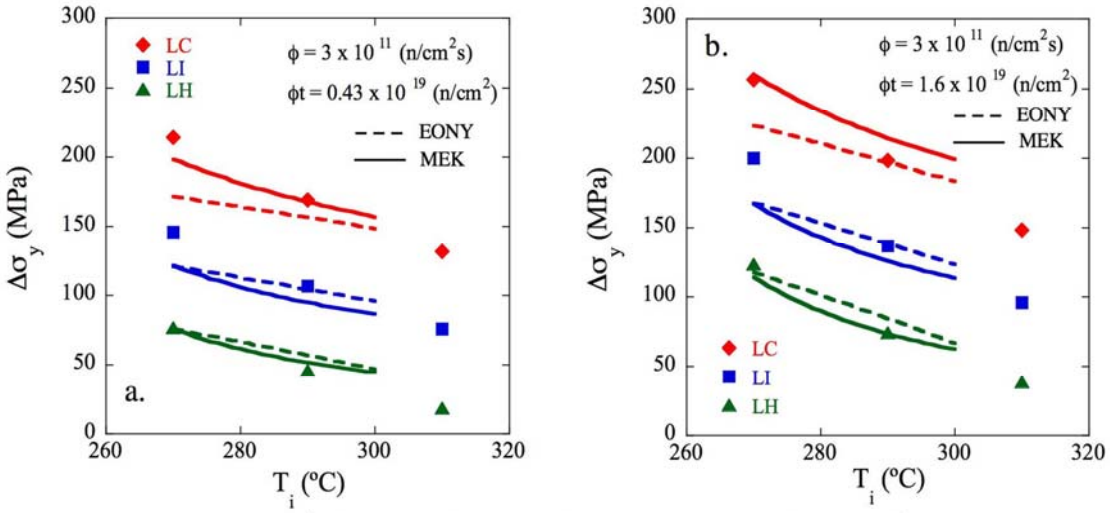

Alloy	Cu	Ni	Mn	P
LH	0.11	0.74	1.39	< 0.005
LI	0.20	0.74	1.37	< 0.005
LC	0.41	0.86	1.44	< 0.005

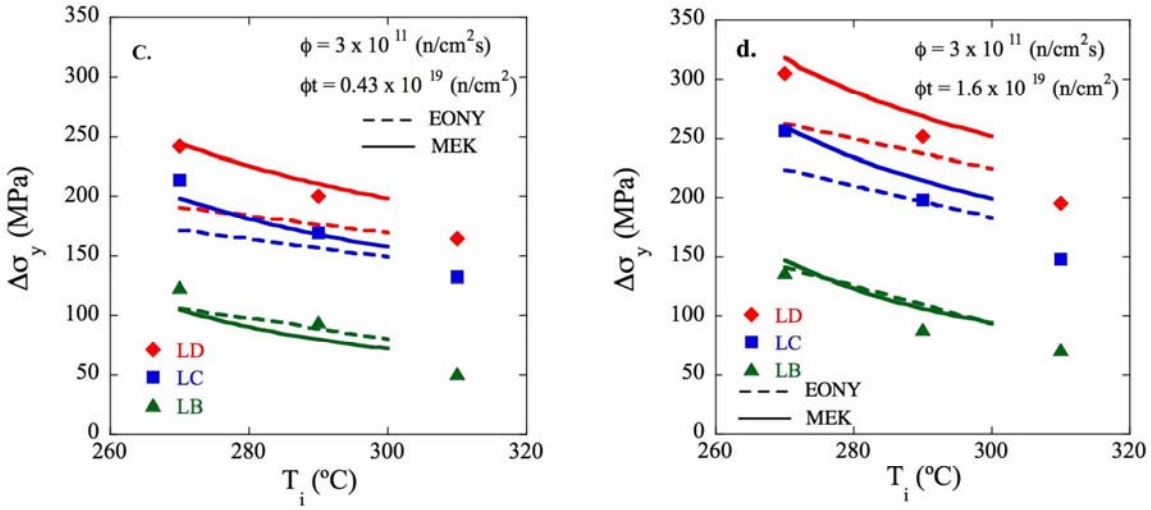

Alloy	Cu	Ni	Mn	P
LB	0.40	0.18	1.35	< 0.005
LC	0.41	0.86	1.44	< 0.005
LD	0.38	1.25	1.38	< 0.005

Fig. 2.15. Comparisons of the MEK and EONY model predictions of the temperature dependence of $\Delta\sigma_y$ (from 270 to 310°C) at two fluences (0.43 and 1.6 × 10^{19} n/cm^2) to IVAR data for three medium Ni (0.8 wt %) IVAR steels (LV series) with Cu contents of 0.1, 0.2, and 0.4 %, and for high 0.4% Cu alloys with Ni contents of 0.2, 0.8, and 1.3%.

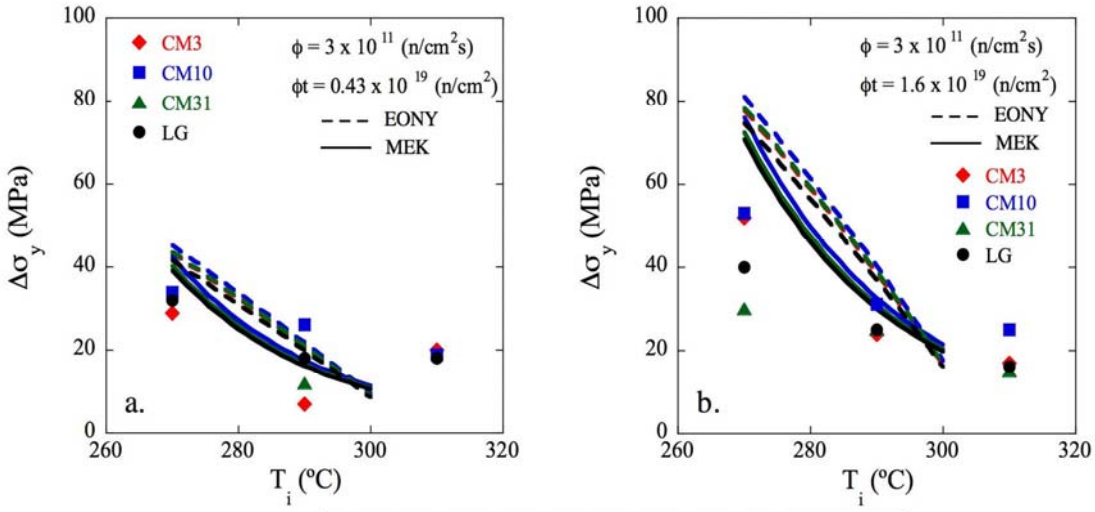

Alloy	Cu	Ni	Mn	P
CM3	0.02	0.85	1.60	0.006
CM10	0.02	0.88	1.66	0.008
CM31	0.01	0.86	1.65	0.006
LG	0.00	0.74	1.37	< 0.005

Fig. 2.16. Comparisons of the MEK and EONY model predictions of the temperature dependence of $\Delta\sigma_y$ (from 270 to 310°C) at two fluences (0.43 and 1.6 × 10^{19} n/cm^2) to IVAR data for four IVAR low (<0.07%) Cu, medium (0.8%) Ni steels.

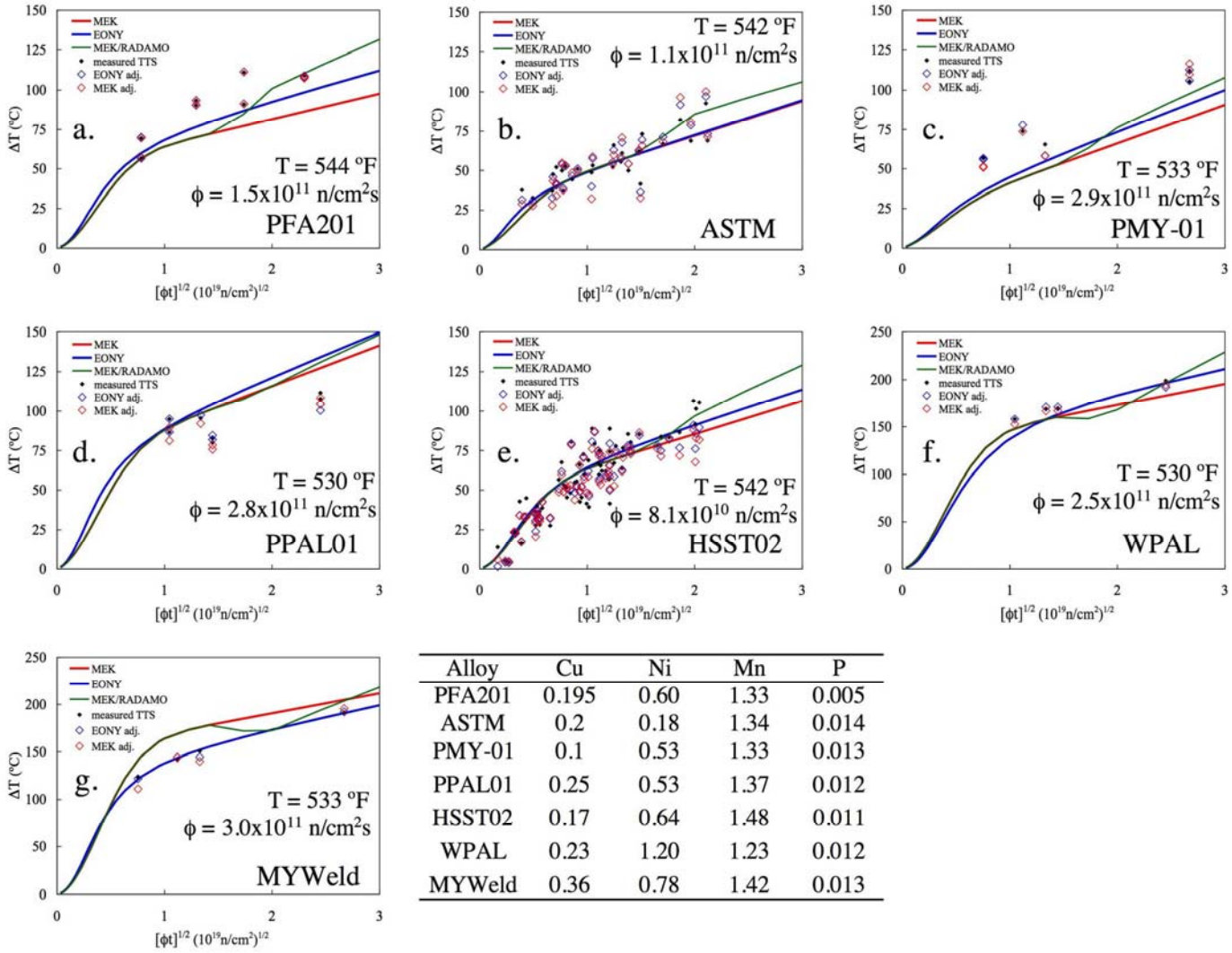

Alloy	Cu	Ni	Mn	P
PFA201	0.195	0.60	1.33	0.005
ASTM	0.2	0.18	1.34	0.014
PMY-01	0.1	0.53	1.33	0.013
PPAL01	0.25	0.53	1.37	0.012
HSST02	0.17	0.64	1.48	0.011
WPAL	0.23	1.20	1.23	0.012
MYWeld	0.36	0.78	1.42	0.013

Fig. 2.17. Comparisons of the MEK, EONY, and combined MEK/RADAMO model predictions of TTS (ΔT) vs the sqrt fluence to data for PWR heats from the SDB at several fluences up to > 4 × 10^{19} n/cm^2/s. The filled symbols are the measured data and the open symbols have been adjusted by the model to the average nominal flux and temperature shown in the figures. The table shows the alloy compositions.

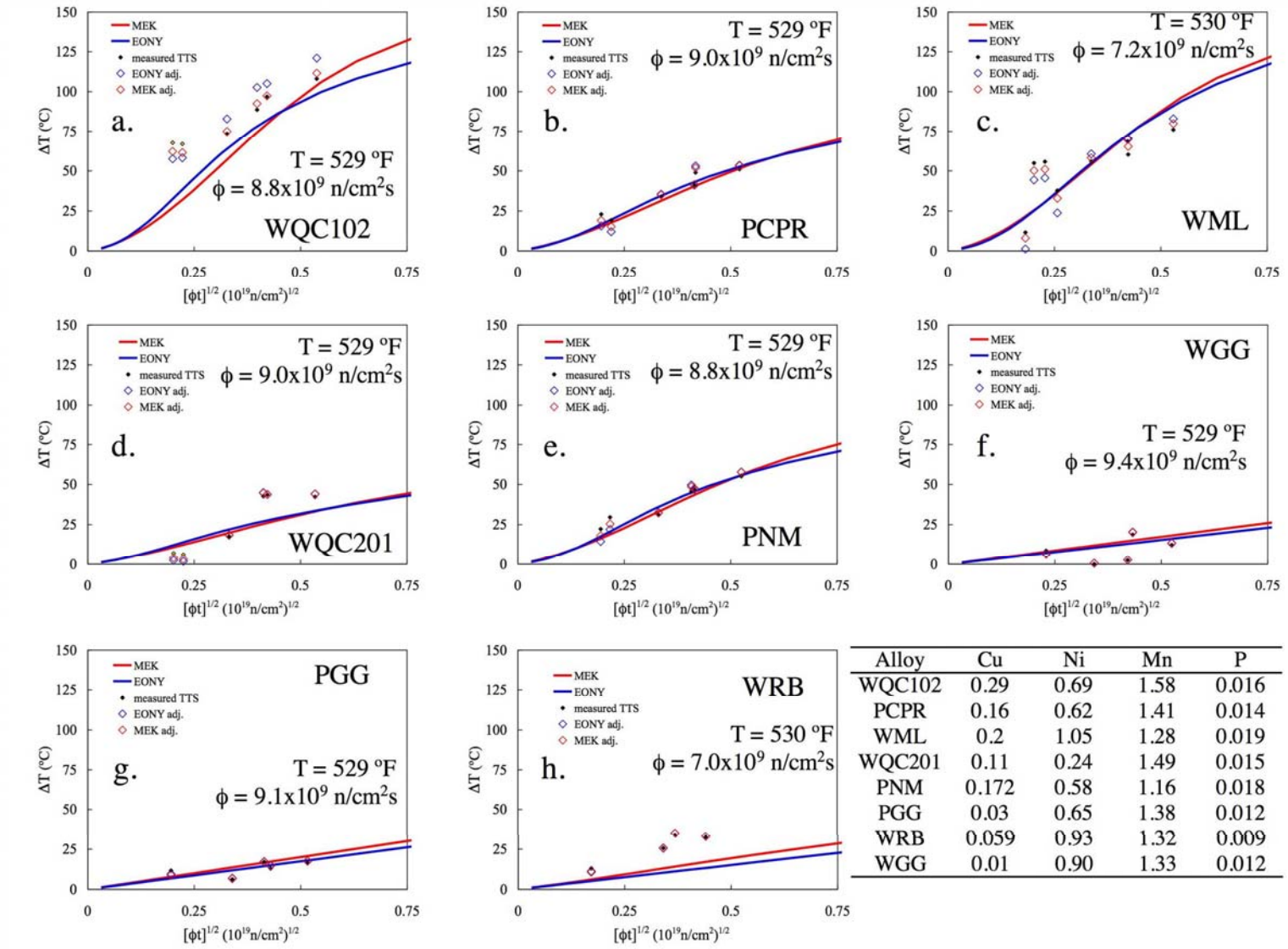

Alloy	Cu	Ni	Mn	P
WQC102	0.29	0.69	1.58	0.016
PCPR	0.16	0.62	1.41	0.014
WML	0.2	1.05	1.28	0.019
WQC201	0.11	0.24	1.49	0.015
PNM	0.172	0.58	1.16	0.018
PGG	0.03	0.65	1.38	0.012
WRB	0.059	0.93	1.32	0.009
WGG	0.01	0.90	1.33	0.012

Fig. 2.18. Comparisons of the MEK and EONY model predictions of TTS (ΔT) vs the sqrt fluence to data for BWR heats from the SDB at several fluences. The filled symbols are the measured data and the open symbols have been adjusted by the model to the average nominal flux and temperature shown in the figures. The table shows the alloy compositions.

number of boiling water reactor (BWR) alloys for low-flux surveillance irradiations. The predictions are in good agreement with the TTS data except for the welds with code designations of WQC102, WQC201, and WRB.2.4 Summary of the MEK and EONY Model Comparisons.

As shown in Fig. 2.1, there are differences in the predictions of the EONY and MEK models even after they have been optimized, although the differences are less than those for the base models. The differences depend on the combination of all the independent variables in the models. An extensive analysis does not suggest that one model is generally better than the other, so we have no clear recommendation as to which one to pick for possible use in RTG 1.99-3. The EONY model has slightly better statistical fit parameters and provides slightly better predictions of the highest fluence data for sensitive welds. The MEK model is in better agreement with the low-Cu IVAR data. The MEK model is also more consistent regarding flux effects and the temperature dependence of irradiation hardening found in the IVAR database. The EONY model may be slightly more conservative for Combustion Engineering (CE) plates but less conservative for high-Cu (> 0.3% Cu) welds in general and Linde 80 welds in particular. The variations in the TTS prediction reflects the major differences in the models that lie in the treatments of product forms and maximum effective Cu contents.

We also note that our analysis did not consider changes to the model variables or form of the model equations. We believe that further research might result in improvements over both models, especially as guided by insight from the IVAR database.

We recommend strongly that the results of the evaluations of the two models be reviewed by a professional statistician. Figure 2.19 provides a specific example of our concerns, where the residuals for the Linde 80 welds are compared for the MEK (a) and EONY (b) models. The residuals for the EONY model are reasonably well centered about zero, whereas there is a clear trend toward overprediction of the TTS by the MEK model at higher Cu content that may or may not be statistically significant. This is not surprising because the MEK model does not have a product form specific Cu_{max} (perhaps it should). The overall residual fit line is not very meaningful in this case because MEK model residuals are well centered up to a Cu content between 0.25 (the approximate limit for the EONY model) and 0.3%. However, there is a much more obvious and significant bias in the MEK residuals at Cu contents greater than 0.3%. Thus, we believe that a better procedure would be to evaluate the statistical significance of differences in the mean residuals above and below an optimized $Cu_{max} \approx 0.25–0.3\%$. The EONY model may have a slight bias in underpredicting the TTS at high Cu. Given these complexities we do simply not have the expertise to exercise a statistical judgment on such matters. We do note, however, that there is significant independent evidence that Cu_{max} is 0.3% or less in low to medium steels that have been stress relieved at about 600°C due to pre-precipitation of Cu. However, if the MEK model is revised to allow a specific Cu_{max} for Linde 80 weld, then it must be fully reoptimized.

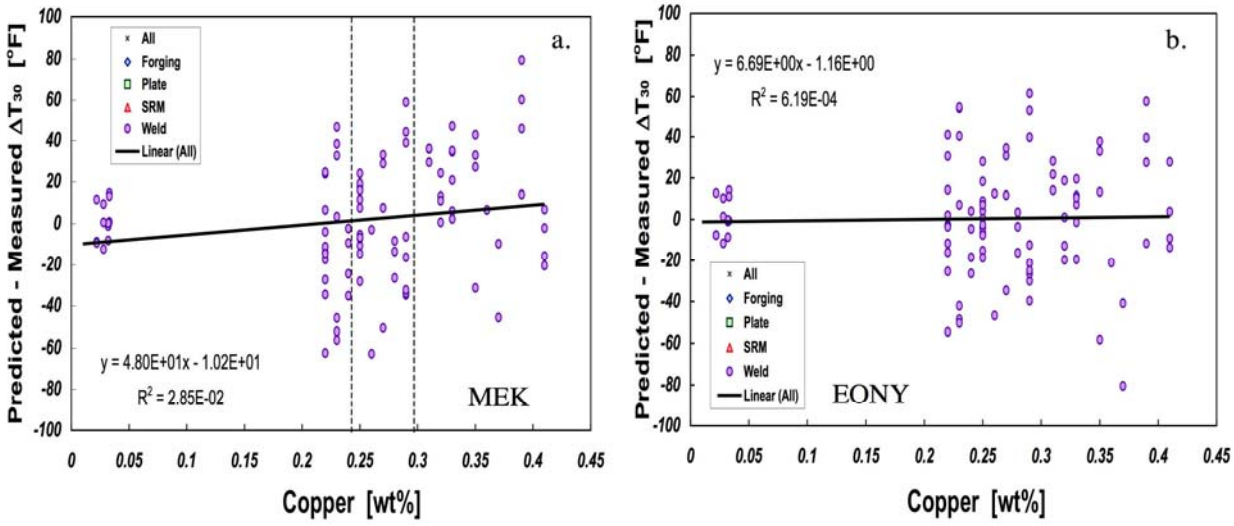

Fig. 2.19. Residuals for the Linde 80 welds comparing the (a) MEK and (b) EONY models. The residuals for the EONY model are reasonably well centered about zero, while there is a clear trend toward overprediction of the TTS by the MEK model at higher Cu content that may or may or not be statistically significant.

3. FLUX EFFECTS AND USE OF THE RADAMO DATA AND MODEL

In this chapter, we discuss dose rate (flux) effects (DRE), including a summary of the basic mechanisms, and especially the effects of high flux at high fluence, and use of the RADAMO model. In support of this analysis we develop a three-feature TTS (3FTTS) model and apply it to analyzing the RADAMO database.

3.1 Dose Rate Effects and Modeling the High-Flux Database

An overview of the mechanisms of irradiation embrittlement of RPV steels is given in Chap. 2 of the EONY report (Eason 07). Briefly, radiation-induced property changes are driven by the excess point defect (vacancy and self interstitial atom [SIA]) fluxes created by displacive irradiation, and the nature of the microstructural evolution that occurs is primarily determined by the kinetics governing the transport and fate of the mobile defects and solute atoms. Flux effects (or DRE) in irradiated materials arises primarily for two reasons: (1) the competition between formation and dissolution of defects that are thermally unstable at the irradiation temperature over irradiation time scales and (2) the influence of the displacement rate on radiation-enhanced solute diffusion (RED) and solute-defect clustering. The effect of variations in dose rate in the low-flux regime, pertinent to SDB and IVAR conditions, is recognized in both the EONY and MEK models. In the low-flux regime the effect of dose rate is believed to be primarily due to solute trap enhanced recombination (SER) of vacancies and SIA (Eason 07, Odette 05). Higher rates of recombination lead to lower rates of RED, thus delaying the CRP contribution to hardening and embrittlement. As discussed in detail elsewhere (Eason 07, Odette 05), the DRE can be approximately described in terms of an effective fluence, ϕt_{eff}, as

$$\phi t_{eff} = \phi t(\phi_r/\phi)^p \qquad (1)$$

Here ϕ_r is a specified reference flux. The DRE scaling exponent *p* depends on the flux, temperature, alloy composition and microstructure, and has a limiting value of 0.5 in the recombination-dominated regime (Eason 07, Odette 05). The SER mechanism diminishes in significance with decreasing flux and is judged to be of only modest importance below about 10^{10} n/cm^2-s. However, thermal diffusion of Cu and other solutes must be considered in this dose rate regime, and *p* may approach 1 at very low flux. The DREs due to thermal diffusion increase at higher temperatures, while the SER decreases.

The DRE expressed by Eq. (1) has been included, either explicitly or implicitly, in treating the CRP term in most classical two-defect CRP plus MD models of hardening and embrittlement (Eason 07, Odette 05, Eason 98, Odette 03, Fisher 88, Williams 02, Carter 02, EricksonKirk 07). The most notable new result in the recent EONY (Eason 07) and MEK RM-9 model fits to the surveillance database is that MDs also appear to be affected by dose rate. The independent data supporting this conclusion is mixed, but a careful analysis of the IVAR database discussed in Chap. 6 of ORNL/TM-2006/530 (Eason 07) revealed a similar behavior. The possibility of a DRE on MD hardening and embrittlement was anticipated in a report summarizing the results of an EPRI sponsored meeting on flux effects(Carter 02), where it was noted that, to the extent that MDs are affected by RED, they will also be affected by dose rate. This conclusion is also consistent with the growing recognition that a continuum of nanoscale MD and precipitate hardening features are formed in irradiated RPV steels that are composed of varying point defect

and solute contents (Eason 07)[3]. Further details on the DRE at low flux can be found elsewhere (Odette 94, Eason 07, Odette 05).

Previous research has also shown that there is another higher-flux regime of DRE found in test reactor irradiations, due to the formation of unstable matrix defects (UMDs) that continuously form and dissolve (anneal) under irradiation (Odette 94, Mader 95, Wirth 01, Odette 98a, Wirth 98, Odette 90). The research by Mader, Odette, and co-workers showed that UMDs play two roles (Odette 94, Mader 95). First, the UMDs directly contribute to irradiation hardening and embrittlement. However, the UMDs also act as defect sinks that destroy vacancies, thereby decreasing the rate of RED. The effect of decreased RED is to delay (shift to higher fluence) the CRP and, presumably, MD contributions to hardening and embrittlement. The p in Eq. (1) also approaches 1 in the UMD sink-dominated regime. *As a result of the dual role played by UMDs, increasing flux can increase, decrease, or leave unaffected hardening and embrittlement, depending on the alloy composition, irradiation temperature, flux, and fluence.*

Mader and Odette estimated the balance of the various hardening features empirically based on postirradiation annealing (PIA) microhardness (ΔH) recovery measurements (Odette 94, Mader 95). The underlying principle is that each of the three types (UMDs, MDs or stable matrix defects [SMDs], and CRPs) of hardening features has a reasonably unique temperature (T_a)-time (t_a) thermal annealing signature. The UMDs are the least thermally stable and can recover in situ over the times characteristic of a high-flux irradiation. At sufficiently high fluence the UMDs reach a steady-state concentration that varies in proportion to the flux. Stable matrix defects are hardening features that accumulate in rough proportion to fluence in both low-Cu and Cu-bearing alloys. SMDs do not recover under irradiation but do anneal to some extent at temperatures about 50°C higher than the nominal irradiation temperature of 290°C. The CRPs are much more thermally stable than either UMDs or SMDs and require annealing temperatures above about 400°C for significant recovery in periods less than several hundred hours.

Very extensive annealing studies (Odette 94, Mader 95) led to estimates of the UMD recovery times, $\tau_{umd} \approx 3.25 \times 10^5$ s (150 h) and $\tau_{umd} \approx 1.8 \times 10^4$ s (5 h) at 290°C and 343°C, respectively. These values are consistent with theoretical estimates of the time for the dissolution of a small vacancy-solute cluster complex (Mader 95). The formal definitions used in the Mader and Odette studies to experimentally determine ΔH_{umd}, ΔH_{smd}, and ΔH_{crp} are shown in Table 3.1 and are schematically illustrated in Fig. 3.1. Here the ΔH_a and ΔH_r are the decrease in microhardness at the specified annealing conditions, and the residual hardening in very low Cu steels at 343°C and 150 h (3.25×10^5 s), respectively. The effects of variables such as Ni, irradiation temperature, flux, and fluence on the hardening contributions of the UMDs, MDs and CRPs were estimated by the PIA measurements on specimens with corresponding variations in composition or irradiation condition.

Table 3.1. Procedure used to define the UMD, MD and CRP contributions to the total irradiation hardening

Feature ΔH	T_a,t_a Definition of the ΔH Feature Contribution
ΔH_{umd}	$-\Delta H_a$(343°C,5h) and $-\Delta H_a$(290°C,150h)
$\Delta H_{smd(md)}$	$-\Delta H_a$(343°C,150h) + ΔH_r(343°C,150h, low Cu) - ΔH_{umd}
ΔH_{crp}	$-\Delta H_r$(343°C,150h) + ΔH_r(343°C,150h, low Cu)

[3] Presentations by an author (G. R. Odette) at IGRDM12 and IGRDM13 as well as the 23rd International Symposium on the Effects of Radiation on Materials in June 2006 discussed the evidence for the continuity of the hardening features in detail.

The effect of flux is most pertinent to this discussion because the number density of UMDs (N_{umd}) scales in direct proportion to dose rate and the hardening scales in proportion to the square root of their number density.

The effect of flux on the balance of hardening contributions is illustrated in Fig. 3.2, which shows the recovery of microhardness as a function of time for 343°C anneals of Cu-bearing steels irradiated at different dose rates (Odette 94, Mader 95). Clearly, the recovery for the high-flux irradiations at 343°C and 1.8×10^4 s (5 h) is much larger than for the corresponding low-flux irradiations. Figure 3.3 plots the individual and combined contributions of CRP, MD (SMD), and UMD that were empirically estimated for the high ≈ 0.3% Cu alloys, based on their respective low-temperature 290 and 343°C thermal annealing signatures, as described above. Figure 3.3 shows that the CRP and MD (SMD) terms decrease with increasing flux, while the UMD increases. Notably, while the balance of defects changes, *the overall hardening is relatively insensitive to flux*. The UMD contribution to hardening also increases with decreasing temperature and increasing Ni, and, by inference, Mn and Cu content. At that time, the UMDs were believed to be small 5-30 vacancy clusters complexed with solutes, which increases their thermal stability and effectiveness as strengthening features. While positron annihilation studies have subsequently shown that such Cu-coated microvoids are indeed present in simple Fe-Cu model alloys, in complex steels (and even simple Fe-Mn model alloys) the UMD and MD features are not associated with clusters containing a significant number of vacancies (Glade 04, 05, 06).

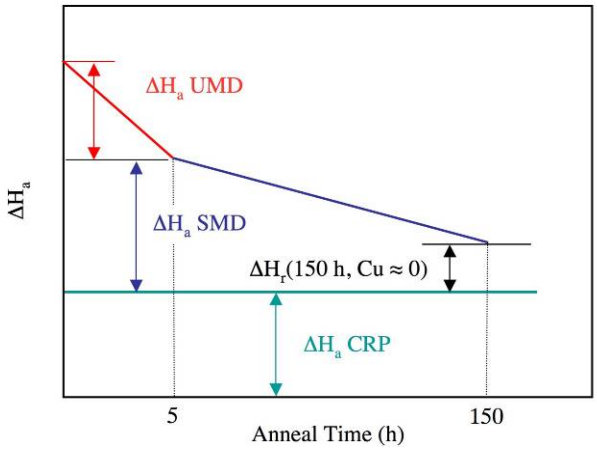

Fig. 3.1. Schematic illustration of the annealing signature procedure used to define the UMD, MD (SMD) and CRP hardening contributions (see Table 3.1).

This three-feature description of irradiation hardening and embrittlement is powerful but certainly approximate. In reality, there is not a sharp delineation between UMDs, MD/SMDs, and CRPs. Such features also implicitly interact with one another by mechanisms such as competition for finite numbers of solute atoms and excluded volume effects. Nevertheless, as shown in Fig. 3.3, it is possible to independently approximate the balance of hardening from those features as a function of flux. The three-feature concept described above was used by Mader and Odette in developing very successful PIA models. However, that concept can also be used to quantitatively model dose rate effects at high flux.

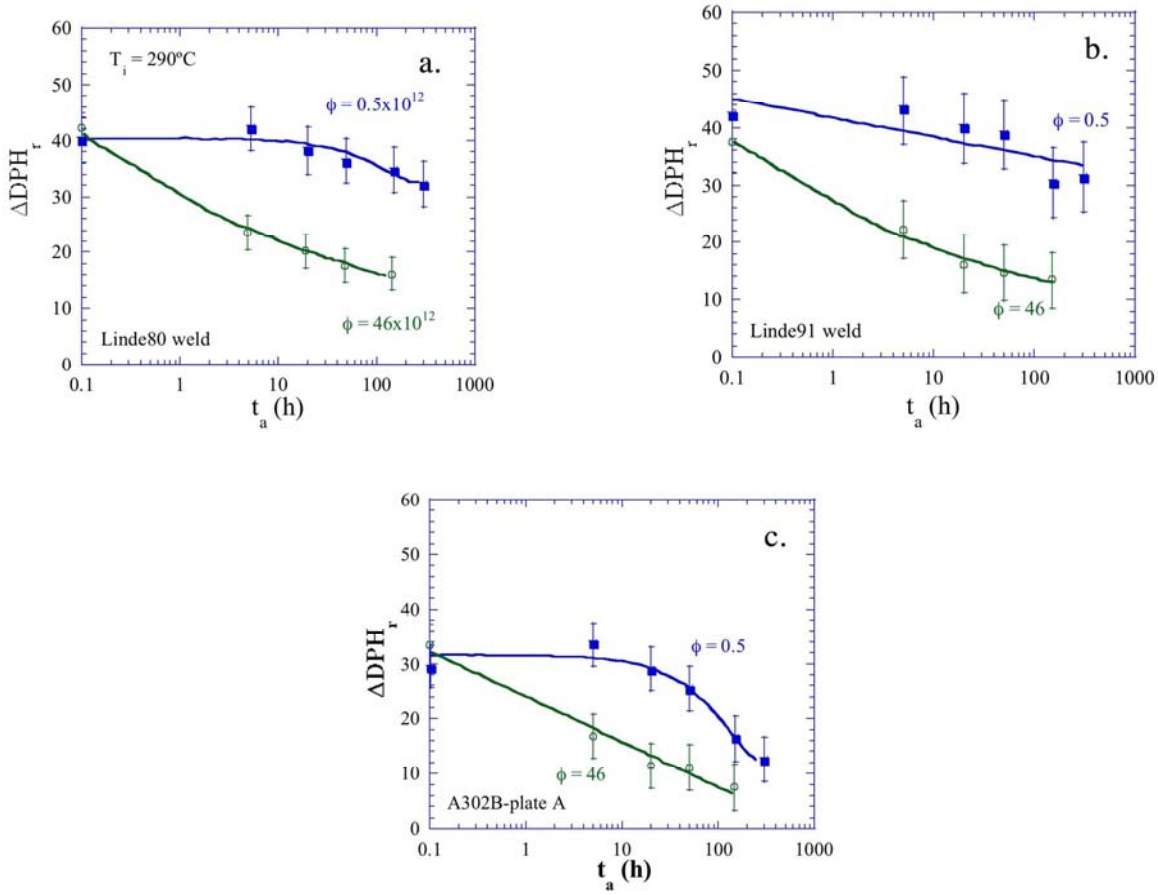

Fig. 3.2. The recovery of microhardness ΔH (ΔDPH, kg/mm^2) as a function of time during a annealing at 343°C for three alloys (two welds and one plate) irradiated at fluxes of 0.5 × 10^{12} and 46 × 10^{12} n/cm^2/s to a fluence of ~0.5 × 10^{19} n/cm^2. While the as-irradiated H are similar, the ΔH in the steels irradiated at high flux is much more rapid.

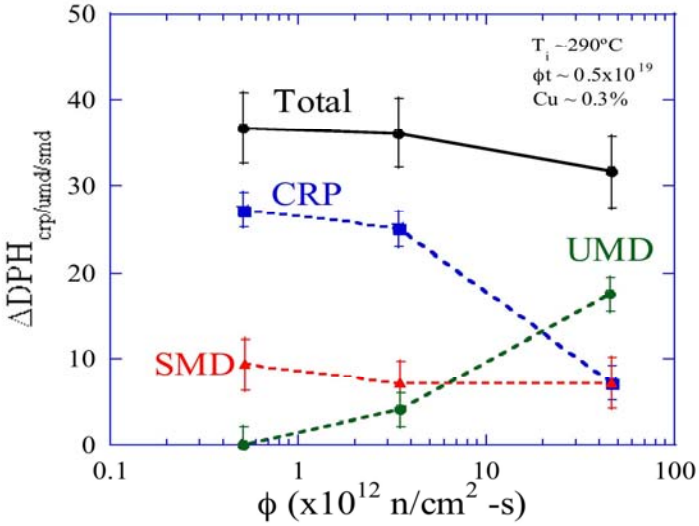

Fig. 3.3. The average micro-hardness contributions from copper-rich precipitates (CRPs), stable matrix defects (SMDs), and unstable matrix defects (UMDs), for high copper (~0.3 wt %) alloys based on their respective low temperature 290 and 343°C thermal annealing signatures.

The number of UMDs (N_{umd}) is governed by their generation rate (G_{umd}) and annealing time (τ_{umd}) as

$$dN_{umd}/dt = G_{umd} - N_{umd}/\tau_{umd} \quad = \phi\sigma_{umd} - N_{umd}/\tau_{umd} \tag{2}$$

Here σ_{umd} is the UMD formation cross section. Integration of this simple differential equation gives

$$N_{umd}(\phi, \phi t) = N_{umds}[1 - \exp(-\phi t/\phi\tau_{umd})] \tag{3}$$

Here, N_{umds} is the steady state number density of UMDs.

$$N_{umds} = \tau_{umd}G_{umd} = \phi\tau_{umd}\sigma_{umd} \tag{4}$$

Since UMD hardening (ΔH_{umd}) approximately scales with the $\sqrt{N_{umd}}$, the corresponding fluence (ϕt) dependence of [$H_{umd}(\phi t)$] is given by

$$\Delta H_{umd}(\phi t) = \Delta H_{urs}(\phi)\{\phi[1-\exp(\phi t/\phi\tau_{umd})]\}^{1/2} \tag{5}$$

Here $\Delta H_{urs}(\phi)$ is the saturation UMD hardening at a specified flux. Figure 3.4 shows the corresponding predictions of UMD ΔH as a function of fluence for a nominal 0.3% Cu alloy at 290°C and various dose rates based on the estimated values of ΔH at lower fluence and $\tau_{umd} = 3.25 \times 10^5$ s. Clearly, UMD hardening is minimal at low flux, but it builds up to a much higher value at high flux. The $H_{urs}(4.6 \times 10^{13})$ is ≈ 33 kg/mm^2. Assuming a conversion factor of 3.3 MPa/kg/mm^2 to convert hardness to yield stress increases and 0.7°C/MPa to convert the yield stress increase to a TTS, the corresponding saturation UMD TTS at 5×10^{13} n/cm^2 is ≈ 80°C.

The effect of the UMD on the RED diffusion coefficient D* can also be modeled crudely in terms of a UMD modified effective fluence, ϕt_{umd}. For simplicity we applied the UMD effective fluence adjustment to ϕt_{eff} at a flux greater than a minimum reference flux, ϕ_{rumd}, as

$$\phi t_{umd} = \phi t_{eff}[(1 + k)/(1 + k\phi/\phi_{rumd})] \qquad \phi > \phi_{rumd} \tag{6}$$

Here ϕ_{eff} accounts for any DREs that are not due to UMDs, and the term in the brackets ([]) accounts for UMD sinks. Above the threshold flux of 10^{12} n/cm^2/s, the UMDs reduce ϕt_{umd}. Table 3.2 summarizes the various regimes of DRE mechanisms and their limiting p-scaling laws. The product of the RED coefficient and time, D*t, is a measure of the amount of precipitation at a specified fluence. Figure 3.5 shows an example of the predicted variation of an effective fluence factor $M_\phi = (\phi t_{eff}$ or $\phi t_{umd})/\phi t$ with flux, which involves all DRE mechanisms, including SER and thermal Cu diffusion as well as UMD sinks for k = 0.1. The M_ϕ is normalized to 1 at $\phi = 3 \times 10^{11}$ n/cm^2/s. The M_ϕ decreases with increasing flux due to the mechanisms described in Table 3.2.

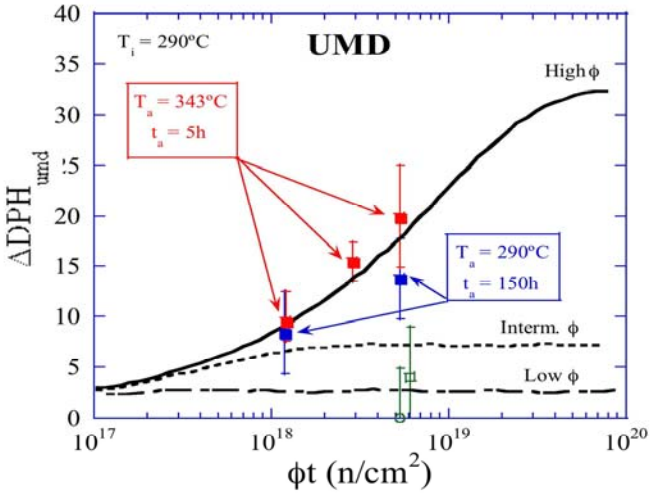

Fig. 3.4. The predicted change in microhardness vs fluence for UMD for a nominal 0.3 wt % Cu alloy at 290°C and at low, intermediate, and high fluxes. The curves are based on a τ_{umd} =3.25 × 10^5 s and the estimates of UMD hardening over a range of lower fluences from 290°C-150 h and 343°C-5 h from annealing signatures.

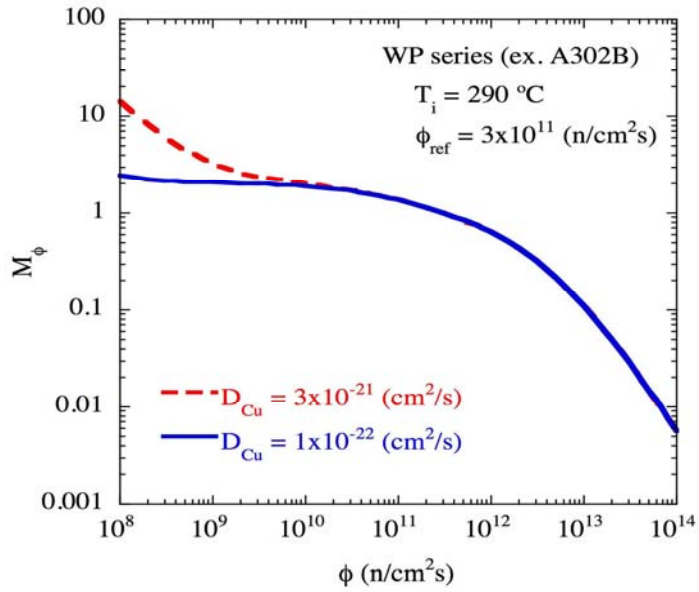

Fig. 3.5. An example of the variation of the ratio of the effective fluence and UMD modified effective fluence (for $\phi > 10^{12}$ n/cm/s) to the actual fluence (M_ϕ) with flux representing all the DRE mechanisms discussed in the text normalized to 1 at a flux of 3 × 10^{11} n/cm²/s. The curves are for a UMD k=0.1 and a set of solute enhanced recombination model parameters discussed in the EONY report (Eason 07) and high and low estimates of the thermal Cu diffusion coefficient. Note this is shown for purposes of illustration. The 3FTTS model used the MEK model to account for DRE on the saturation fluence and used a UMD modified fluence at $\phi > 10^{12}$ n/cm²/s.

Table 3.2. Flux dependence mechanisms, regimes and scaling laws for T_i = 290°C

Dominant mechanism	ϕ-regime ($n/cm^2/s$)	Limiting scaling p[a]	Comments[b]
Thermal diffusion assisted	$< \approx 10^{10}$	$D^*t \alpha \phi t \alpha 1/\phi$	Depends on low-temperature D_{cu}. Thermal precipitation is observed in sensitive model alloys and sensitive steels at 290 to 350°C. This flux range is pertinent to BWR vessels and some low-flux surveillance capsules.
Solute trap recombination	$> 10^{10}$	$D^*t \alpha \phi t \alpha 1/\sqrt{\phi}$	Depends on alloy Ni & Mn contents, microstructure Pertinent to PWR surveillance capsules and test reactor irradiations as well as higher flux regions in PWR vessels.
Unstable matrix defect sinks	$> 10^{12}$	$D^*t \alpha \phi t$ a $1/\phi$	Pertinent to materials test reactor irradiations and high flux

[a]The flux-scaling varies smoothly in transitions between regimes that are dominated by a specific mechanism that may overlap between some regimes.
[b]The flux levels at actual surveillance and vessel locations vary greatly, depending on the reactor type and details of the design and fuel assembly arrangements and surveillance capsule locations.

The concepts represented in Eqs. (5) and (6) were used to develop a three feature TTS (3FTTS) model for application to subsets of the high-flux database complied in Appendix G of the draft NUREG report.

$$TTS = TTS_{md} + TTS_{crp} + TTS_{umd} \tag{7}$$

The MD and CRP contributions are calculated by using the ϕt_{eff} and ϕt_{umd} in the low flux MEK or EONY TTS models. The results presented here use the optimized MEK model where $\phi t_{eff} = \phi t$ and the effect of flux, other than that due to the UMDs, is represented in terms of its effect on the saturation fluence. The UMD contribution is based on Eq. (7) as

$$TTS_{umd}(\phi t) = TTS_{urs}\{(\phi/5 \times 10^{13})[1-\exp(\phi t/\phi\tau_{umd})]\}^{1/2} \tag{8}$$

Here TTS_{urs} is the saturation TTS contribution at $\phi = 5 \times 10^{13}$. As noted previously, at 290°C TTS_{urs} was estimated to be about ≈ 80°C for high-Cu steels. Thus, the saturation TTS_{umd} at other fluxes is given by

$$TTS_{umd}(\phi) = TTS_{urs}\sqrt{(\phi/5 \times 10^{13})} \tag{9}$$

Note, in a number of cases in the data in Appendix G the flux and fluence are directly proportional, since the irradiations are for a fixed time (t_{irr}) at different fluxes: $\phi t = \phi t_{irr}$. In this case the TTS_{umd} is simply

$$TTS_{umd} = TTS_{urs}\sqrt{[\phi t/(5 \times 10^{13} t_{irr})]} \tag{10}$$

This trend is observed in a number of the data subsets in Appendix G of the draft NUREG report.

The τ_{umd}, k, and TTS_{uos} relate to the UMD annealing time, sink strength, and saturation hardening, respectively. The latter two parameters are for the specified reference flux (5×10^{13} n/cm^2/s). In principle, the parameters can be related to physical quantities, such as vacancy binding energies and the self-diffusion coefficient, in the case of τ_{umd}, for example. Indeed, such models have been developed by Mader and Odette (Odette 94, Mader 95) for irradiations around 290°C. However, detailed development of more general models is beyond the scope of this effort. Another approach would be to treat τ_{umd}, k, and TTS_{urs} as fitting parameters to establish the UMD contribution to the TTS at high flux as well as their corresponding effect on the fluence dependence of the MD and CRP contributions. However, our initial application of the 3FTTS model revealed a practical problem related to a high degree of covariance between the fitting parameters; for example, the delay imposed by k in the MD and CRP TTS can trade off with the fluence dependence of the UMD contribution, which is controlled by τ_{umd}.

Thus, the application of the 3FTTS model reported here was based on fixing τ_{umd} at a nominal value of 3.25×10^5 s at 290°C and scaling it at other temperatures of 266 and 300°C by the activation energy corresponding to the ratio of $\tau_{umd}(290)/\tau_{umd}(343) = 30$. This gives $\tau_{umd}(300°C) = 1.63 \times 10^5$ s and $\tau_{umd}(266°C) = 1.9 \times 10^6$ s, respectively. A k (at 290°C) = 0.1 was found to give a reasonable fit to some of the appendix G data at a nominal irradiation temperature of 290°C. Since at saturation k scales with τ_{umd}, the corresponding k (at 266°C) is 0.58 and k (at 300°C) is 0.05. This leaves TTS_{urs} as the only remaining fitting constant.

Figures 3.6 to 3.8 show three examples of the application of the 3FTTS model to data in Appendix G. Figure 3.6 shows the 0.31% Cu 73W data at both high-flux (BR2) and low-flux (IVAR) conditions and at both 266°C (510°F) in Fig. 3.6 (a) and 300°C (572°F) in Fig. 3.6 (b).

We have adjusted the IVAR data at 290°C to the higher temperature using the 3FTTS model. The solid red curves are the 3FTTS model predictions at a flux of 5×10^{13} n/cm^2/s. The dashed blue line is the MEK model that is not modified for UMD sinks; the dashed green line is the UMD-modified MEK curve for the MD and CRP TTS contributions. The effect of the UMD sinks in shifting the MD and CRP curves to higher fluence is clear, especially at the lower temperature. The short dashed purple line is the UMD contribution to the TTS. The small filled diamonds are the actual data for a range of irradiation conditions, and the open diamonds are the data adjusted by the model to the specified flux and temperature. The fitted TTS_{urs} are ≈ 180°C and ≈ 50°C at irradiation temperatures of 266°C and 300°C, respectively. The decrease in the TTS_{urs} with increasing temperature is not unexpected and is qualitatively consistent with the observations of Mader and Odette (Odette 94, Mader 95). The interpolated TTS_{urs} to 290 is ≈ 89°C which is only slightly higher than the previous estimate for such high-Cu alloys of ≈ 80°C. Figure 3.6 (c) shows that the corresponding 3FTTS model prediction at a low flux of 5×10^{10} n/cm^2/s, with a minimal contribution from the UMD, is also in good agreement with the adjusted TTS data.

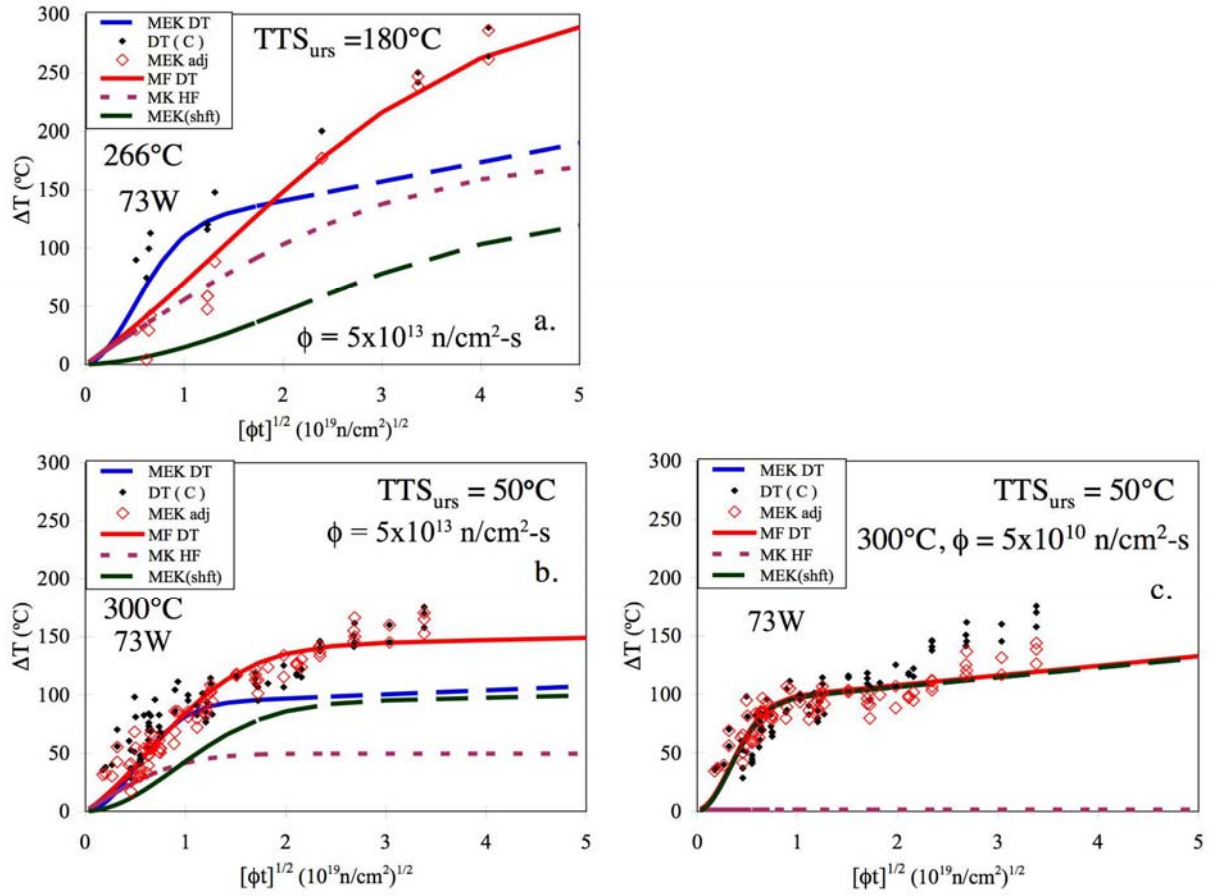

Fig. 3.6. The 3FTTS model predictions vs the sqrt fluence for the high 0.31 wt % Cu HSSI Weld 73W at high flux (5 × 10^{13} n/cm^2/s) at both nominal temperatures of 511 and 572°F (266 and 300°C). The predictions for low flux (5 × 10^{10} n/cm^2/s) at 300°C are also shown.

Figure 3.7 shows a similar plot for a low 0.05% Cu A508 forging. The TTS_{urs} are 84°C, 63°C, and 23°C at irradiation temperatures of 266°C, 290°C, and 300°C, respectively. The TTS_{urs} are lower than those for 73W, probably reflecting the low ≈0.05% Cu content of that alloy. In this case the adjusted data show a large amount of scatter around the predicted TTS curve at 290°C, and at both low and high flux, but the absolute values of the shifts are small.

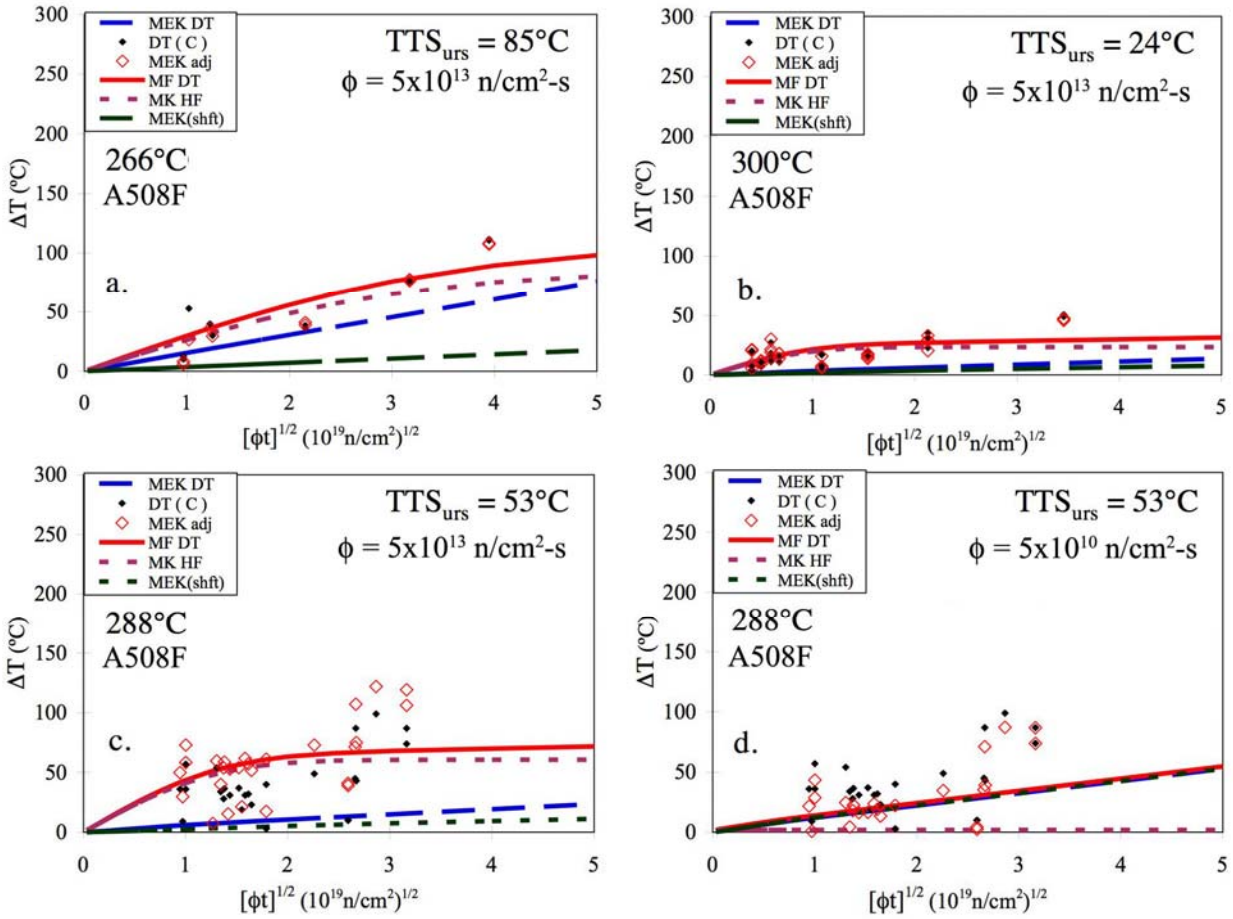

Fig. 3.7. The 3FTTS model predictions vs the sqrt fluence for a low-Cu (0.05 wt %) A508 forging at high flux (5×10^{13} n/cm^2/s) at nominal temperatures of 266, 288, and 300°C (511, 552, and 572°F). The predictions for low flux (5×10^{10} n/cm^2/s) at 288°C are also shown. The filled diamonds are RADAMO (high-flux) data. The open diamonds are the data adjusted to the reference conditions by the 3FTTS model.

Figure 3.8 shows similar plots for the intermediate 0.14% Cu JRQ plate at three irradiation temperatures for the RADAMO and IVAR databases, again over a wide range of flux. The TTS_{urs} again decrease with increasing temperature with values of 145°C, 87°C, and 52°C at irradiation temperatures of 266°C, 288°C and 300°C, respectively. The intermediate Cu JRQ plate falls between the low-Cu A508 and the high-Cu 73W. The 3FTTS model predictions at low flux are again consistent with the adjusted TTS data.

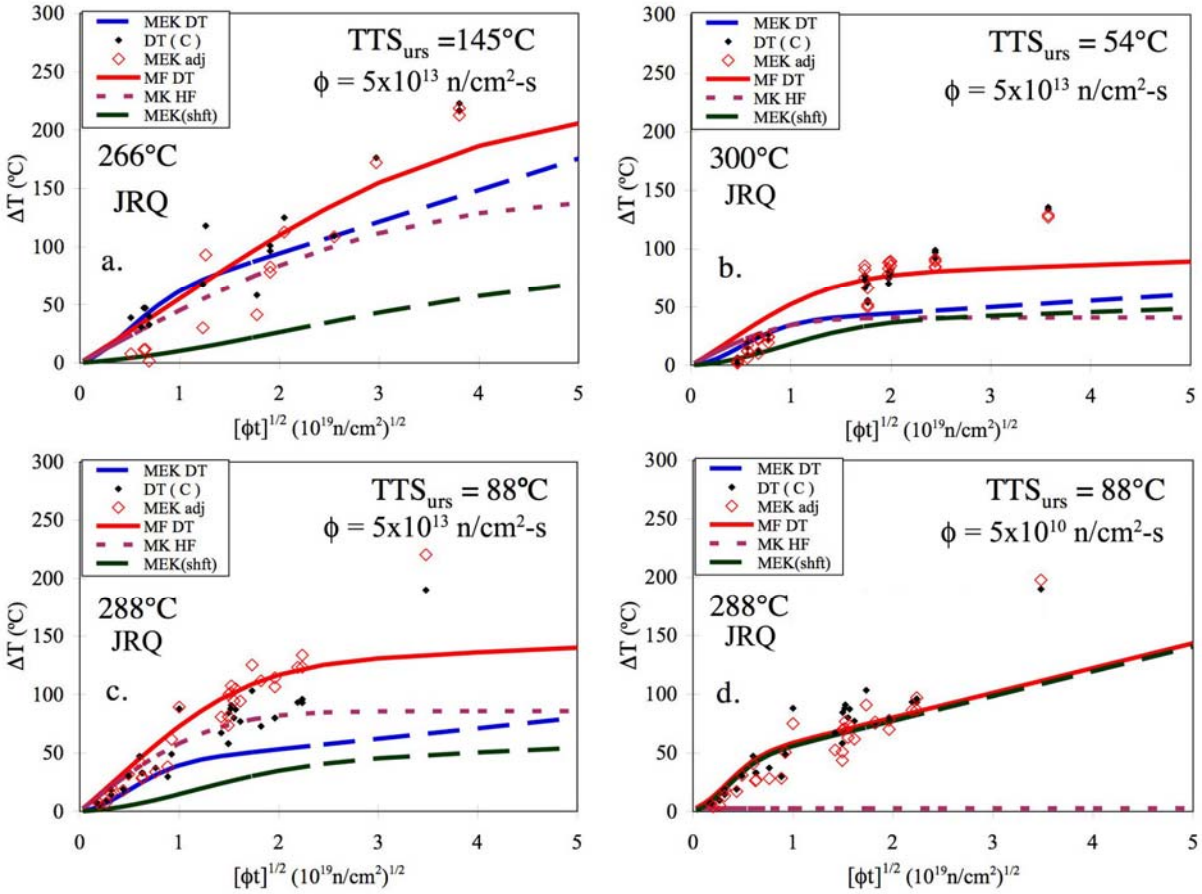

Fig. 3.8. The 3FTTS model predictions vs the sqrt fluence for the intermediate Cu (0.14 wt %) JRQ plate at high flux (5 × 10^{13} n/cm^2/s) at nominal temperatures of 266, 288, and 300°C (511, 554, and 572°F). The predictions for low flux (5 × 10^{10} n/cm^2/s) at 288°C are also shown. The filled diamonds are both IVAR (low-flux) and RADAMO (high-flux) data. The open diamonds are the data adjusted to the reference conditions by the 3FTTS model.

Figure 3.9 plots the TTS_{urs} for the three alloys and nominal irradiation temperatures, showing the systematic trends in Cu and irradiation temperature described above. We have not applied the 3FTTS model to all the alloys and high-flux irradiation conditions in Appendix G, but in the other cases we examined, the results were generally similar to those illustrated in Figs. 3.6 to 3.8. The unmodified MEK model worked well for the low-flux Chooz data, as shown in Fig. 3.10. Extension of the 3FTTS approach to a *general* TTS model encompassing the entire range of flux, irradiation temperature, and alloy chemistry is beyond the scope of the present work but is certainly possible.

For the present purposes, the most important conclusion is that including a UMD TTS contribution in the 3FTTS model rationalizes most of the high-flux TTS data in Appendix G up to relatively high fluence. Further, at low flux the 3FTTS model provides reasonable predictions of the adjusted TTS up to about 6×10^{19} n/cm^2 or more. However, we do not claim that the very simple 3FTTS model fully represents all the physics of embrittlement at high flux and fluence. Indeed, it almost certainly does not. However, the 3FTTS model does have a solid and *independent* physical basis. Most importantly, *the model can be tested* by future low-temperature (e.g., 290 to 350°C) annealing studies of a large number of RPV alloys that we have included in both IVAR and BR2 irradiations.

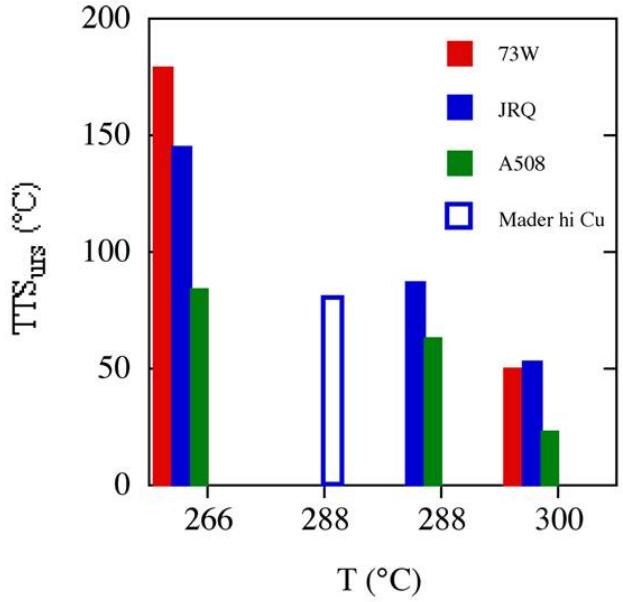

Fig. 3.9. The saturation TTS$_{urs}$ for the A508 forging, JRQ plate, and HSSI Weld 73W showing the systematic effect of the (nominal) irradiation temperatures of 510, 550, and 570°F (266, 288, and 300°C) and alloy composition.

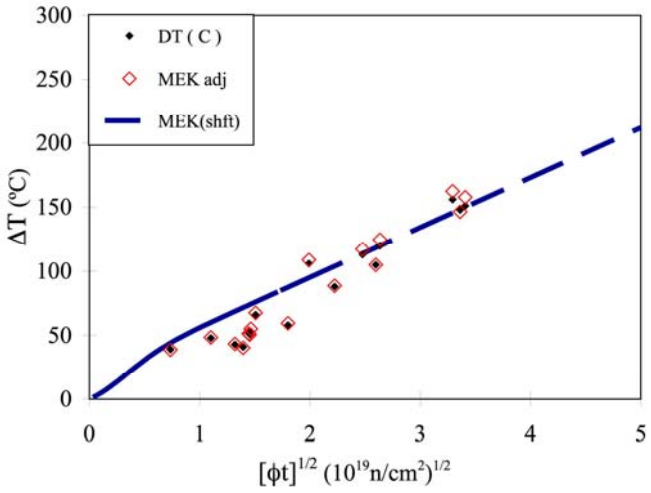

Fig. 3.10. Predictions of the MEK model for the Chooz reactor steels at low flux of 1.2×10^{11} n/cm^2/s and a low irradiation temperature of 504°F (262°C).

It is also important to note limitations of the 3FTTS in fitting some subsets of the Appendix G data. First, in most cases, the predicted minus measured TTS decreased relatively slowly, but systematically, with increasing measured TTS, yielding negative residuals at the highest TTS. However, the residuals are much smaller than those found for the RM-6(2) model in the draft NURG report, and the amount of underprediction generally did not exceed -20°C, except at fluences above, and generally well above, 6×10^{19} n/cm^2. The residual trends suggest that the simple 3FTTS model does not fully capture the shape of the TTS fluence dependence, especially at high dose. Overpredictions are observed at low dose, especially for alloys with Cu contents above the threshold but below ≈ 0.2% Cu. The 3FTTS model worked very well for the high-Cu welds in spite of the fact that the lowest irradiation temperature in the RADAMO database is outside the SDB. We believe that the differences at low fluence are primarily due to limitations in the base MEK (or EONY) model in these cases.

The 3FTTS model did not work as well for the Doel and BR2 data reported by Gérard et al. (Gérard 06) for a low-Cu forging and weld. In this case a low- to high-flux UMD-type effect was not observed. The predictions of the 3FTTS model systematically fell about 20°C higher for the high vs low flux data. However, even in that case the adjusted data scattered around the predicted curve to about 4.5×10^{19} n/cm^2 with larger deviations occurring only at higher fluence. Both the MEK and EONY low-flux models underpredict the Gérard data at intermediate to high fluence. The best fit TTS_{urs} values in that case were 23 to 29°C, consistent with the A508 results shown in Fig. 3.7. Other references suggest that the Doel welds have higher Cu than reported in Appendix G (Gérard 96, Hasagawa 07), with minimum levels of 0.13%, which is well above the threshold for forming CRPs that are indeed observed in a variety of microanalytical studies showing these features are enriched in Mn, Si and Ni. Thus we must conclude that the deviations observed in the case of the Doel welds are not terribly significant.

In a number of other cases we examined, including the relatively low flux Kussmaul data on Gundremmingen steels, the TTSs are underpredicted by all the models at fluences greater than 6×10^{19}. Thus, it appears that at very high fluence additional embrittlement mechanisms come into play, *adding to* (not replacing) the effects of hardening features formed at lower fluence. This will be discussed further in the following section. The issue of what happens at a combination of *higher fluence and low flux* remains an especially critical open question.

3.2 High Fluence Effects—Late Blooming Phases and Dislocation Loops

We believe that the analysis described in the previous section to some extent decreases the degree of concern about the nonconservative deviations between the high-flux, high-fluence data in Appendix G and the predictions of the TTS models calibrated to the low-flux surveillance database. However, these results do NOT address the issue of higher fluence data at lower flux. For example, work by Odette and co-workers predicted the formation of so-called “late blooming phases” (LBPs) (Odette 98b, Odette 01a, Odette 98, Odette 97a, Odette 97b, Odette 95, Odette 90, Odette 04, Odette 01b, Miller 06) that could lead to severe embrittlement even at low Cu levels. LBPs are Mn-Ni-Si rich precipitates that can cause severe hardening and embrittlement, potentially even in excess of that experienced by sensitive high-Cu, medium-Ni steels. The LBP predictions, were based on thermodynamic theory, but have recently been experimentally confirmed.

The Mn-Ni-Si precipitates are described as late blooming because they are slow to nucleate and require an extended incubation dose before they start to rapidly grow to produce large volume

fractions of nanoscale hardening features. The thermodynamic models predict that LBPs are enhanced by higher Ni, low but some Cu that acts as a catalyst for nucleation, lower irradiation temperatures, and *lower flux*. The widespread recognition that LBPs are real has been reflected in recent meetings of the International Group for Radiation Damage Modeling (IGRDM), the American Society for Testing and Materials (ASTM), and the Minerals, Metals, and Materials Society (TMS). (Presentations by an author (G. R. Odette) at a number of IGRDM meetings dating from the early 1990s trace the history of theoretical and experimental research on LBPs. More recent presentations include at the Twenty-Third International Symposium on the Effects of Radiation on Materials in June 2006 and the Annual TMS Meeting in February 2007. At the last few IGRDM meetings the presence of LBPs was reported by researchers from both Europe and Asia. A recent newsletter on the European Ageing Materials European Strategy (AMES) program (AMES 08) noted that research on LBPs would be a major thrust of its future research).

Thus, it is clearly important to place fluence limits on the applicability of current low-flux TTS models. The draft NUREG proposes a limit of 3×10^{19} n/cm^2. We have carefully examined the limited data in the SDB at higher fluence to determine whether the limit is appropriate. Figure 2.17 includes comparisons of the optimized EONY and MEK TTS model predictions to Maine Yankee and Palisades plate and weld data extending to high fluence. In both cases the weld data are well predicted by the models, while the plate TTSs are moderately overpredicted and underpredicted for Palisades and Maine Yankee plates, respectively. In all of those cases, the combined high-flux RADAMO–low -flux surveillance database calibrated model and MEK and EONY TTS predictions are similar. However, even for the Maine Yankee plate, the underprediction may not be a high fluence effect but rather may be a systematic effect of uncertainties in other variables such as the unirradiated transition temperature and/or a combination of the chemistry factor and product form factor. Table 3.3 summarizes the MEK and EONY model prediction residuals for surveillance data between 3 and 8×10^{19} n/cm^2/s. While the data are limited, the results do not suggest that there is any large and sudden trend toward underpredicting the surveillance data above 3×10^{19} and below 8×10^{19} n/cm^2. For example, there are 36 data points above 4×10^{19} n/cm^2, with an average residual of 2.3 and -0.6°C for the EONY and MEK models, respectively.

Based on the behavior of high-sensitivity steels at high fluence and the results shown in Table 3.3, we believe that a provisional fluence limit of 5×10^{19} n/cm^2 for the MEK and EONY TTS models represents a reasonable engineering judgment. However, we fully recognize that any decision on this matter is a decision to be made by the NRC staff. As noted in the draft NUREG report, a modest increase in margin term above 3×10^{19} n/cm^2 is an option to mitigate such concerns. Indeed, we believe that any provisional decision on TTS predictions at high fluence should be supported by further research. In particular, we note combinations of lower-flux, high-fluence conditions may accelerate the formation of LBPs or other hardening features and may introduce other embrittlement mechanisms.

The increasing deviation of the high-flux TTS data from the model predictions at very high fluence could be an indication of the onset of the formation of LBP. However, another possibility is the development of a population of dislocation loops that produce significant hardening and embrittlement. Dislocation loops first form in displacement cascades as small self-interstitial atom (SIA) clusters (Phythian, 95, Stoller 96a, Wirth, 00). In principle, they may grow due to a preferential bias for SIAs, but they can also shrink by absorbing vacancies. Molecular dynamics computer simulations suggest that small loops are mobile in pure iron. Highly mobile SIA

Table 3.3. Data points and average model prediction residuals for the surveillance data base at high fluence

ϕt_{min} (10^{19}n/cm^2) $E_{min} \geq$ MeV	# Data points	Av. EE residual (°C)	Av. MEK residual (°C)
3	74	0.1	–3.1
4	36	2.3	–0.6
5	9	4.3	–11.8
6	6	5	–12

clusters would be expected to undergo one-dimensional diffusion to sinks, which would reduce their accumulation in the material. However, the corresponding mobility in complex alloys is not known. Small loops may be trapped by impurities and are also observed to decorate dislocations, which can cause source hardening. Rate theory models suggest that loop formation is favored at higher fluxes, with loop production proceeding by a combination of direct in-cascade formation and a classical cluster dynamics nucleation mechanism (Stoller 93, Stoller 96b, Stoller 04). Growth is further enhanced by collisions between mobile (glissile) loops that react to produce larger sessile loops (Marian 02, Osetsky 00). Recent atomistic simulations indicate that interstitial loops change from relatively weak dislocation obstacles to strong obstacles as their size increases[4]. This could also increase their impact on hardening and embrittlement at high fluence.

It is well established that loops are a major source of hardening in 9Cr normalized and tempered martensitic steels for high-flux irradiation at doses above a few tenths of a dpa (Wakai 00, Klueh 01). Loop hardening and embrittlement also scale with the square root of fluence at a rate that is similar to low-dose, low-flux hardening in RPV steels (Yamamoto 06). Loops and loop hardening have been reported in the literature at even lower doses for high-flux irradiations of RPV alloys (Smidt 73) and at relatively low flux in commercial-purity iron (Jenkins 01). Thus, a key issue is to determine the degree to which loops contribute to MD hardening, particularly at low flux and high fluence. To the best of our knowledge these issues have not been resolved.

3.3 High-Fluence Effects—Use of the RADAMO Model

The draft NUREG proposes combining the MEK model calibrated to the low-flux SDB with the high-flux RADAMO model. In addition to the analysis provided above, we believe that, while this approach is understandable and well motivated, it does not have a solid technical basis for other reasons as well. These include the following.

- The basic physics reflected in RADAMO is at odds with what is known about the microstructures for CRP hardening at low flux. For example, there is no Ni effect on the CRP contributions in the RADAMO model. Nickel effects on CRP are well established based on a large number of microstructural observations, as well as mechanical property trends described in the draft NUREG. See Chap. 2 in ORNL/TM-2006/530 (Eason 07) for further discussion.
- The temperature dependence of the TTS in the RADAMO model is also very different from those found in the low-flux models and data trends. Lower temperature dependence at high flux can be rationalized based on the corresponding effect of temperature on recombination

[4] Bacon, D. J., private communication, unpublished, 2007.

and UMD sinks. It is also well established that the rate is lower at higher temperatures, but hardening extends to more than 350°C and more at very high fluence. Both of these effects may be reflected in the RADAMO database.

- The RADAMO model shows a different balance of MD and CRP hardening contributions from those found with low-flux models and data. Specifically, RADAMO predicts higher contributions from MD, and generally lower contributions from CRPs. These differences are very consistent with a 3FTTS model of the effect of high flux on the balance of defects, including UMDs, as discussed in the previous section.
- There is also an inherent logical problem with using a high-flux model with a very different microstructural basis above 4×10^{19} n/cm^2 to replace a low-flux model at less than 2×10^{19} n/cm^2. There is absolutely no evidence that the low-flux microstructures somehow disappear at higher fluence and are somehow replaced by high-flux microstructures. We have not surveyed low- to intermediate-flux higher fluence microstructural data that may be available, but we believe that data exist to demonstrate this conclusion. Rather, as in the case of UMDs at high flux, it is logical to be concerned that *new* hardening features may emerge at low flux at high fluence that add to the effects of the lower dose microstructure, as discussed in Sect. 3.2.
- The RADAMO model does not always work as intended. Indeed, it systematically *underpredicts* the low-flux TTS models in perhaps what are the most important embrittlement regimes associated with high-sensitivity steels irradiated at lower flux and temperature. Underprediction is illustrated in Fig. 3.11, which shows TTSs for the MEK and EONY optimized models for alloys with compositions similar to Maine Yankee (0.36 Cu, 0.8 Ni) and Palisades (0.23 Cu, 1.2 Ni) welds. Moreover, as shown in Fig. 3.11, the blended curves (i.e., RM-9 and RADAMO combined) often exhibit abrupt changes in slope (e.g., from positive to negative) with increasing fluence.

Thus, in summary, we do not find the recommendation in the draft NUREG report related to the use of the RADAMO model to be acceptable for predicting low-flux TTS.

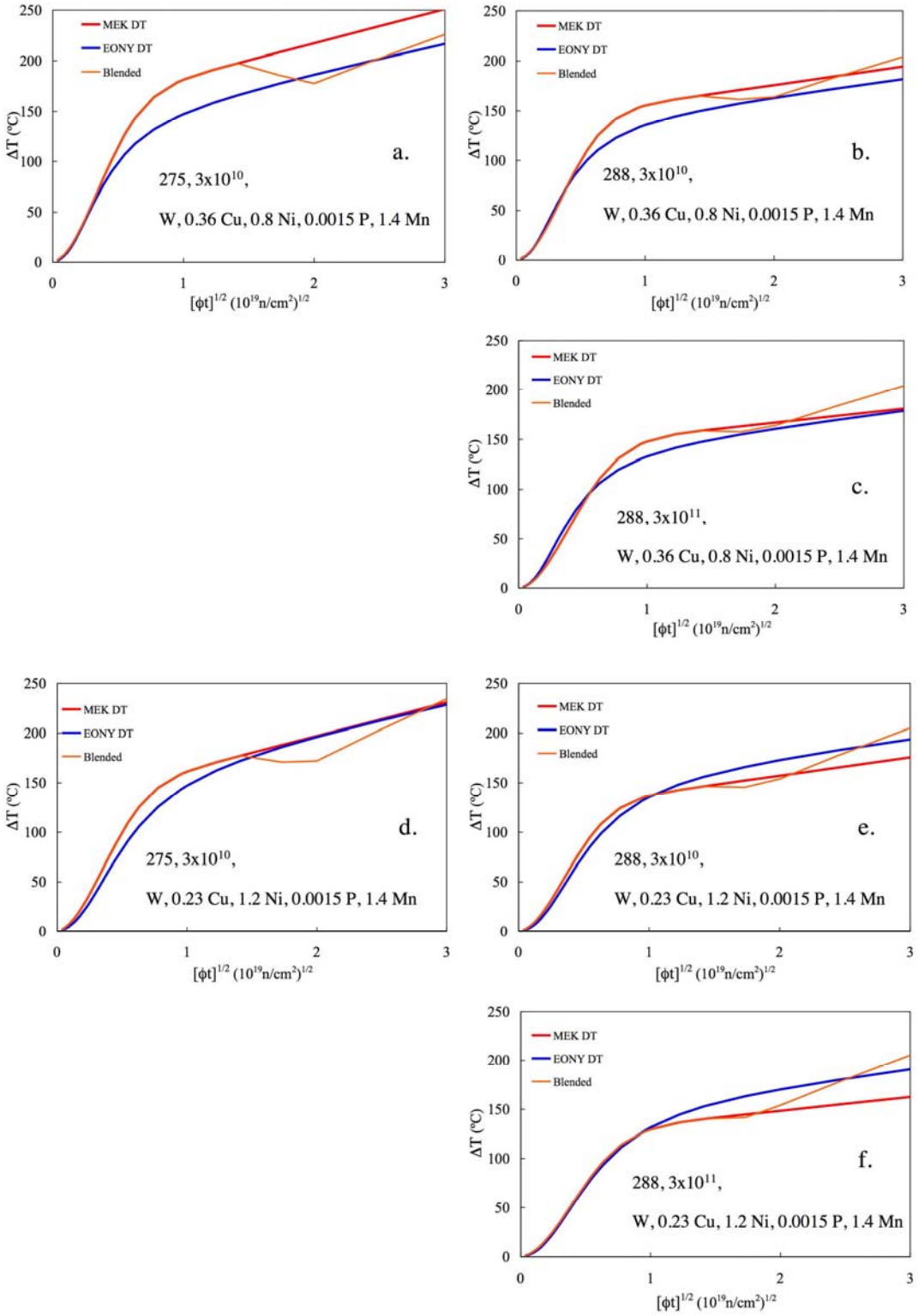

Fig. 3.11. TTS vs sqrt fluence for the MEK, EONY and MEK/RADAMO-blended models for alloys with compositions similar to Maine Yankee (0.36 Cu, 0.8 Ni) and Palisades (0.23 Cu, 1.2 Ni) welds, and for two different fluxes and temperatures of 275 and 288°C. Note the blended model underpredicts the MEK and EONY models over a range of high fluences in a number of cases.

4. REVIEW COMMENTS ON CHAPTER 5, UPPER-SHELF ENERGY DROP

As stated in Chap. 5 of the draft NUREG, the last systematic analysis of the U.S. SDB for the purpose of developing a model for prediction of irradiation-induced upper-shelf energy drop (ΔUSE) was performed by Eason, Wright, and Odette (EWO) in NUREG/CR-6551 (Eason 98). The draft NUREG notes that two approaches were used for the analysis in the EWO report, one in which a functional relationship between ΔUSE and both composition and exposure variables was developed, and another in which a simple linear relationship was developed between ΔT_{30} and ΔUSE. The standard error for the detailed functional relationship was 11.2 ft-lb, whereas it was 12.9 ft-lb for the simple linear relationship.

Because the standard errors are relatively close in value, the draft NUREG developed a similar linear correlation with the updated SDB. The correlation presented in Chap. 5 is

$$\Delta USE = 0.18 \cdot \Delta T_{30} \tag{11}$$

This correlation has a standard error of 13 ft-lb, about the same as that reported by EWO. Thus, the standard error for such a relationship has not changed despite the fact that a substantially larger surveillance database has been used for the draft NUREG analysis.

The regulatory context for the ΔUSE evaluation is that the *Federal Register* (in 10CFR50, Appendix G) requires specific actions be taken if the Charpy upper-shelf energy falls below the requirement of 50 ft-lb (67.7 J). In 1993, based on work of the Working Group on Flaw Evaluation of American Society of Mechanical Engineers (ASME) Code Section XI (WGFE 96), simplified procedures for evaluation of reactor vessels that do not meet the Charpy upper-shelf requirements were adopted into the ASME Code as Code Case N-512 (in effect through the 1995 edition of the code) and as Appendix K to Section XI (ASME 93). Those procedures applied to Level A and B Service Loadings only and, in 1995, Code Case N-512 and Appendix K were updated to include procedures for evaluation of Levels C and D Service Loadings (WGFE 96). The evaluation procedures adopted into the ASME code are based on elastic-plastic fracture mechanics and require the J-integral resistance curve for the material. However, if J-R curve data are not available for the material of interest, Appendix K allows for an indirect method of estimating the J-R curve (provided that the method is justified for the specific material); procedures are described in *WRC Bulletin 413* (WGFE 96) for use of Charpy upper-shelf energy to estimate the parameters of the J-R curve. Example calculations described in *WRC Bulletin 413* demonstrate acceptable fracture toughness for a material with a Charpy upper-shelf energy of 38.1 ft-lb (51.6 J). Thus, because prescribed acceptable procedures are available for using measured Charpy impact upper-shelf energy data from surveillance programs for the evaluation of the structural integrity of irradiated RPVs, the development of a more complicated parametric correlation is not considered necessary at this time.

One issue noted by the review panel is that the recommended correlation for ΔUSE does not include a limit of applicability for neutron fluence. Presumably, the same limit recommended for the ΔT_{30} model based on the SDB would apply, but it needs to be explicitly stated. Other than that minor discrepancy, the panel members believe that the correlation recommended for ΔUSE in the draft NUREG is adequate.

5. REVIEW COMMENTS ON CHAPTER 8, ATTENUATION

The so-called attenuation issue revolves around the need to predict the properties of RPV steel as a function of depth into the vessel. For example, the properties at a location three-quarters of the way through the vessel (3/4-T) are required for analysis during heat-up and cool-down conditions. In principle, the embrittlement model derived from analysis of surveillance data can be used to predict the ductile-to-brittle transition temperature (DBTT) at any location within the vessel as long as it is done in a self-consistent way with respect to the use of fast neutron flux and fluence (> 1 MeV) and if changes in the neutron energy spectrum, and flux are properly accounted for. Additionally, the actual temperature at the location of interest should be used since it is an explicit variable in the embrittlement model.

It is necessary to consider the neutron energy spectrum because the embrittlement model uses fast neutron fluence (E > 1.0 MeV) as the neutron exposure parameter. This measure of dose is inadequate if the neutron energy spectrum at the location of interest in the vessel wall differs from that at the reactor surveillance location. Radiation-induced embrittlement is better correlated with displacement damage as measured by the standard Norgett, Robinson, and Torrens (NRT) dpa (Norgett 75) because neutrons with energies much lower than 1.0 MeV produce displacements. This is not an issue for the damage model as long as the energy dependence of the neutron flux is the same in the environments being compared. Indeed, if the spectra are the same, any measure of the neutron fluence (e.g., E > 1.0 MeV, E > 0.1 MeV, total fluence) could be used to correlate the property changes. However, this is not the case when comparing the spectrum in the surveillance locations to those within the interior of the RPV. Neutron scattering reactions quickly reduce the flux with E > 1.0 MeV, leading to an increase in the flux at energies lower than 1 MeV. Since the lower-energy neutrons produce displacement damage, the ratio of dpa damage to fast fluence increases.

The difference between neutron exposure parameters is illustrated in Fig. 5.1 (Stoller 01), where the fluence with E > 1.0 MeV is compared with the fluence with E > 0.1 MeV, dpa, and the exponential attenuation function currently specified in RG 1.99-2 (RG 1.99-2). Results are shown for typical pressurized water reactor (PWR)

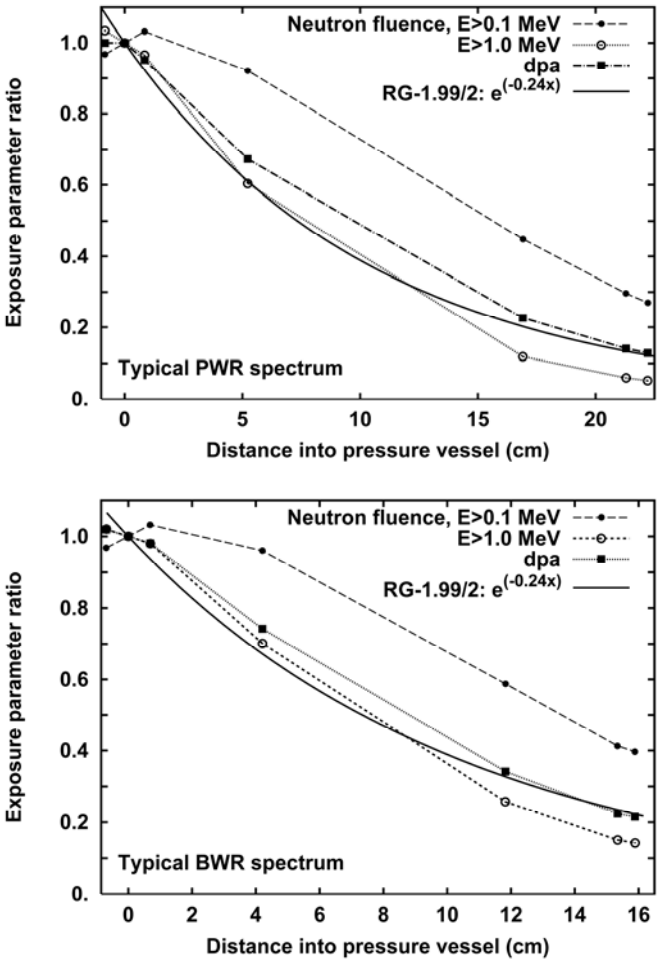

Fig. 5.1. Attenuation of neutron fluence, E > 0.1 MeV and E > 1.0 MeV, dpa, and the exponential formula from RG 1.99-2 for typical PWR and BWR vessels.

and boiling water reactor (BWR) neutron spectra and vessel thicknesses, with the values normalized to 1.0 at the inner surface of the vessel. While the fluence > 1.0 MeV decreases rapidly as a function of distance into the RPV wall, the fluence > 0.1 MeV initially increases until it peaks at a depth of about 1 cm. Fluence > 0.1 MeV is always much higher than fluence > 1.0 MeV. The reduction in dpa as a function of distance into the RPV is intermediate between the two measures of neutron fluence. At any given depth, there are slight differences between the PWR and BWR cases because of neutron backscattering in the thicker PWR vessel.

Depending on the vessel thickness and the location in the vessel, the exponential function may be greater or less than either fluence > 1.0 MeV or dpa. The best correspondence between dpa and the RG 1.99-2 exponential function, which occurs for depths greater than about 15 cm (6 in.), is a result of the procedure that was used for RG 1.99-2 to obtain the exponent of -0.24, which involved averaging the calculated dpa to fast fluence ratio at a depth of 8 in. for six PWR cases (Randall 86).

The recommendation contained in the draft NUREG follows the current practice of RG 1.99-2; i.e., the neutron energy spectrum effect is accounted for by increasing the effective fast fluence at the given location. However, it neglects the flux effect that is explicit in the embrittlement models. A self-consistent application of the model absolutely requires that differences in both neutron energy spectrum and flux level be taken into account when calculating changes in the DBTT for locations within the vessel.

The best approach would be to calculate the actual fast flux and fluence (E > 1.0 MeV), and dpa for the specific location of interest as well as the values for the inner wall of the vessel. Then, an effective fast flux and fluence should be determined and applied in the embrittlement model as follows.

1. The effective fast fluence, $\phi t^*(X)$, at a depth X within the vessel is equal to the fast fluence (RG 1.99-2) at the inner wetted wall, $\phi t(0)$, times the ratio of the dpa at depth X to the dpa at the inner wetted wall:

$$\phi t^*(X) = \phi t(0) \cdot \frac{dpa(X)}{dpa(0)} \tag{12}$$

In this case the effective fluence will be greater than the actual fluence, leading to an increase in the predicted DBTT shift at depth X.

2. An effective fast flux, $\phi^*(X)$ should be calculated in a similar way because the change in energy spectrum responsible for increasing the fluence also gives rise to a higher effective damage rate:

$$\phi^*(X) = \phi(0) \cdot \frac{dpa(X)}{dpa(0)} \tag{13}$$

The flux effect in the embrittlement model will also lead to a higher predicted TTS shift at depth X, but the use of a higher effective fast flux will slightly reduce the magnitude of the change.

The procedure assumes that the neutron spectrum is approximately the same at the inner wall and the prototypic surveillance location; that may not always be the case. The influence of the changes is illustrated for a simple case in Table 5.1 for both the EONY model (Eason 07) and the RM-9 version of the draft NUREG model. The following variables were used: product form weld, Cu = 0.20, Ni = 0.75, Mn = 1.5, P = 0.003, T = 288°C, and the fast flux and fluence at the inner wall of the vessel were 3×10^{10} n/cm^2/s and 2×10^{19} n/cm^2, respectively. The PWR exposure parameters for the 3/4-T (16.9 cm [6.65 in.]) location in Fig. 5.1 were employed. In this case the fast fluence and flux would be reduced by a factor of 0.118, whereas the reduction in dpa is 0.226. The reduction based on the RG 1.99-2 exponential function would be 0.202. Six cases are shown in Table 5.1 for both embrittlement models. In cases 1 to 3, the change in flux between the inner wall and the 3/4-T position was not taken into account when calculating the DBTT.

- For Case 1, the DBTT shift values are based on the actual computed fast fluence at the 3/4-T location.
- For Case 2, inner wall fast fluence was reduced in proportion to the exponential equation in RG 1.99-2.
- For Case 3, Eq. (12) was used to determine the effective fast fluence from the actual dpa ratio.
- Cases 4 and 5 use the same effective fluence as Case 3. The actual flux at the 3/4-T location was used for Case 4, whereas Case 5 accounts for an increased effective fast flux using the dpa ratio as shown in Eq. (13).
- The results for Case 6 are obtained if the current RG 1.99-2 exponential function is used to correct both the fluence and the flux rather than using the dpa ratio in Eqs. (12) and (13).

The authors of this report recommend the procedure employed in Case 5.

The values listed in Table 5.1 are compared in Fig. 5.2. For the conditions used here, the DBTT shifts predicted by the EONY correlation are higher than those from RM9 for each case, but the relative change is the same from one case to another. Depending on any given reactor vessel's composition and fluence, it is clear that the differences among the various cases may be larger or smaller than those observed in this particular example. However, this example illustrates the

Table 5.1. Influence of assumed damage attenuation in DBTT shift predicted for typical PWR at 3/4-T (16.9 cm [6.65 in.])

Cases of assumed damage attenuation behavior	Actual or effective fast fluence (n/cm^2)	Actual or effective fast flux (n/cm^2/s)	EONY DBTT Shift (°C/°F)	EricksonKirk RM9 DBTT Shift (°C/°F)
1: no flux attenuation, actual 3/4-T fluence	2.36×10^{18}	3×10^{10}	59.7/107	51.7/93.1
2: no flux attenuation, RG 1.99-2 fluence	4.04×10^{18}	3×10^{10}	74.0/133	66.0/119
3: no flux attenuation dpa-adjusted fluence	4.52×10^{18}	3×10^{10}	76.5/138	68.6/123
4: actual flux at 3/4-T, dpa-adjusted fluence	4.52×10^{18}	3.54×10^{9}	85.8/154	75.0/135
5: dpa-adjusted flux, dpa-adjusted fluence	**4.52×10^{18}**	**6.78×10^{9}**	**84.1/151**	**73.0/131**
6. RG 1.99-2 flux, RG 1.99-2 fluence	4.04×10^{18}	6.06×10^{9}	82.6/149	70.9/128

sense of the changes that will occur with the recommended attenuation procedure.

Since the differences between the calculated dpa profiles and the exponential formula shown in Fig. 5.1 are not large, an alternate procedure would be to permit the use of the exponential function in RG 1.99-2 as a substitute for the dpa ratio in the equations shown above. However, this will be slightly nonconservative in some cases, and it is believed that current neutronic practice in the industry already includes calculation of the required dpa values.

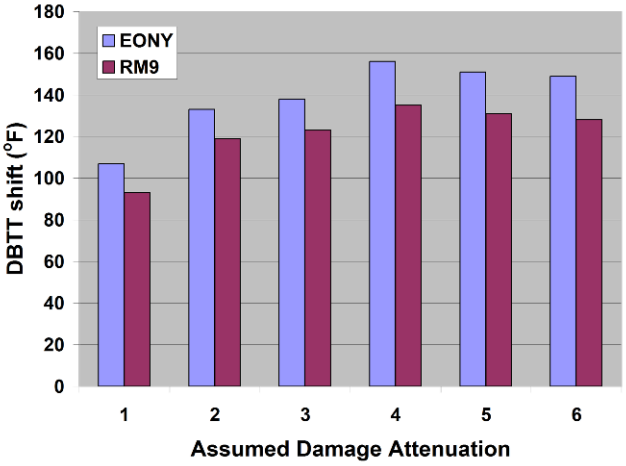

Fig. 5.2. Impact of six different damage attenuation models on predicted DBTT shifts at the 3/4-T position for EONY and RM9 embrittlement correlations.

In summary, the current Regulatory Guide 1.99-2 procedure recommended in the draft NUREG for attenuation should not be employed. Whichever embrittlement model is used, it is important that it be applied in a self-consistent manner with respect to flux, spectral effects, and irradiation temperature when predicting embrittlement at locations within the RPV wall. The authors of this report recommend the two-step procedure enumerated earlier in this section.

6. CONCLUSIONS AND RECOMMENDATIONS

Chapter 4 in the draft NUREG report, on Prediction of Transition Temperature Shift (ΔT_{30}) includes a number of statements that require correction and/or clarification. Also, a substantial rewrite is required because the draft report was written with model RM-6(2) in mind, whereas the subsequently developed model RM-9 is the model evaluated by the review team. The members of the review team believe that the RM-9 model is superior to RM-6(2).

Extensive fitting of the SDB showed that the draft NUREG embrittlement model provides reasonably good fits to a variety of subsets of the database. Also, extensive comparisons show that the draft NUREG embrittlement model provides reasonably good fits to single-variable subsets of the IVAR database.

It was not clear that the current formulation of RM-9 is the best possible model. Comparisons have been also made between the draft NUREG model and the EONY model. Although the general trends in flux, fluence, temperature, copper, nickel, and phosphorus are broadly similar, there are both similarities and significant differences in the TTSs predicted by the two models, depending on the specific combination of variables. The largest differences are associated with variations in the treatment of product form effects and maximum Cu levels.

The conclusions and recommendations of the authors of this report are as follows.

- There are some statistical differences between the models that are described in the report, including those associated with using different Excel fitting procedures.
- The significance of the similarities and differences for the various models have been qualitatively evaluated based on analysis of subsets of the surveillance database as well as insights from comparisons to the IVAR database.
- A very important basis on which to compare the models is differences in the predictions for the combination of metallurgical and irradiation variables that produce the largest TTS and perhaps the highest irradiated transition temperature.
- Subsets of data at high fluence have also been examined to especially assess the relative fidelity of the models above 3×10^{19} n/cm^2. The same type of assessment has been carried out for low-flux, low-fluence data.
- An extensive analysis does not suggest that one model is generally better than the other so we have no clear recommendation as to which one to pick for use in Reg. Guide Revision 3.
- Our assessment does not include a statistical evaluation of the differences between the models, and we recommend that this be done by a professional statistician.

Regarding the use of high-flux test reactor data, the current understanding of radiation damage mechanisms suggests that it is not appropriate to use highly accelerated test reactor data directly to predict high-fluence behavior for RPV or surveillance conditions. It is known that the balance of hardening features, and associated radiation damage mechanisms, differ at high vs low flux, even in those cases where the overall hardening is the same. For example, the RADAMO model itself highlights differences between high- and low-flux embrittlement microstructures because it predicts enhancement of matrix damage, effects of nickel on matrix damage, and a corresponding suppression of CRP hardening contributions, in general agreement with current understanding of radiation damage mechanisms.

A 3FTTS model was developed and applied to subsets of data in Appendix G of the draft NUREG report. This model generally rationalizes the differences between TTS predictions of the MEK and EONY models fit to the low flux SDB and the high-flux RADAMO data. Thus, it is mechanistically inappropriate to use the RADAMO data to predict TTS at high fluence for low-flux irradiation conditions. Beyond the question of different mechanisms, there are also logical and practical issues associated with the use of RADAMO in a combined model that are described in the body of this report.

The draft NUREG proposes combining the MEK model calibrated to the low-flux surveillance database with the high-flux RADAMO model. In addition to the analysis provided in the report, we believe that, while this approach is understandable and well motivated, it does not have a solid technical basis for other reasons as well. Thus, in summary, we do not find the recommendation in the draft NUREG report related to the use of the RADAMO model to be acceptable for predicting low-flux TTS. Nevertheless, there are many opportunities to carry out research using high- and low-flux irradiation conditions to help develop a better understanding of radiation damage mechanisms. The issues raised in this report suggest that there is a compelling need for such research.

The ΔUSE correlation recommended in the draft NUREG provides a reasonable basis for prediction with the current database.

The current Regulatory Guide 1.99, Revision 2 procedure recommended in the draft NUREG for attenuation should not be employed. Whichever embrittlement model is used, it is important that it be applied in a self-consistent manner with respect to flux, temperature, and spectral effects when predicting embrittlement at locations within the RPV wall. A recommended procedure is described in the body of this report.

Based on the behavior of high sensitivity steels at high fluence, and the results shown in Table 3.3, we believe that a provisional fluence limit of 5×10^{19} n/cm^2 for the MEK and EONY TTS models represents a reasonable engineering judgment. However, we fully recognize that any decision on this matter is to be made by the NRC staff. As noted in the draft NUREG report, a modest increase in margin term above 3×10^{19} n/cm^2 is an option, and we would support that approach if the extra margin is justified. Indeed, we believe that any provisional decision on TTS predictions at high fluence should be supported by further research. In particular, we note combinations of lower flux-high fluence conditions may accelerate the formation of late blooming phases (LBP) or other hardening features and may introduce other embrittlement mechanisms.

7. REFERENCES

AMES 08. AMES Newsletter

ASME 93. "Assessment of Reactor Pressure Vessels with Low Upper shelf Charpy Impact Energy Levels," Nonmandatory Appendix K, Section XI, *ASME Boiler and Pressure Vessel Code*, The American Society of Mechanical Engineers, New York, New York, 2007.

ASTM 02. E 900-02, "Standard Guide for Predicting Radiation-Induced Transition Temperature Shift in Reactor Vessel Materials, E706 (IIF)," *Annual Book of ASTM Standards, 2007*, ASTM International, West Conshohocken, Pennsylvania, 2007.

Carter 02. Carter, R. G., and N. Soneda, *Workshop on Dose Rate Effects in Reactor Pressure Vessel Materials*, Electric Power Research Institute Conference Proceedings, EPRI 1006981, CD, 2002.

Chaouadi 05. R. Chaouadi, *An Engineering Radiation Hardening Model for RPV Materials*, SCK/CEN Report R-4235, September 2005.

Debarberis 05. Debarberis, L., A. Kryukov, F. Gillemot, B.Acosta, and F. Sevini, "Semi-Mechanistic Analytical Model for Radiation Embrittlement and Re-embrittlement Data Analysis," *International Journal of Pressure Vessels and Piping* 82 (2005), pp. 195-200.

Eason 98. Eason, E. D., J. E. Wright, and G. R. Odette, *Improved Embrittlement Correlations for Reactor Pressure Vessel Steels*, NUREG/CR-6551, U.S. Nuclear Regulatory Commission, Washington DC, 1998.

Eason 07. Eason, E. D., G. R. Odette, R. K. Nanstad, and T.Yamamoto, *A Physically Based Correlation of Irradiation-Induced Transition Temperature Shifts for RPV Steels*, ORNL/TM-2006/530, Oak Ridge National Laboratory, Oak Ridge, Tennessee, November 2007.

EricksonKirk 07. EricksonKirk, Mark, Technical Basis for Revision of Regulatory Guide 1.99: NRC Guidance on Methods to Estimate the Effects of Radiation Embrittlement on the Charpy V-Notch Impact Toughness of Reactor Vessel Materials, Draft NUREG-XXXX, U. S. Nuclear Regulatory Commission, Washington, D. C., October 1, 2007.

Fisher 88. Fisher, S. B., and J. T. Buswell, "A Model For PWR Pressure-Vessel Embrittlement," *Int. J. of Pressure Vessels and Piping* 27 (2), 91(1988).

Gérard 96. Gérard, R., A. Fabry, J. Van de Velde et al., "In Service Embrittlement of the Pressure Vessel Welds at the Doel I and II Nuclear Power Plants, Effects of Irradiation on Materials," ASTM STP 1270, ed. D. S. Gelles, R. K. Nanstad et al. (1996), 294–319.

Gérard 06. Gérard, R., E. Lucon, M. Scibetta, and E. Van Walle, "Reactor Pressure Vessel Steels Embrittlement at Very High Neutron Doses," *Fontevraud 6th International Symposium on Contribution of Material Investigations to Improve Safety and Performance of LWRs*, September 18-22, 2006, Fontevraud-L'Abbaye, France.

Glade 04. Glade, S. C., B. D. Wirth, P. Asoka-Kumar, P A. Sterne, and G. R. Odette, "Positron Annihilation Spectroscopy of Nanostructural Features in Model Reactor Pressure Vessel Steels," *Materials Science Forum* 445-446 (2004) 87.

Glade 05. Glade, S. C., B. D. Wirth, G. R.. Odette, P. Asoka-Kumar, P. A., Sterne, and R. H. Howell, "Positron Annihilation Spectroscopy and Small Angle Neutron Scattering Characterizations of the Effect of Mn on the Nanostructural Features Formed in Irradiated Fe-Cu-Mn Alloys," *Philosophical Magazine* 85 (2005) 629.

Glade 06. Glade, S. C., B. D. Wirth, G. R. Odette and P. Asoka-Kumar, "Positron Annihilation Spectroscopy and Small Angle Neutron Scattering Characterization of Nanostructural Features in High-Nickel Model Reactor Pressure Vessel Steels," *J. Nucl. Mater* 351 (2006) 197.

Hasegawa 07. Hasagawa, M., Y. Nagai et al., "Evolution of Irradiation Induced Cu Precipitates and Defects in Surveillance Test Specimens of Pressure Vessel Steels of Nuclear Reactors: Positron Annihilation and 3 Dimensional Atom Probe Study," *Proceedings of the International Symposium on Research for Aging Management of Light Water Reactors*, October 22–23, 2007, Fukui City, Japan, Institute of Nuclear Safety Systems, Fukui, Japan.

Jenkins 01. Jenkins, M. L., A. C. Nicol, and M. A. Kirk, "Matrix Damage In Iron," pp. R1.3.1-R1.3.6 in *Microstructural Processes in Irradiated* Materials – *2000*, MRS Proceeding 650, ed. G. E. Lucas, L. L. Snead, M. A. Kirk, and R. G. Ellman, Materials Research Society 506 Keystone Drive, Warrendale, Pennsylvania, 2001.

Klueh 01. Klueh, R, L. and D. R. Harries, *High Chromium Ferritic and Martensitic Steels for Nuclear Applications*, ASTM International, West Conshohocken, PA, 2001.

Mader 95. Mader, E. V., "Kinetics of Irradiation Embrittlement and the Post-Irradiation Annealing of Nuclear Reactor Pressure Vessel Steels," PhD. Thesis, the University of California, Santa Barbara, 1995.

Marian 02. Marian, J., B. D. Wirth and J. M. Perlado, "On the Mechanism of Formation and Growth of <100> Interstitial Loops in Ferritic Materials," *Physical Review Letters* 88 (2002) 255507.

Miller 06. Miller, M. K., K. Russell, and G. R, Odette, "Clustering and Precipitation in Low Copper and Copper Free Steels and Model Alloys," International Field Emission Symposium, 2006.

Nanstad 93. Nanstad, R. K. and R. G. Berggren, "Effects of Irradiation Temperature on Charpy and Tensile Properties of High-Copper, Low Upper-Shelf, submerged-Arc Welds," pp. 239–67 in *Effects of Radiation on Materials*, ASTM STP 1175, ed. A. S. Kumar, D. S. Gelles, R. K. Nanstad, and E. A. Little, American Society of Testing and Materials, Philadelphia, 1993.

Norgett 75. Norgett, M. J., Robinson, M. T., Torrens, I. M., *Nucl. Eng. Des.*, 33 (1975), 50.

Odette 85. Odette, G. R., P. M. Lombrozo, and R. A. Wullaert, "Relationship Between Irradiation Hardening and Embrittlement of Pressure Vessel Steels," pp. 840–60 in *Effects of Radiation on Materials*, ASTM STP 870, ed. F. A. Garner and J. S. Perrin, American Society of Testing and Materials, Philadelphia, 1985.

Odette 90. Odette, G. R., and G. E. Lucas, "The Effect of Nickel in Irradiation Hardening of Pressure Vessel Steels," E*ffects of Radiation on Materials: 14th International Symposium*, ASTM STP 1046, ed. N. H. Packan et al., American Society for Testing and Materials, West Conshocken, PA,, 323, 1990.

Odette 93. G. R. Odette, E. V. Mader, G. E. Lucas, W. J. Phythian, and C. A. English, "The Effect of Flux on the Irradiation Hardening of Pressure Vessel Steels," *Effects of Radiation on Materials*, *ASTM STP 1175*, A. S. Kumar, D. S. Gelles, R. K. Nanstad, and E. A. Little, Editors, American Society of Testing and Materials, Philadelphia, 1993, 373–394.

Odette 94. Odette, G., R. E. V. Mader, G. E. Lucas, et al., "The Effect of Flux on the Irradiation Hardening and Embrittlement of Pressure Vessel Steels," *Effects of Radiation on Materials: 16th International Symposium*, ASTM-STP 1175, ed. A.S. Kumar et al., American Society for Testing and Materials, West Conshohocken, PA, 373, 1994 .

Odette 95. Odette, G. R., "Radiation Induced Microstructural Evolution in Reactor Pressure Vessel Steels," *Microstructural Evolution During Irradiation*, Mat Res. Soc. Symp. Proc. 373, ed. I. M. Robertson et. al., Materials Research Society, Warrendale, PA, 137, 1995.

Odette 96. G. R. Odette, G. E. Lucas and D. Klingensmith, "The Influence of Metallurgical Variables on the Temperature Dependence of Irradiation Hardening in Pressure Vessel Steels," Effects of Radiation on Materials-17 International Symposium, ASTM-STP-1270, American Society for Testing and Materials, 1996, 606-622.

Odette 97a. Odette, G. R., and B. D. Wirth, "A Computational Microscopy Study of Nanostructural Evolution in Irradiated Pressure Vessel Steels," *J. Nuc. Mat.* 251, 157, 1997.

Odette 97b. Odette, G. R., C. L. Liu, and B. D. Wirth, "On the Composition and Structure of Nanoprecipitates in Irradiated Pressure Vessel Steels," *Microstructural Evolution During Irradiation*, MRS Symp. Proc. 439, ed. I. M. Robertson et. al., Materials Research Society, Warrendale, PA, 457, 1997.

Odette 98a. Odette, G. R., "Modeling of Irradiation Embrittlement in Pressure Vessel Steels," *Irradiation Effects on Pressure Vessel Steels*, IAEA IRRWG-LMNPP98-3, International Atomic Energy Agency, Vienna, Austria, 438, 1998 .

Odette 98b. Odette, G. R. and G. E. Lucas, "Recent Progress in Understanding Reactor Pressure Vessel Embrittlement," *Radiation Effects and Defects in Solids* 144, 189, 1998.

Odette 01a. Odette, G. R., B. D. Wirth, D. J. Bacon and N. M. Ghoneim, "Multiscale-Multiphysics Modeling of Radiation-Damaged Materials: Embrittlement of Pressure Vessel Steels," *MRS Bulletin* 26, 176, 2001.

Odette 01b. Odette, G. R., and C. Cowan, "Use of Combined Electrical Resistivity and Seebeck Coefficient Measurements to Characterize Solute Redistribution Under Irradiation and Thermal Aging," *Proceedings of the 10th International Symposium on Environmental Degradation of Materials in Light Water Reactors*, ed. G. S. Was et. al., NACE, CD, 2001.

Odette 03. Odette, G. R., T. Yamamoto, R. D. Klingensmith, et al., *The Effect of Flux and Irradiation, Temperature on Hardening in RPV Steels*, UCSB-NRC-LR-03/2, 2003 .

Odette 04. Odette, G. R., T. Yamamoto, and B. D. Wirth, "Late Blooming Phases and Dose Rate Effects in RPV Steels: Integrated Experiments and Models," p. 355 in *Proceedings of the Second International Conference on Multiscale Materials Modeling*, ed. N. M. Ghoniem, Univeristy of California, 2004.

Odette 05. Odette,G. R., T. Yamamoto, and R. D. Klingensmith, "On the Effect of Dose Rate on Irradiation Hardening of RPV Steels," *Phil. Mag.* 85, 2005 779.

Osetsky 00. Osetsky, Y. N., A. Serra, and V. Priego, "Interactions Between Mobile Dislocation Loops in Cu and alpha-Fe," *Journal of Nuclear Materials* 276, (2000), 202-212.

Phythian 95. Phythian, W. J., R. E. Stoller, A. J. E. Foreman, A. F. Calder, and D. J. Bacon, "A Comparison of Displacement Cascades in Copper and Iron by Molecular Dynamics and its Application to Microstructural Evolution," *Journal of Nuclear Materials* 223 (1995) 245–261.

Randall 86. Randall, P.N., "Basis for Revision 2 of the U.S. Nuclear Regulatory Commission's Regulatory Guide 1.99,"pp. 149–62 in *Radiation Embrittlement of Nuclear Reactor Pressure Vessel Steels: An International Review (Second Volume)*, ASTM STP 909, ed. L.E. Steele, American Society for Testing and Materials, Philadelphia, 1986.

RG 1.99-2. "Radiation Embrittlement of Reactor Vessel Materials," *Regulatory Guide 1.99, Revision 2*, U.S. Nuclear Regulatory Commission, May 1988.

Smidt 73. Smidt, F. A and J. A. Sprague, "Property Changes Resulting from Impurity-Defect Interactions in Iron and Pressure Vessel Steel Alloys," pp. 78–91 in *Effects of Radiation on Substructure and Mechanical Properties of Metals and Alloys*, ASTM STP 529, American Society of Testing and Materials, Philadelphia, 1973.

Stoller 93. Stoller, R. E., "The Influence of Damage Rate and Irradiation Temperature on Radiation-Induced Embrittlement in Pressure Vessel Steels," pp. 394–426 in *Effects of Radiation on Materials*, ASTM STP *1175*, ed. A. S. Kumar, D. S. Gelles, R. K. Nanstad, and E. A. Little, American Society of Testing and Materials, Philadelphia, 1993.

Stoller 96a. Stoller, R. E., "Point Defect Survival and Clustering Fractions Obtained from Molecular Dynamics Simulations of High *Energy* Cascades," *Journal of Nuclear Materials* 233-237 (1996) 999-1003.

Stoller 96b. Stoller, R. E., "Pressure Vessel Embrittlement Predictions Based on a Composite Model of Copper Precipitation and Point Defect Clustering," pp. 25–59 in *Effects of Radiation on Materials*, ASTM STP 1270, ed. D. S. Gelles, R. K. Nanstad, A. S. Kumar, and E. A. Little, American Society of Testing and Materials, Philadelphia, 1996.

Stoller 01. Stoller, R. E. and L. R. Greenwood, "An Evaluation of Through-Thickness Changes in Primary Damage Production in Commercial Reactor Pressure Vessels," *Effects of Radiation on Materials: 20th International Symposium*, ASTM STP 1405, ed. S. T. Rosinski, M. L. Grossbeck, T. R. Allen, and A. S. Kumar, American Society for Testing and Materials, West Conshohocken, Pennsylvania, 2001.

Stoller 04. Stoller, R. E., "The Effect of Neutron Flux on Radiation-Induced Embrittlement in Reactor Pressure Vessel Steels," *Journal of ASTM International* 1 (2004) JAI11355 (see also *Effects of Radiation on Materials, ASTM STP 1447*).

Wakai 00. Wakai, E., A. Hishinuma, K. Usami, T. Kato, S. Takaki, and K. Abiko, "Damage Structures and Mechanical Properties of High-Purity Fe-9Cr Alloys Irradiated by Neutrons," *Materials Transaction*, JIM 41 (2000) 1180–83.

WGFE 96. Working Group on Flaw Evaluation of ASME Section XI, "Development of Criteria for Assessment of Reactor Vessels with Low Upper Shelf Fracture Toughness," *WRC Bulletin 413*, Pressure Vessel Research Council of Welding Research Council, Inc., July 1996.

Williams 02. Williams, T. J., D. Ellis, C. A. English, and J. Hyde, "A Model of Irradiation Damage in High Nickel Submerged Arc Welds," *Int. J. of Pressure Vessels and Piping* 79, 964, 2002.

Wirth 98. Wirth, B. D., "On the Character of Nano-Scale Features in Reactor Pressure Vessel Steels under Neutron Irradiation," PhD. Thesis University of California, Santa Barbara, 1998.

Wirth 00. Wirth, B. D., G. R. Odette, D. Maroudas, and G. E. Lucas, "Dislocation Loop Structure, Energy and Mobility of Self-Interstitial Atom Clusters In bcc Iron," *Journal of Nuclear Materials* 276 (2000) 33–40.

Wirth 01. Wirth, B. D., G. R. Odette, and R. E. Stoller, "Recent Progress Toward an Integrated Multiscale-Multiphysics Model of Reactor Pressure Vessel Embrittlement," Multiscale Modeling of Materials, *MRS Soc. Symp. Proc.* 677, ed. V. Bulatov et. al., Materials Research Society, Warrendale, Pennsylvania, AA5. 2, 2001.

Yamamoto 06 Yamamoto, T., G. R. Odette, H. Kishimoto, J. W. Rensman, and P. F. Miao, "On the Effects of Irradiation on the Yield Stress Changes and Hardening and Non-Hardening Embrittlement of 8Cr Tempered Martensitic Steels: Compilation and Analysis of Existing Data," *J. Nucl. Mater.* 356 1–3, 27–49 (2006).

APPENDIX A. DETAILS OF MODEL STATISTICS

APPENDIX A. DETAILS OF MODEL STATISTICS

MEK model (RM-9)

		orig.	imprvd	optmzd
CRP	Weld	0.3	0.30696	0.31563
	Plate & SRM	0.233	0.24282	0.25731
	Forging	0.235	0.2316	0.24081
	Cu exponent	0.5	0.5	0.5
	Cu_{min}	0.048	0.0492	0.052
	Cu: B_{1m}	530.8	555.22	561.93
	Cu: $B_{Cu(max)}$	185	170.99	163.78
	$\Delta B_{Cu(max)}$ -L80	0	-0.0002	-0.0002
	Ni: B_2	0	0	0
	Cu*Ni: B_3	2500	2562.4	2554.8
	Mn: B_4	0	0	0
	P: B_5	0	0	0
	Si: B_6	0	0	0
	Φ_{SAT}: C_0	10	10.8872	11.3974
	Φ_{SAT}: ϕ: C_2	11	11.8115	11.8543
	Φ_{SAT}: Ni: C_1	2.3	2.32702	2.09494
	Φ_{SAT}: Mn: C_4	0	0	0
	Φ_{SAT}: Cu : C_3	0	0	0
	Φ_{SAT}: P : C_3	0	0	0
	Φ_{SAT}: Si : C_3	0	0	0
	Etemp	-1.74	-1.7636	-1.76363
	Eflux	5	4.91271	5.15835

MD	Efluence	0.5	0.5	0.5
	Etemp	-14.64	-14.1521	-13.8117
	E-Flux	-3.44	-2.94977	-3.01284
	Weld	6.7	6.60582	6.58483
	Plate & SRM	8.1	7.76829	7.60261
	Forging	4.75	4.82563	4.89567
	CF-Ni	0	0	0
	CF-Mn	0	0	0
	CF-P	35	33.3596	34.2992
	CF-Si	0	0	0
	CF-Cu	0	0	0

t-total	7.4364	2.3693	2.0375
S-error	24.301	23.81	23.669

fluence	0.7935	0.0299	6E-06
	0.81	0.0299	6E-06
	1.6036	0.0598	1E-05
flux	0.866	0.0302	0.0061
	0.8923	0.0302	0.0061
	1.7583	0.0604	0.0121
Temperature	0.48	9E-06	1E-05
	0.4906	9E-06	3E-06
	0.9705	2E-05	1E-05
Copper	0.2493	0.3816	1E-05
	0.4873	0.3269	0.0002
	0.7366	0.7085	0.0002
Nickel	0.1652	3E-07	8E-07
	0.3542	1E-06	0.0001
	0.5194	2E-06	0.0001
Pred TTS	0.4695	0.641	0.944
	0.0684	0.5169	0.7597
	0.5379	1.1579	1.7037
Phos	0.4338	6E-06	0.0001
	0.241	4E-06	2E-05
	0.6749	1E-05	0.0001
Mn	0.166	1E-06	0.0001
	0.0596	1E-07	3E-05
	0.2256	1E-06	0.0001
Product Form	0.1425	0.1429	0.1288
	4E-05	0.008	0.0003
	0.2671	0.2317	0.1919
	0.4097	0.3827	0.321

EONY model (Simplified)

	orig.	imprvd	optmzd
Weld	155	157.055	163.052
Plate	102.5	100.74	104.373
CE _add	32.7	32.5419	30.7628
Forging	102.3	105.375	115.954
SRM	128.2	124.945	128.8
Cu_{min}	0.072	0.07429	0.072
Pmin	0.008	0.008	0.008
P_coef	1.359	1.36604	1.22611
E_CuP	0.668	0.67842	0.67422
Ni_coef	3.77	3.66691	3.59167
E_Ni	1.191	1.16633	1.06535
Cue_max	0.301	0.30228	0.301
Cue_max_LINDE80	0.243	0.25048	0.26279
Linde80_Ni_min	0.5	0.5	0.5
g: C_0	-18.12	-18.1894	-18.2025
g: Ni: C_1	-0.448	-0.45004	-0.45722
g: Cu : C_3	1.139	1.13978	1.13461
g: denom	0.629	0.63036	0.75075
Etemp	0	0.00375	-0.001
E_flux_max (x1e10)	4.39	4.38698	4.64117

Efluence	0.5	0.5	0.5
K_temp (x 1e-3)	-1.718	-1.70958	-1.70969
E-Flux	0.259	0.29951	0.26659
Weld	1.417	1.42334	1.29057
Plate & SRM	1.561	1.49271	1.44141
Forging	1.14	1.14549	1.1005
E-Mn	2.47	2.45591	2.43807
CF-P	6.13	6.10614	6.05447

t-total	12.893	7.9252	1.5674
S-error	22.672	22.707	22.584

fluence	0.4389	0.0004	0.0932
	0.5068	0.0004	0.0931
	0.9457	0.0008	0.1863
flux	0.0487	0.1608	0.0054
	0.062	0.1605	0.0054
	0.1107	0.3213	0.0108
Temperature	2.1936	0.9354	0.0102
	2.2365	0.9352	0.0102
	4.4301	1.8706	0.0205
Copper	0.343	1.503	0.0019
	0.8115	1.2866	0.0021
	1.1546	2.7895	0.004
Nickel	1.3935	0.2451	0.0002
	0.4752	0.2275	0.0001
	1.8687	0.4726	0.0003
Pred TTS	1.9909	5E-06	0.3787
	0.3297	0.0012	0.3045
	2.3206	0.0012	0.6832
Phos	0.0652	0.3841	0.0008
	0.6244	0.3633	0.0005
	0.6896	0.7474	0.0013
Mn	0.7539	0.1071	0.002
	0.3228	0.1054	0.0018
	1.0767	0.2124	0.0039
Product Form	0.1209	0.8029	0.1918
	0.1583	0.5513	0.0526
	0.0171	0.1549	0.4129
	0.2963	1.5092	0.6572